การวิเคราะห์สมบัติเชิงโครงสร้างและสมบัติเชิงแสงของบ่อศักย์เดี่ยว $In_xGa_{1-x}P_{1-y}N_y/GaP$ แบบแลตทิชแมทช์ปลูกโดยวิธีเอ็มโอวีพีอี

นางสาวดาเรศ แก้วเกตุ

STRUCTURAL AND OPTICAL PROPERTIES ANALYSIS OF
LATTICE-MATCHED $In_xGa_{1-x}P_{1-y}N_y$/GaP SINGLE QUANTUM WELL
GROWN BY MOVPE

Miss Dares Kaewket

A Thesis Submitted in Partial Fulfillment of the Requirements
for the Degree of Master of Science Program in Physics
Department of Physics
Faculty of Science
Chulalongkorn University
Academic year 2006

Thesis Title   STRUCTURAL AND OPTICAL PROPERTIES ANALYSIS OF LATTICE-MATCHED $In_xGa_{1-x}P_{1-y}N_y$/GaP SINGLE QUANTUM WELL GROWN BY MOVPE

By   Miss Dares Kaewket

Field of study   Physics

Thesis Advisor   Assistant Professor Sukkaneste Tungasmita, Ph.D.

Thesis Co-advisor   Sakuntam Sanorpim, Ph.D.

Accepted by the Faculty of Science, Chulalongkorn University in Partial Fulfillment of the Requirements for the Master's Degree

....Dean of the Faculty of Science

(Professor Piamsak Menasveta, Ph.D.)

THESIS COMMITTEE

.........Wichit Sritrakool............. Chairman

(Associate Professor Wichit Sritrakool, Ph.D.)

....Thesis Advisor

(Assistant Professor Sukkaneste Tungasmita, Ph.D.)

.... Thesis Co-advisor

(Sakuntam Sanorpim, Ph.D.)

....Member

(Assistant Professor Rattachat Mongkolnavin, Ph.D.)

....Member

(Burin Asavapibhop, Ph.D.)

ดาเรศ   แก้วเกตุ: การวิเคราะห์สมบัติเชิงโครงสร้างและสมบัติเชิงแสงของบ่อศักย์เดี่ยว
In$_x$Ga$_{1-x}$P$_{1-y}$N$_y$/GaP แบบแลตทิซแมทช์ปลูกโดยวิธีเอ็มโอวีพีอี
(STRUCTURAL AND OPTICAL PROPERTIES ANALYSIS OF LATTICE-
MATCHED In$_x$Ga$_{1-x}$P$_{1-y}$N$_y$/GaP SINGLE QUANTUM WELL GROWN BY
MOVPE) อ. ที่ปรึกษา: ผศ. ดร. สุคคเณศ ตุงคะสมิต, อ. ที่ปรึกษาร่วม: ดร.สกุลธรรม
เสนาะพิมพ์, 81 หน้า.

ในวิทยานิพนธ์นี้ สมบัติเชิงโครงสร้างและสมบัติเชิงแสงของบ่อศักย์เดี่ยว In$_x$Ga$_{1-x}$P$_{1-y}$N$_y$
/GaP แบบแลตทิซแมทช์ที่ปลูกผลึกลงบนซับสเตรต GaP ระนาบ 001 ด้วยวิธีเมทอลออแกนิกเว
เปอร์เฟสอีพิแทกซี (MOVPE) ได้ถูกตรวจสอบ   ผลกระทบจากการเปลี่ยนแปลงของทั้งค่าความ
กว้างของบ่อศักย์และองค์ประกอบทางเคมีภายในบ่อศักย์ได้ถูกพิสูจน์   ผลการทดลองที่ได้จาก
เทคนิคการเลี้ยวเบนของรังสีเอ็กซ์กำลังแยกสูง (HRXRD) บ่งชี้ว่าบ่อศักย์เดี่ยว In$_x$Ga$_{1-x}$P$_{1-y}$N$_y$
/GaP แบบแลตทิซแมทช์ที่มีคุณภาพของผลึกดีและมีผิวต่อประสาน (interface) ที่เรียบได้ถูกเตรียม
ให้เกิดขึ้นจริง โฟโตลูมิเนสเซนส์ (PL) สเปกตราแสดงการเปล่งแสงจากบ่อศักย์เดี่ยวในช่วงความ
ยาวคลื่นที่มองเห็นได้ (ช่วงแสงสีเหลืองถึงแสงสีแดง)   โดยการทำให้ความกว้างของบ่อศักย์แคบ
ลง ตำแหน่งของยอด PL และจุดเริ่มเกิดการดูดซับพลังงานของโฟโตลูมิเนสเซนส์เอกไซเตชัน
(PLE) แสดงการเลื่อนไปทางด้านพลังงานที่สูงขึ้น จากผลนี้ได้ยืนยันถึงอิทธิพลของควอนตัมคอน
ไฟน์เมนต์ด้วยบ่อศักย์เดี่ยว ในทางตรงข้ามโดยการเพิ่มความเข้มข้นของ In และ N ตำแหน่ง
ของยอด PL และจุดเริ่มเกิดการดูดซับพลังงานของ PLE แสดงการเลื่อนไปทางด้านพลังงานที่
ต่ำลง ซึ่งบ่งชี้ถึงการลดลงของขอบแถบการนำของ InGaPN ความแตกต่างของแถบการนำ
(conduction band offset, ΔE_c) ของโครงสร้างบ่อศักย์ In$_x$Ga$_{1-x}$P$_{1-y}$N$_y$/GaP มีค่าประมาณ 270-490
มิลลิอิเล็กตรอนโวลต์ (meV) ขึ้นอยู่กับความเข้มข้นของ In และ N ในบ่อศักย์ อย่างไรก็ตาม
ค่าความแตกต่างของแถบการนำนี้ถูกจำกัดด้วยความบกพร่องที่เกี่ยวเนื่องกับกระบวนการไม่เปล่ง
แสง ซึ่งก่อเกิดขึ้นในชิ้นงานที่มีปริมาณความเข้มข้นของ In และ N สูง

ภาควิชา ....ฟิสิกส์............	ลายมือชื่อนิสิต	
สาขาวิชา........ฟิสิกส์............	ลายมือชื่ออาจารย์ที่ปรึกษา	
ปีการศึกษา ....2549............	ลายมือชื่ออาจารย์ที่ปรึกษาร่วม...............	

4772300923: MAJOR   PHYSICS

KEY WORDS: InGaPN / SINGLE QUANTUM WELL / METAL ORGANIC VAPOR PHASE EPITAXY / STRUCTURAL PROPERTY / OPTICAL PROPERTY

DARES KAEWKET: STRUCTURAL AND OPTICAL PROPERTIES ANALYSIS OF LATTICE-MATCHED $In_xGa_{1-x}P_{1-y}N_y$/GaP SINGLE QUANTUM WELL GROWN BY MOVPE. THESIS ADVISOR: ASST. PROF. SUKKANESTE TUNGASMITA, PH.D. THESIS CO-ADVISOR: SAKUNTAM SANORPIM, PH.D., 81 pp.

In this thesis, structural and optical properties of the lattice-matched $In_xGa_{1-x}P_{1-y}N_y$/GaP single quantum wells (SQWs) grown on GaP (001) substrates by metalorganic vapor phase epitaxy (MOVPE) have been investigated. The effects of both well-width and compositional variations are established. The results from high-resolution X-ray diffraction (HRXRD) measurements indicate that the lattice-matched $In_xGa_{1-x}P_{1-y}N_y$/GaP SQWs were realized with excellent crystal quality and fairly flat interfaces. Photoluminescence (PL) spectra show the visible light emission (yellow-red emission) from the SQWs. With decreasing well-width, the PL peak position and the absorption edge of PLE spectra exhibit the blue-shift in energy. This result confirms the quantum confinement effect by the well. On the other hand, with increasing In and N concentrations, the PL peak position and the absorption edge of PLE spectra exhibit the red-shift to lower energy, indicating the lowering of the InGaPN conduction band edge. The conduction band offset (ΔE_c) of the InGaAPN/GaP quantum structure is estimated to be about 270 - 490 meV, which depends on the In and N concentrations in the well. However, the value of conduction band offset is limited by the large number of non-radiative defects caused in the high In and N incorporating samples.

Department.......Physics........	Student's signature................................
Field of study....Physics........	Advisor's signature................................
Academic year....2006..........	Co-advisor's signature............................

Acknowledgements

CONTENTS

List of Tables

List of Figures

CHAPTER I

INTRODUCTION

In this first chapter, the literatures and properties of InGaPN are presented. The objectives and organization of the thesis are also described.

1.1 Overviews

Dilute nitride semiconductors have attracted intense interest during the recent decade, especially, GaAsN and GaPN alloys. The incorporation of small amount of nitrogen can lead to novel physical properties of these alloys. This results in drastically reduction of the bandgap energy. Figure 1.1 shows the bandgap energy as a function of lattice constant for the ternary and quaternary III-V compounds. Notice that, the incorporation of 1% of N into GaAs can cause the bandgap energy to reduce from 1.42 to 1.25 eV at room temperature [1], although the bandgap energy of GaN is much larger (3.299 eV). This is an advantage for the bandgap engineering which done by controlling the amount of nitrogen in the III-V based materials. Moreover, this bandgap reduction, which is due to the incorporation of nitrogen, comes from lowering of the conduction band edge [2]. These lead to a large conduction band offset which is beneficial for heterostructures. Recently, the variety of materials in this group, such as GaAsN [3], InGaAsN [4] and GaPN [5], have been grown and investigated. The GaPN was discovered in the late 1960s [6], and later leads to the fabrication of light emitting diodes (LEDs) [7, 8]. For GaAsN and InGaAsN, they have received a great deal of the attention because their bandgap bowing makes possible 1.3 and 1.55 μm Bragg reflectors (as shown in Fig. 1.1) which can be applied in many devices, such as optical fiber.
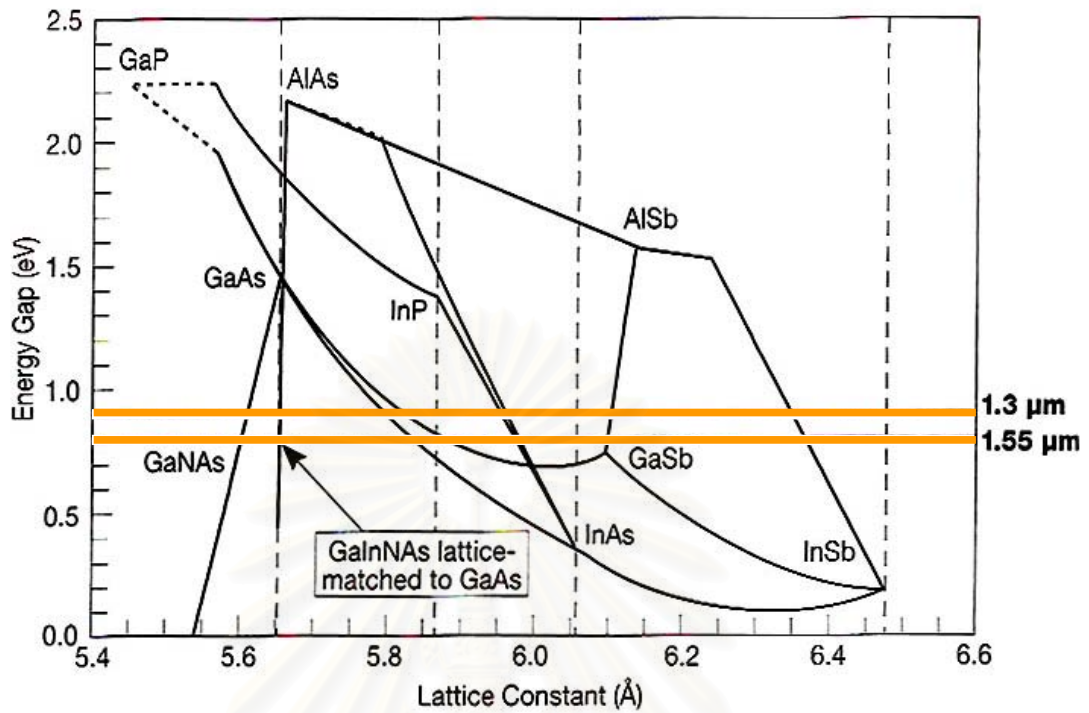
Figure 1.1: The relationship between the bandgap energies and the lattice constants of III-V compounds [9].

Nowadays, $In_xGa_{1-x}P_{1-y}N_y$ (or InGaPN for short), which is a novel material in this group, have attracted intense interest for optoelectronic devices operating at the visible wavelength regions (yellow to red region). As the major material, GaP, the InGaPN has a zinc-blende structure. This alloy material becomes much interesting because it could have a large impact in materials science and device applications. Since it is a quaternary alloy, so its lattice constant can be tuned by adjusting the compositions (*x*, *y*) of the material. An indium (In) atom has atomic size larger than that of gallium (Ga), phosphorus (P) and nitrogen (N), so adding In results in an increase of the lattice constant of the alloy. On the other hand, a nitrogen atom has the atomic size smaller than others, so adding N results in a decrease of the lattice constant. This can make the lattice-matching with many commercial substrates such as GaP, InP and GaAs. The lattice-matching condition between InGaPN and GaP can be determined using an interpolation method, as follows

$$x = \frac{0.947\,y}{0.418 + 0.059\,y} \quad , \quad x, y \leq 1 \quad , \tag{1.1}$$

where *x* and y are the concentrations of In and N, respectively. The lattice-matching condition between the film and substrate prevents the epitaxial layers from a misfit dislocation, which degrades the quality of the grown layers. The physical properties of the InGaPN alloy can be estimated by the properties of the related binary compounds, as shown in Table 1.1. For the bandgap engineering, by adjusting the compositions of InGaPN, its bandgap energy also can be tuned. The bandgap energy of InGaPN is in the range between the bandgap energy of InP (1.4236 eV) and that of GaN (3.299 eV). This is of interest for a variety of high-brightness light-emitting and laser applications such as automotive lighting, optical media reader/writer, billboard, media display panel and traffic light etc.

The InGaPN alloy can be invented for optoelectronic devices, like the GaPN and GaPAsN based devices. In the late 1960s, Thomas and Hopfield discovered the N isoelectronic trap in GaP:N for low N concentration ($\sim 10^{18}$ cm^{-3}) [6], which led this structure to fabrication of high-efficient green light emitting diodes (LED's) [7, 8]. This phenomenon is caused by the producing of localized N-related trap states in the bandgap which lower than the indirect bandgap energy level of GaP [6], as shown in Fig. 1.2. The A-line (or N state in Fig. 1.2) is due to an exciton bound to an isolated N atom. It is known that the exciton is a one type of carriers in semiconductors. Because the free hole and the free electron are opposite charges, so there is the coulomb

Physical properties / Binary compounds	Lattice constant (Å), (RT)	Bandgap energy (eV), (0K)	Electron effective mass (m_e)
GaP	5.4505	2.35*	0.13
InP	5.8697	1.4236	0.0795
GaN	4.50	3.299	0.15
InN	4.98	1.94	0.12

*indirect bandgap

Table 1.1: Physical properties of binary compounds [10] which are components of InGaPN alloy.
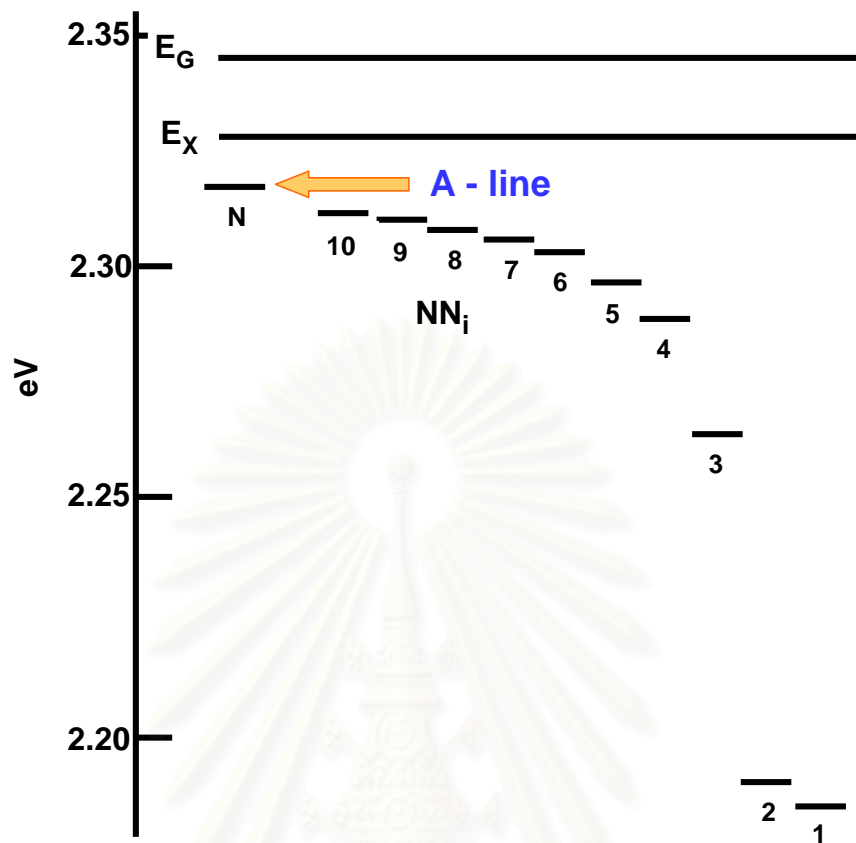
Figure 1.2: The N trap states which lie under the indirect gap of GaP (labeled by E_G) and free exciton level (labeled by E_X) [11]. A-line (or N) state [12] is also denoted by an arrow.

attraction. Hence, the electron orbits around the hole as a hydrogen-like atom and exhibits as the neutral carrier. In addition, the deeper series of NN lines are bound states of the exciton to two nitrogen atoms at various interatomic spacing. Figure 1.3 depicts the NN_1, NN_2 and NN_3. As a result, the carriers are attracted by these strong localized states and then recombination. These make the GaPN material to be the quasi-direct semiconductor with lowering the optical transitions. The same effect is also expected for the InGaPN material.

InGaPN/GaP lattice-matched single quantum wells (SQWs) was first purposed by Onabe *et al* [13]. They have demonstrated that the InGaPN alloy can be lattice-matched to GaP substrate with a narrower bandgap than GaP. This material also exhibit the large reduction of the bandgap energy which caused by lowing of the

(a) NN$_1$ pair

(b) NN$_2$ pair
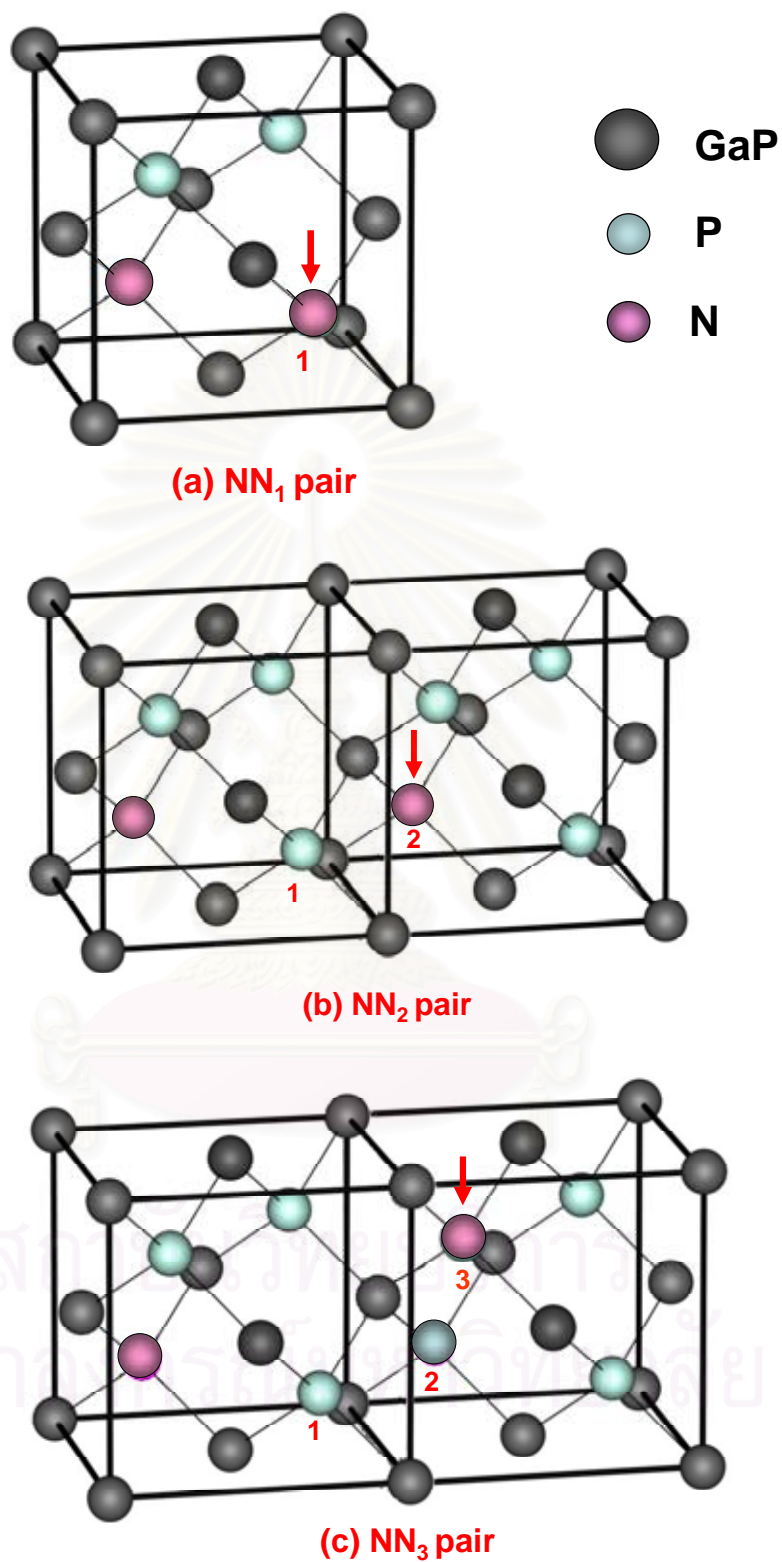
(c) NN$_3$ pair

Figure 1.3: Schematic illustration showing the NN$_i$ ((a) NN$_1$, (b) NN$_2$ and (c) NN$_3$) pairs which can be bound the excitons.

conduction band edge. As a result, these introduce the InGaPN/GaP structure as an alternative heterostructure with a large barrier height for an electron confinement in the InGaPN/GaP quantum structures, and exhibit higher characteristic temperature for laser application. Also, the InGaPN/GaP strained quantum well by molecular beam epitaxy (MBE) is reported by Odnoblyudov and Tu [14]. From above promising advantages, InGaPN/GaP will allow brighter and cheaper LED chips.

1.2 Objectives and Organization of the Thesis

The objectives of the thesis is to investigate structural and optical properties of lattice-matched InGaPN/GaP single quantum wells (SQWs) grown by metalorganic vapor phase epitaxy (MOVPE). Effects of well-width and composition on both the structural and optical properties of the lattice-matched SQWs are discussed.

The thesis is organized as follows:

In Chapter I, as described above, the literature and physical properties of III-V-Nitrides are reviewed. Especially, InGaPN alloy, InGaPN/GaP heterostructure and their applications are focused.

In Chapter II, the basic knowledge which related to the single quantum well (SQW) structures are introduced. The superior properties of quantum well structures (2-dimentional system) over the bulk film (3-dimentional system) are described. Then, characterization methods are briefly described.

In Chapter III, the InGaPN/GaP SQWs with different well-widths were investigated. Structural quality, well-thickness and alloy compositions, which were analyzed by high resolution X-ray diffraction (HRXRD) and the dynamical theory simulation software, are described. Effects of the well-width variation on optical properties of the SQWs, which were characterized by photoluminescence (PL) and photoluminescence-excitation (PLE), are discussed.

In Chapter IV, effects of the compositional variation on both structural and optical properties of the SQWs, which were investigated by HRXRD, PL and PLE, are discussed in details.

In Chapter V, the valence and conduction band offsets of the InGaPN/GaP heterostructures were examined. The comparison results between the transition energy, which was obtained from the PL peak positions and PLE absorption edge, and that from the finite square well method, are mainly focused.

Finally, the conclusions of the thesis are given in Chapter VI.
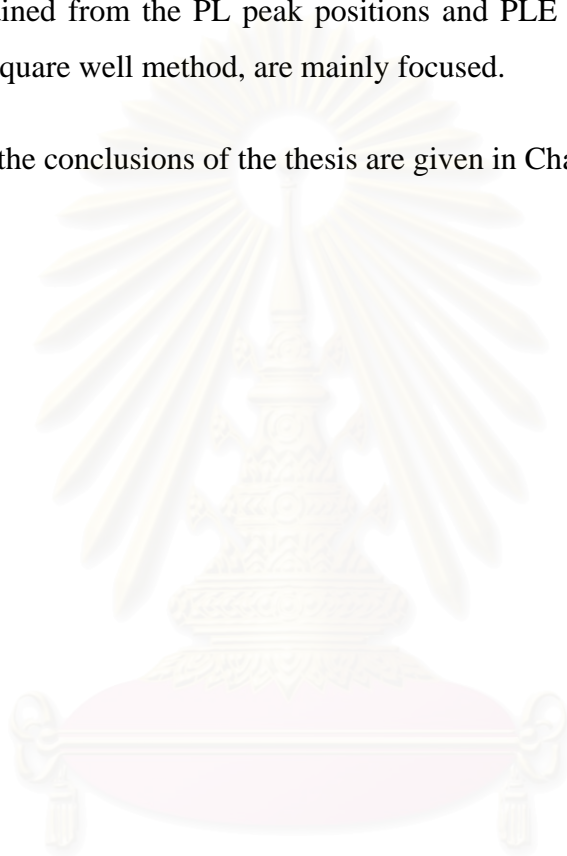
CHAPTER II

QUANTUM WELL STRUCTURE
AND CHARACTERIZATION

In this chapter, the physics of quantum well structure and characterization methods are briefed. For the physical characteristics of quantum well structure, the calculation of a finite-depth square quantum well and the advantages of heterostructure are demonstrated. Moreover, several characterization methods for the quantum well structure are introduced.

2.1 Basic Physics of Quantum Well Structures

2.1.1 Introduction

In a semiconductor quantum well (QW) structure (often abbreviated as heterostructure), two different semiconductors with different bandgap energies are brought into physically contact. In practice, a very thin semiconductor A is epitaxially grown on top of a semiconductor B and then the semiconductor B is repeatedly grown over the thin semiconductor A again, as shown in Fig. 2.1 (a). The semiconductor A is called "well layer" which usually not thicker than 10 nm and semiconductor B is called "barrier". Typically, the bandgap energy of the well layer is smaller than that of the barrier. This structure generates the potential well which can confine the carriers. The energy of the carriers will be quantized. The difference of the conduction band edge between the well layer and the barrier is called "conduction band offset, ΔE_c"
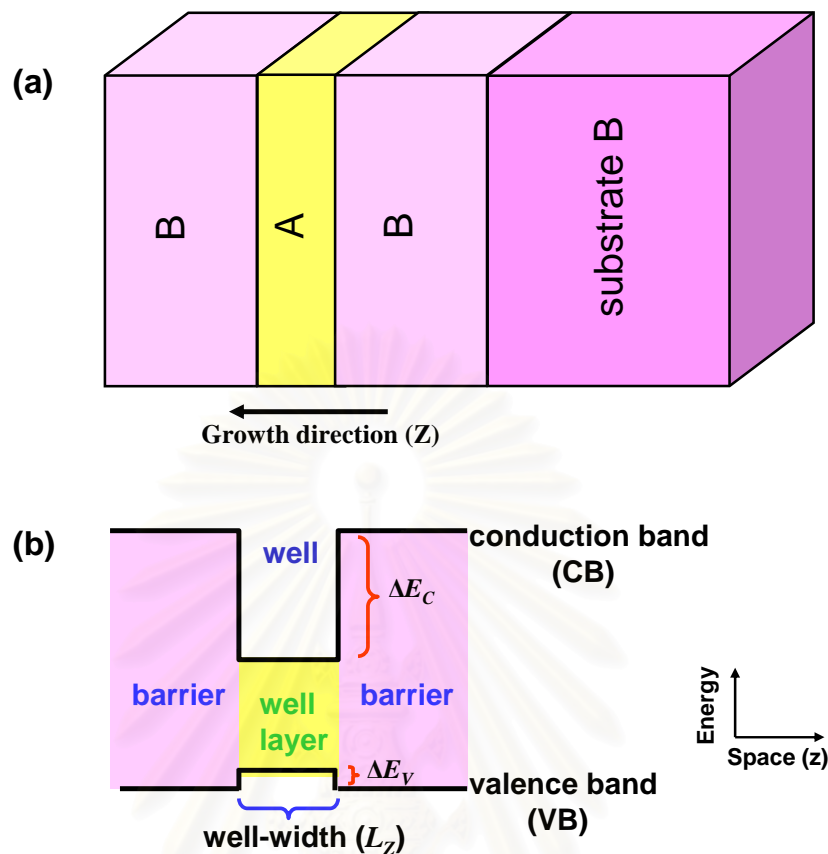
Figure 2.1: (a) Single quantum well structure (SQW). (b) Electronic structure of SQW.

and that of the valence band edge is called "valence band offset, ΔE_v", see Fig 2.1 (b). For the dilute nitride semiconductors, it is known that adding small amount of N decreases the bandgap, which mainly affects the conduction band (CB) states. This led the heterostructure to a large ΔE_c and only a small valence-band offsets (ΔE_v). For example, the effect of ~1% of N on the valence band of GaAs is negligible [2]. So, the valence band offset which is depicted in the Fig. 2.1 (b) is estimated to be very small comparing to the conduction band offset.

However, the heterostructures can be classified according to the alignment of the band of the two semiconductors. Two different alignments of the conduction and valence bands and of the forbidden gap are shown in Fig. 2.2. In Fig. 2.2 (a), this shows the most common alignment which will be referred to as the "straddled alignment" or "Type-I" alignment. This type of the alignment shows the valence band edge of the well layer is higher than that of the barrier. Another type is shown as
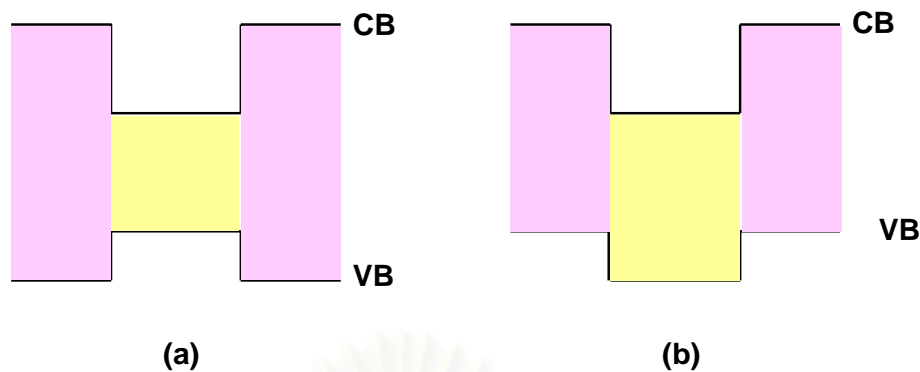
Figure 2.2: Types of energy band lineups: (a) straddled or Type-I lineup. (b) staggered or Type-II lineup.

Fig. 2.2 (b) which called "staggered alignment" or "Type-II" alignment. In the contrast, Type-II alignment shows the valence band edge of the well layer is lower than that of the barrier. In the case of Type-I alignment, the carriers will recombine down to the quantum level in the well region. But, for Type-II, they are instead recombining to the valence band of the barrier. The recombination efficiency in this case is lower than that of the Type-I because it is the indirect transition. So, the applications for light emitting and laser diodes prefer the Type-I alignment due to its higher recombination efficiency.

2.1.2 Finite-Depth Square Quantum Wells

Consider an electron in the conduction band of the quantum well of width L and the finite well height of V_0, as in Fig. 2.3. This finite well height is equal to the conduction band offset between the well layer and the barrier. The electron effective mass in the well and the barrier are m_w^* and m_b^*, respectively (in the case of two barriers are the same materials). The potential energy profile in z direction is given as seen in Fig. 2.3. On the other hand, the potential energy along the x-y plane is constant. Therefore, the Schrödinger's equation can be separated in the x, y, and z directions. The wave function of electron must satisfy the Schrödinger's equation. In the well region, the Schrödinger's equation for the z direction can be written as:
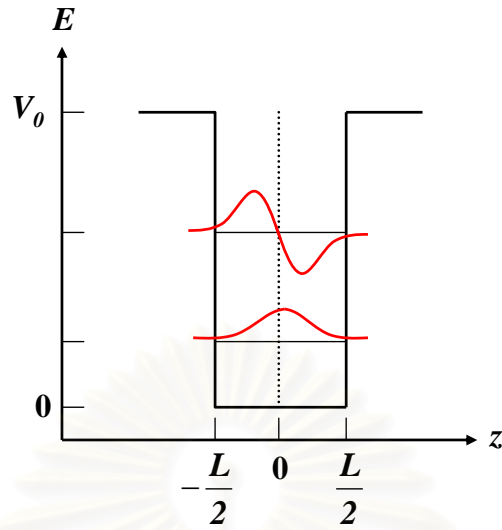
Figure 2.3: The finite-depth square potential well.

$$-\frac{\hbar^2}{2m_w^*}\frac{d^2\varphi_w(z)}{dz^2} = E\varphi_w(z) \quad , \tag{2.1}$$

where m_w^*, $\varphi_\omega(z)$, and E are the electron effective mass, the wave function of electron in the well region along the z direction and the energy of electron for the z direction, respectively. Hence, the wave function of electron inside the well in the z direction is:

$$\varphi_w(z) = A\cos(k_1 z) + B\sin(k_1 z) \quad , \tag{2.2}$$

where $k_1^2 = \dfrac{2m_w^* E}{\hbar^2}$

The Schrödinger's equation in the barrier region is:

$$\left(-\frac{\hbar^2}{2m_b^*}\frac{d^2}{dz^2} + V_0\right)\varphi_b(z) = E\varphi_b(z) \quad , \tag{2.3}$$

where m_b^* and $\varphi_b(z)$ are the electron effective mass and the wave function of electron in the barrier along the z direction, respectively. So, the wave functions of electron in the barrier are:

$$\varphi_b(z) = C \exp(-k_2 z) \quad , \quad z \geq \frac{L}{2} \quad , \tag{2.4}$$

$$\varphi_b(z) = D \exp(k_2 z) \quad , \quad z \leq -\frac{L}{2} \quad , \tag{2.5}$$

where $k_2^2 = \dfrac{2m_b^*(V_0 - E)}{\hbar^2}$.

The boundary conditions are:

1)
$$\varphi_w\left(\pm\frac{L}{2}\right) = \varphi_b\left(\pm\frac{L}{2}\right) \tag{2.6}$$

2)
$$\frac{1}{m_w^*}\frac{\partial\varphi_w(z)}{\partial z}\bigg|_{z=\pm\frac{L}{2}} = \frac{1}{m_b^*}\frac{\partial\varphi_b(z)}{\partial z}\bigg|_{z=\pm\frac{L}{2}} \tag{2.7}$$

The symmetric solution ($B = 0$) can be calculated from the equation:

$$\tan\left(k_1\frac{L}{2}\right) = \frac{m_w^*}{m_b^*}\frac{k_2}{k_1} \tag{2.8}$$

For asymmetric solution ($A = 0$):

$$\tan\left(k_1\frac{L}{2}\right) = -\frac{m_b^*}{m_w^*}\frac{k_1}{k_2} \tag{2.9}$$

Notice that the number of energy states lying within the well decreases as L becomes smaller. For $L < 30$ Å only one energy state exist which is the ground state. In order to obtain the ground state solution, the symmetric solution is selected. Eq. (2.8) can be written as:

$$\tan(x) = \sqrt{\frac{m_w^*}{m_b^*}}\frac{\sqrt{\xi - x^2}}{x} \quad , \tag{2.10}$$

where $x = \dfrac{k_1 L}{2}$ and $\xi = \dfrac{m_w^* L^2 V_0}{2\hbar^2}$.

Eq. (2.10) can be solved numerically or graphically for the value of *x* and then the lowest quantized state can be obtained.

2.1.3 Advantages of the Lattice-matched Quantum Wells

There are several advantages for the fabrication of the quantum well structures.

First, the density of states property for the quantum well is superior over that of the bulk. The density of states for a parabolic two-dimensional system is given by

$$\rho_{2D} = \frac{m^*}{\pi\hbar^2} \quad , \tag{2.11}$$

where *m** is the electron effective mass. This density of states is constant for all energies above the energy threshold. Because the quantum well has the subband more than one, it yields a staircase density of states profile, as shown in Fig. 2.4 for a square quantum well. For the comparison, the density of states for the bulk layer is also shown in the dashed line which follows:

$$\rho_{3D}(E) = \frac{(2m^{*3})^{\frac{1}{2}} E^{\frac{1}{2}}}{\pi^2 \hbar^3} \tag{2.12}$$

From the comparison, it is seen that the absorption edge for the case of quantum well
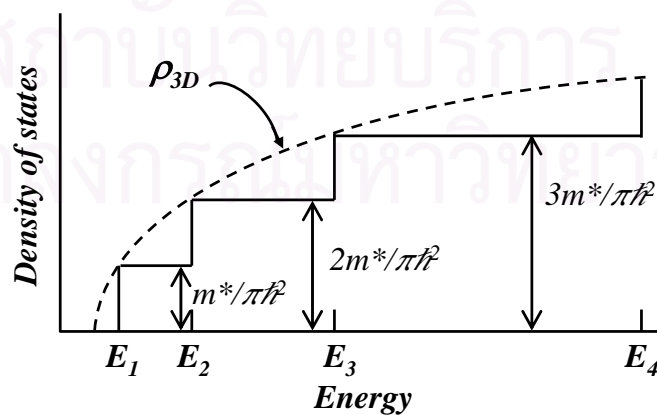
Figure 2.4: Staircase density of states for a 2D quantum well. The dashed line is the 3D case.

has the density of states higher than that of the bulk. This indicates that for the lowest threshold, the quantum well provides the number of carriers larger than that for the bulk. In addition, for the same number of carriers, the quantum well yields the smaller energy fluctuation, which is advantage for the laser applications.

Secondly, the quantum well structure improves the capture efficiency. The electrons are down into the potential well in the conduction band and the same situation occurs with the holes in the valence band. This condition enhances the electron and hole wave functions overlapping which leads to the increasing of recombination efficiency. Moreover, the effects of surface states are reduced because the electron and hole are trapped by the potential wells. From above reasons, the quantum well structure yields the increasing of the emission efficiency. This is advantage for both light emitting diode (LED) and laser diode (LD) applications.

The benefits of the lattice-matched condition are next described. The lattice-mismatch between the layers in the sample induces the misfit dislocations which are believed to cause the non-radiative recombination. The non-radiative recombination is the recombination between the electron and hole with no emission of light or photon. It is not required for the optoelectronic devices. Moreover, in the quantum well structure, the lattice-mismatch induces the strain in the samples. This strain distorts the potential well as drawn in the Fig. 2.5. The distorted potential well reduces the overlap of electron and hole wave functions. This reduces the probability of recombination between electron and hole, leading to the lower emission intensity.
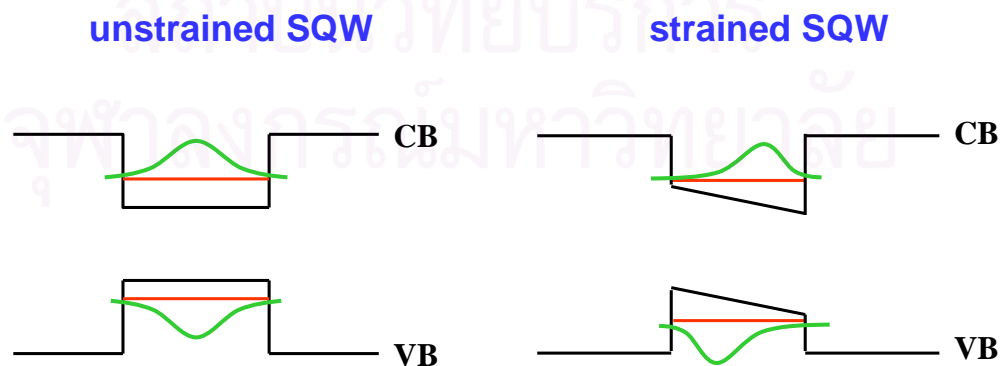
Figure 2.5: The wave functions of electron and hole in SQW for both of unstrained and strained cases.

2.2 Characterization Methods

2.2.1 High-resolution X-ray Diffraction

High-resolution X-ray diffraction (HRXRD) is a versatile ex-situ investigation of the epitaxial layer and structure. The measurement is done by projecting the X-ray beam onto the sample. This X-ray beam is diffracted by the atomic planes in the sample. The d-spacing between the atomic planes cause the path difference of the diffracted X-ray beam, and then result in the diffraction patterns (see Fig. 2.6). The obtained diffraction patterns concern the composition, the uniformity of each layer, their thickness, the built-in strain and strain relaxation, and the crystalline perfection related to their dislocation density.

The measurement was done using the Bruker-AXS D8 DISCOVER at the Scientific and technological research equipment centre, Chulalongkorn University. The $K_{\alpha 1}$ radiation from the anode at a wavelength of 1.54056 Å was selected for the experiment. The monochromator consists of two components, a graded parabolic mirror and a (022) channel-cut Germanium crystal. The graded parabolic mirror eliminates the K_{β} radiation and the Ge crystal removes the $K_{\alpha 2}$ component from the beam. The sample is placed on an Euler cradle. The Euler cradle permits an
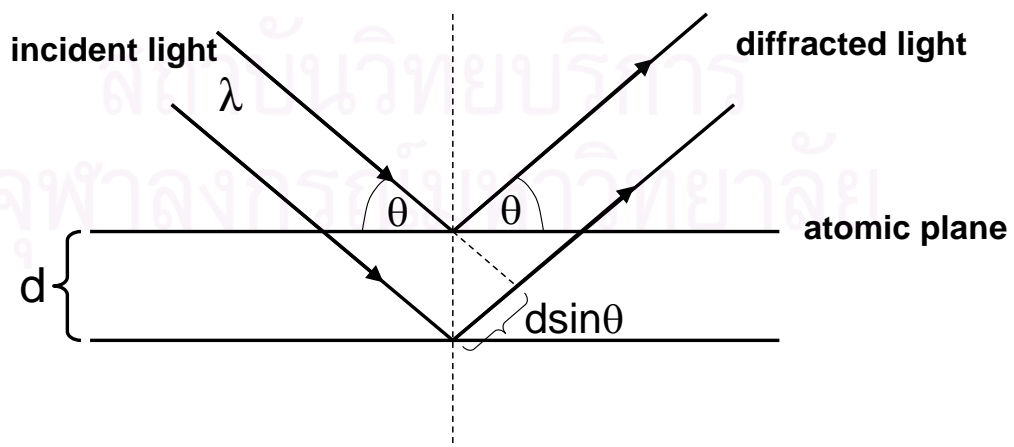
Figure 2.6: X-ray scattering geometry. **d**: d-spacing of atomic plane, θ: Bragg angle.

independent variation of the incident angle (ω), the angle around the surface normal and the angle around an in-plane horizontal direction. Moreover, for the high resolution, the measurement was performed with a secondary Ge (220) crystal monochromator in front of the detector. The setup is shown in Fig. 2.7.

There are several scan modes in the routine HRXRD measurements, i.e. "ω–scan", "2θ–scan" and "2θ/ω–scan". For the "ω–scan" mode, it can do by varying the angle of the incident X-ray beam. The information obtained is the orientation of the Bragg planes in the sample. The "2θ–scan" is achieved by varying the angle of the detector scanning, and the result shows the d-spacing fluctuation of the one Bragg plane that we intentionally observe. Finally, for the "2θ/ω–scan", which we adopt in our experiment, it is done by varying both the incident angle and the detector scanning angle. The diffraction pattern which obtained from this mode provides information about the lattice parameters and quality of the sample. For the bulk layer, we can gain the lattice parameters, i.e. lattice constants of all layers in the sample which relate directly to the peak position of each layer. The composition which relate to the peak position is also obtained. However, for the single quantum well structure, because of the well layer is very thin, the XRD peak of the well layer cannot be observed, and the composition cannot be directly obtained. So, the simulation software with a dynamical theory is used to determine the composition and the thickness of each layer.
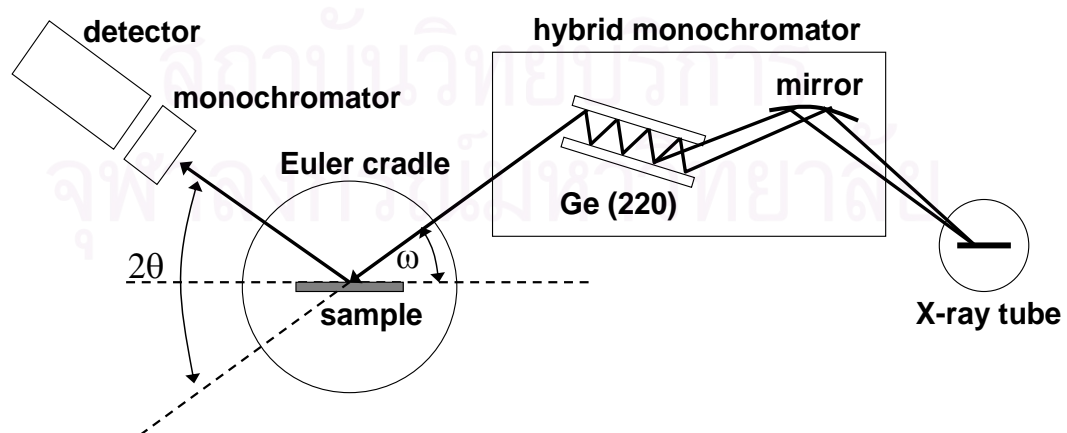
Figure 2.7: Schematic drawing of the HRXRD setup.

2.2.2 Photoluminescence

Photoluminescence (PL) spectroscopy is a routine, powerful, contactless and nondestructive method for probing the electronic structure of materials. The measurement is done by projecting monochromatic light or photon direct onto the sample. This photon is absorbed by the sample and then an electron-hole pair is created. The electron is excited to the permissible excited states which cause the electron unstable. So, the electron recombines down to the equilibrium state and simultaneously release the excess energy. This excess energy can be dissipated through the emission of light or photon, which called "luminescence". Because the source which excites the electron is light or photon, so this measurement method is called "photoluminescence".

In general case of quantum well, the bandgap energy of barrier material is larger than that of the well layer material. So, the energy of exciting photon should be larger than the bandgap energy of the barrier. When light is projected direct to the quantum well sample, the electron is first excited to the conduction band of the barrier. Then, it relaxes to the energy level of quantum states lining in the well. After that, in case of Type-I quantum well, it recombines to the valence band of the well layer. However, for Type-II quantum well, it instead recombines to the valence band of the barrier.

In this thesis, the raw data from PL results were obtained from Prof. Kentaro Onabe's laboratory, Department of Advanced Materials Science, the University of Tokyo. The PL setup is shown in Fig. 2.8. In this experiment, the He-Cd laser with 325 nm (3.815 eV) line of continuous-wave at the power density of 1.0 W/cm^2 was used as the light source. The laser is focused by the focusing lens onto the mirrors before reflecting onto the sample fixed in a cryostat. The cryostat is used for cooling the sample. The luminescent light from the sample is collected by the collecting lens. Then, it is dispersed to the monochromator for distinguishing photon energy before count by the detector. The lock-in amplifier and chopper are applied to increase the signal-noise ratio.
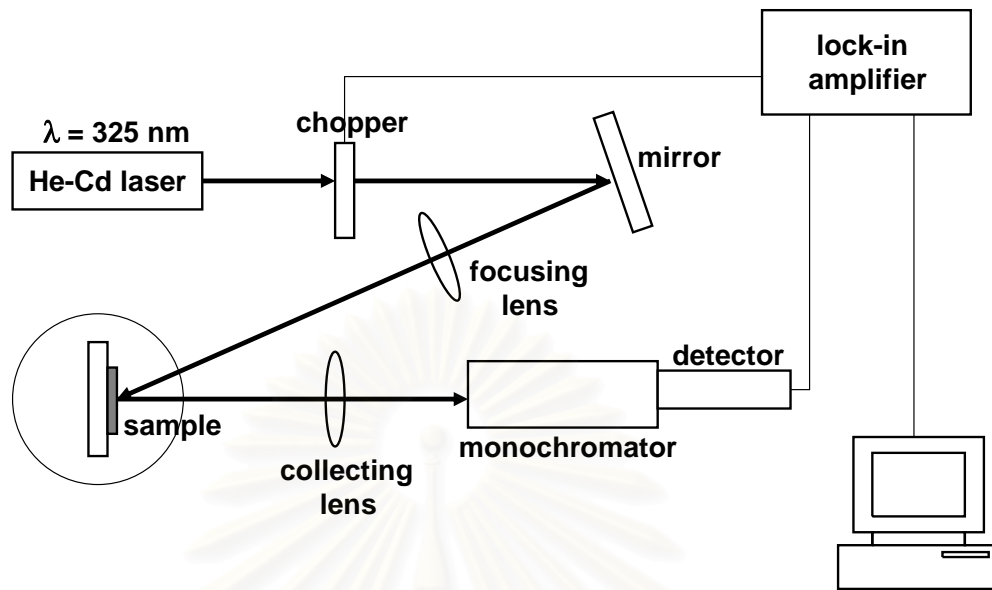
Figure 2.8: Schematic drawing of photoluminescence setup.

2.2.3 Temperature Dependent Photoluminescence

Thanks to the technology of cryostat sample holder, the temperature of the sample can be adjusted in the range of 4 – 300 K. The increasing temperature causes the thermal energy of carriers in the sample to increase. So, the carriers are excited up to higher permissible excited states. The results from the temperature dependent PL show the evolution of PL features with the temperature. Moreover, a fitting of the graph which is plot between an integrated PL intensity and temperature provides the parameters which relate to the localized energy or the activation energy.

2.2.4 Photoluminescence-excitation

Photoluminescence-excitation (PLE) spectroscopy is essential an inverse of photoluminescence spectroscopy. In this technique, the detection system is set to detect emission of the particular photon energy which inside the photoemission band of the sample. The exciting light shined onto the sample is tuned. In this thesis, the raw PLE results were also obtained from Prof. Kentaro Onabe's laboratory,

Department of Advanced Materials Science, the University of Tokyo. The PLE system is shown in Fig. 2.9. The 500 W Xe-lamp is used as the exciting light source. This halide lamp emits the light with the wide range of frequency. Thus, it is dispersed by the monochromator A to be a monochromatic light. So, we can tune the exciting light by changing the slit in the monochromator A. If the energy of the exciting light coincides with a permissible excited state in the sample, this photon is absorbed and then the electron-hole pair is created. The electron is excited to that state. Next, the electron relaxes down to the excited discrete states which lower in energy than that before recombination which is radiative or non-radiative. After the absorption and relaxation processes, the emitted light which identical to the setting photon energy of the monochromator B is then collected and passed to the detector for counting. Thus, the intensity of this emission is then recorded as a function of the excitation photon energy.

The result from PLE shows the mechanism of excitation and relaxation of carriers. It demonstrates the origin of the carrier which recombines at the setting energy state (interesting energy state). Moreover, the PLE spectrum is roughly
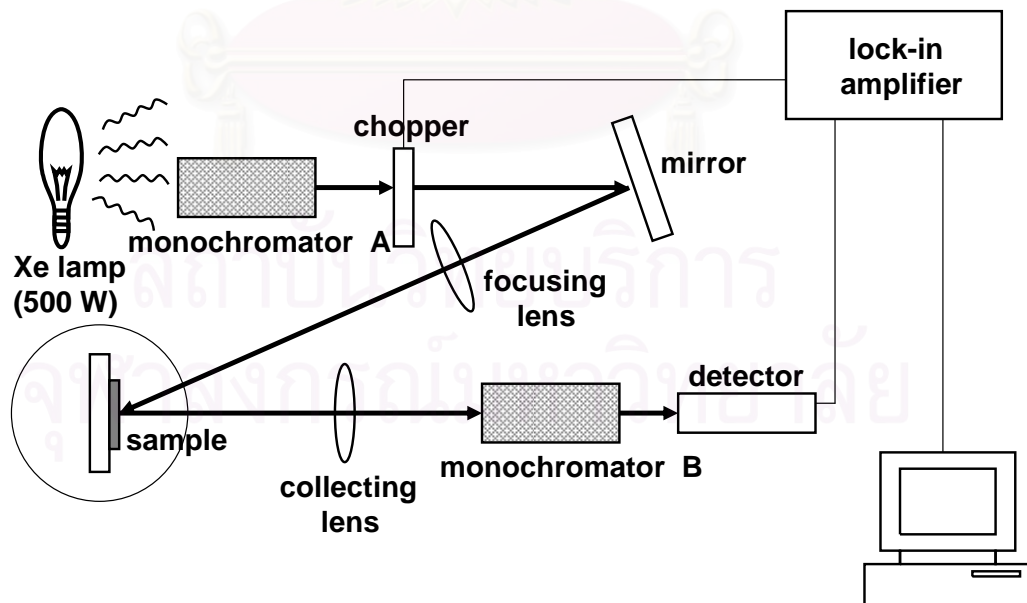
Figure 2.9: Schematic drawing of photoluminescence-excitation setup.

equivalent to the absorption spectrum of the sample. However, the intensities of the different features do not represent actual absorption strengths. Rather, they reflect the effect that such absorption has the recombination efficiency at the setting energy state. Thus, absorption in regions where recombination is very efficient could, in principle, produce considerable intensity of features in the PLE spectrum.

　　　PLE technique is popular for studying thin epilayers grown on opaque bulk substrates. It is not necessary to polish the substrate out, in contrast to the absorption spectroscopy which requires removing the substrate. PLE measurement can therefore be performed on the quantum well structure which typically thin sample and difficult to remove the substrate.

CHAPTER III

EFFECTS OF WELL-WIDTH VARIATION

In this chapter, structural and optical investigation results of InGaPN/GaP SQWs with different well-widths are described. The high-resolution X-ray diffraction (HRXRD) and optical microscopy are used to characterize alloy compositions, layer thickness, interface properties and surface morphology, respectively. For the optical characterization, photoluminescence (PL) and photoluminescence-excitation (PLE) techniques are employed.

3.1 Sample Description

All the $In_xGa_{1-x}P_{1-y}N_y$/GaP SQWs and the $In_xGa_{1-x}P_{1-y}N_y$ bulk layers used in this study were grown on GaP (001) substrates by metalorganic vapor phase epitaxy (MOVPE) at Prof. Kentaro Onabe's laboratory, the University of Tokyo by Dr. Nobuhiro Nakadan and Dr. Tokuharu Kimura. The precursors for Ga, In, P and N are trimethyl-gallium (TMGa), trimethyl-indium (TMIn), PH_3 and 1,1-dimethyl-hydrazine (DMHy), respectively. The carrier gas is H_2. After the growth of the around 0.3 µm-thick GaP buffer layer at 710°C, a thin $In_xGa_{1-x}P_{1-y}N_y$ well layer and a GaP cap layer were respectively grown at 635°C. The compositions of $In_xGa_{1-x}P_{1-y}N_y$ well layer for all of samples were controlled in the same compositions which were nominally lattice-matched to GaP. The well-widths of $In_xGa_{1-x}P_{1-y}N_y$ were varied by the growth time of $In_xGa_{1-x}P_{1-y}N_y$ layer (2 - 8 seconds). The $In_xGa_{1-x}P_{1-y}N_y$ bulk layers without the GaP cap layer were also prepared for a comparative study. The growth
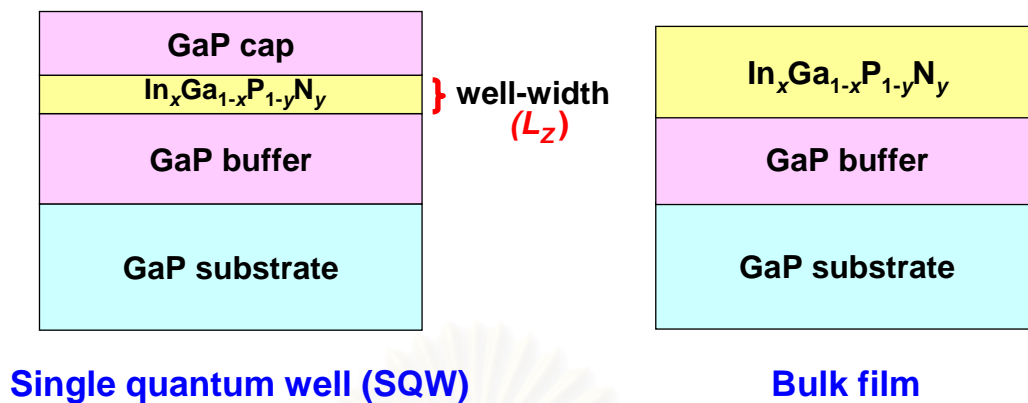
Figure 3.1: Schematic illustration of the InGaPN/GaP SQW and InGaPN bulk layer.

parameters such as V/III ratio, DMHy flow rate, were based on the growth of the $In_xGa_{1-x}P_{1-y}N_y$ bulk layers [15, 16].

3.2   Structural Investigation

3.2.1   HRXRD and Simulation Results

All the samples were investigated by HRXRD in order to determine the well-width and alloy composition and check the structural quality. As in Fig. 3.2, shows (004) 2θ/ω-scan HRXRD patterns of four InGaPN/GaP SQWs with different well-widths. The InGaPN well layers were grown at the same growth rate and flow rate of precursors but the growth time were different (2, 3, 4 and 8 seconds). These different growth time lead to the different well thickness. All the samples show a similar shape of diffraction patterns. The main sharp peaks at the angle of 68.8° correspond to the reflection from the (004) GaP. In addition, the additional diffracted peaks at lower angles, the broad satellite fringes and the frequent Pendellösung fringes are clearly observed.

For the bulk layer, the composition can be obtained directly from the angle position of the diffracted peak. In the case of SQWs, the well layer is very thin, not larger than 10 nm. So, the diffracted peak of the well layer cannot be clearly observed.
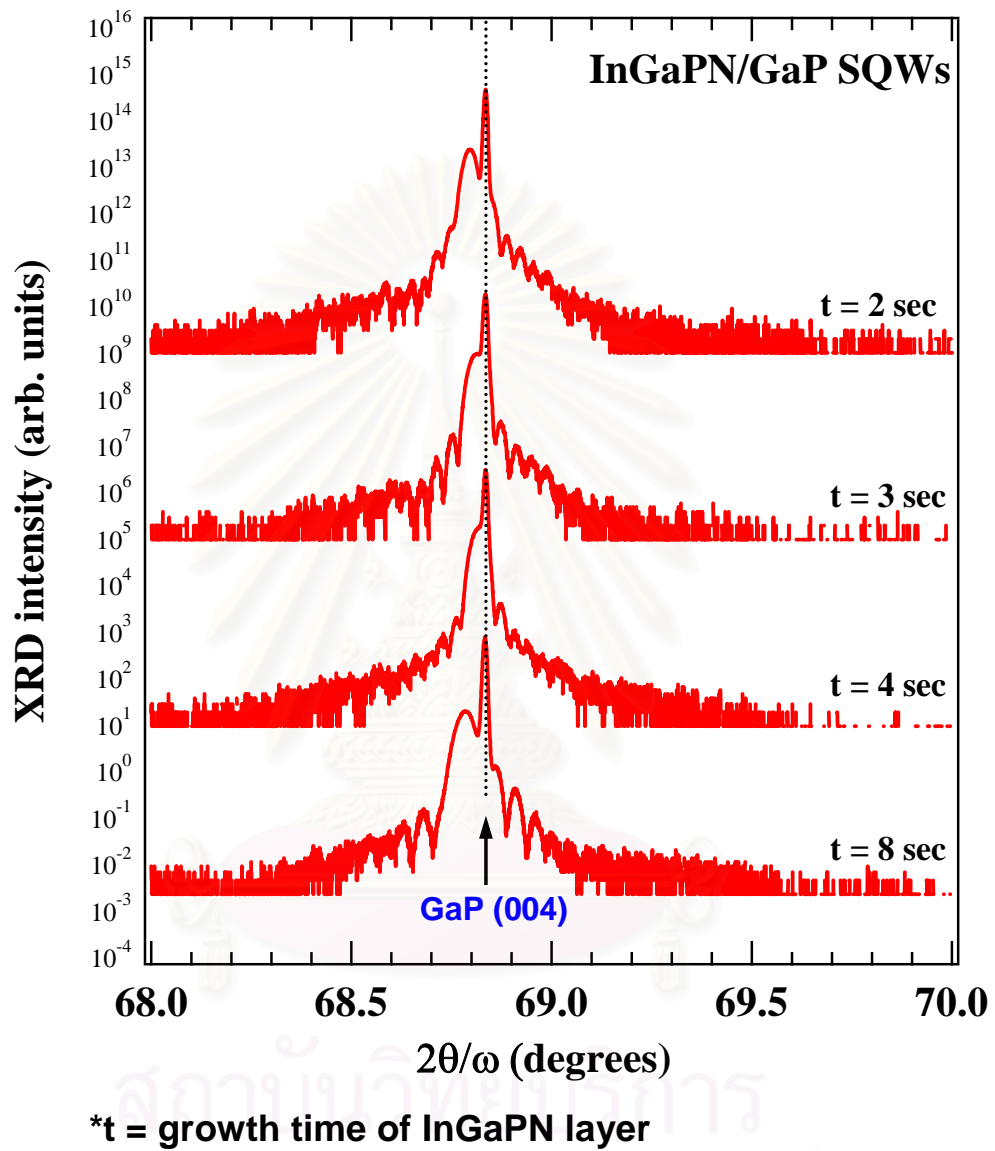
Figure 3.2: HRXRD patterns of InGaPN/GaP SQWs with the growth time of InGaPN layer were different.

The existence of this layer is shown through the interference fringe which called "satellite fringes". In order to determine the composition and the thickness of each layer in the SQWs, the dynamical theory [17] simulation software is employed. The initial parameters that need in the simulation software are the composition and the thickness of each layer, and the strain of whole sample.

In this experiment, the initial composition and the thickness of well layer were estimated from the bulk growth condition. The strain was approximated to be zero due to lattice-matching condition. The simulation results from the software are depicted in Fig. 3.3, along with the experimental patterns, which show a very match to the experimental results. From the simulation, the In and N concentrations in the $In_xGa_{1-x}P_{1-y}N_y$ well layer are almost the same for all the SQWs. The In and N concentration were examined to be at $x = 0.050$ and $y = 0.025$, respectively. But the well thickness or well-width are different as labeled in Fig. 3.3. Moreover, the additional diffracted peak at the lower angle is corresponding to (004) InGaP. The existence of InGaP is due to the diffusion of a small amount of In (~ 0.5%), which has been existed in the growth system, into the GaP buffer layer during the growth. In addition, the clearly observed interference fringes from the experimental results indicate that the excellent crystal quality and fairly flat interface have been grown. Furthermore, the extremely matching between the GaP diffracted peak and the zero order of satellite fringes, as shown by dashed line in Fig. 3.3, indicate the lattice-matching between InGaPN well layer and GaP barriers. These demonstrate that the lattice-matched InGaPN/GaP SQWs were successfully achieved.

3.2.2 Surface Images from the Optical Microscopy

In order to indicate the lattice-matching condition, surface morphologies were investigated for the other evidence. Figure 3.4 illustrates the surfaces of SQWs (Fig. (a) – (d)) which are the same series shown in last section together with the film surface of GaP substrate (Fig. 3.4 (e)). All the samples show the smooth surface without appearing of cross-hatch patterns, which is usually observed in the highly lattice-mismatched films. For the comparison, the surface morphology of highly lattice-mismatched $GaP_{1-x}N_x$ ($x = 0.023$)/GaP with cross-hatch patterns [18] is shown
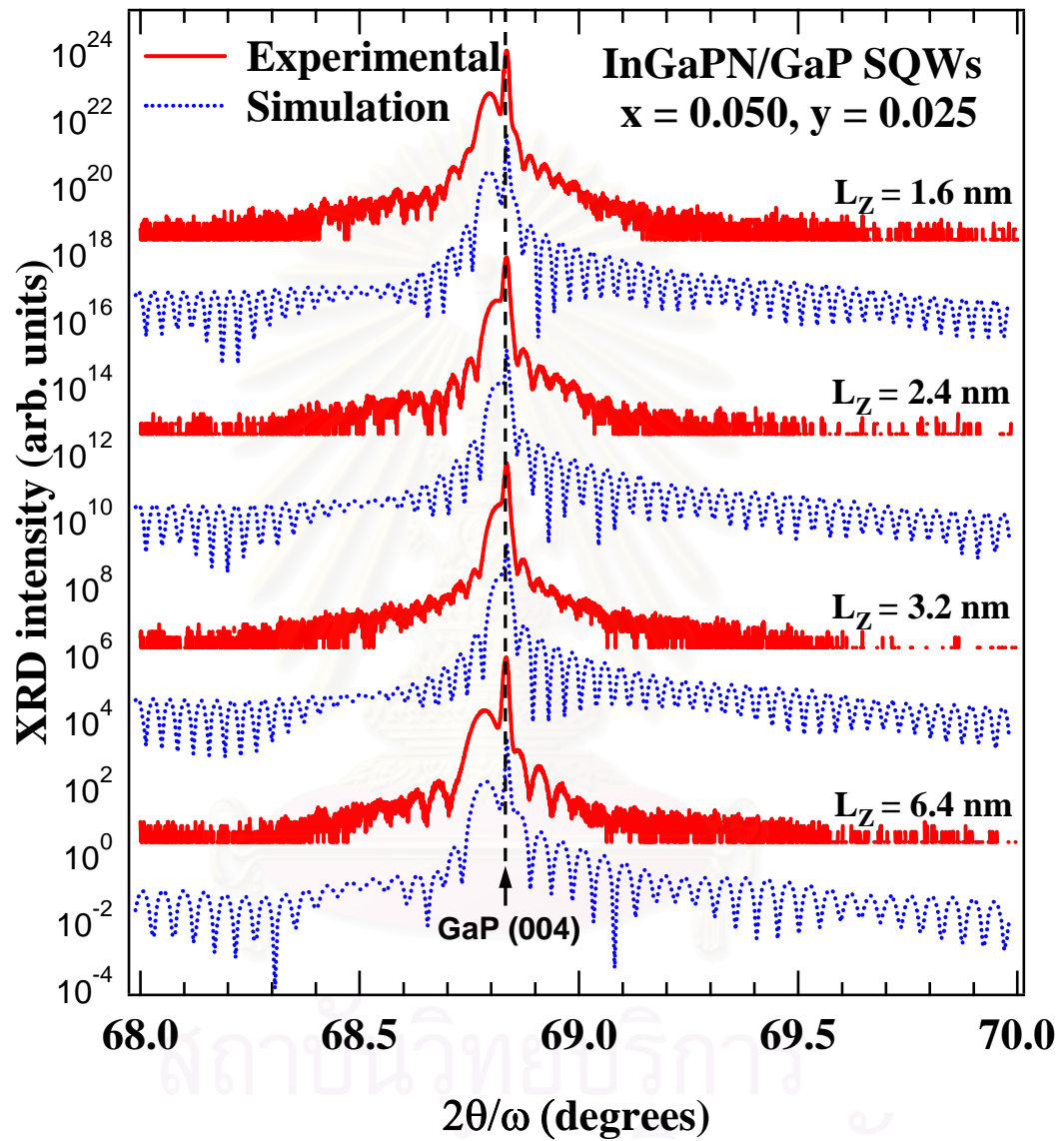
Figure 3.3: HRXRD patterns of InGaPN/GaP SQWs with different well-widths (L_Z = 1.6 -6.4 nm) and the simulations.
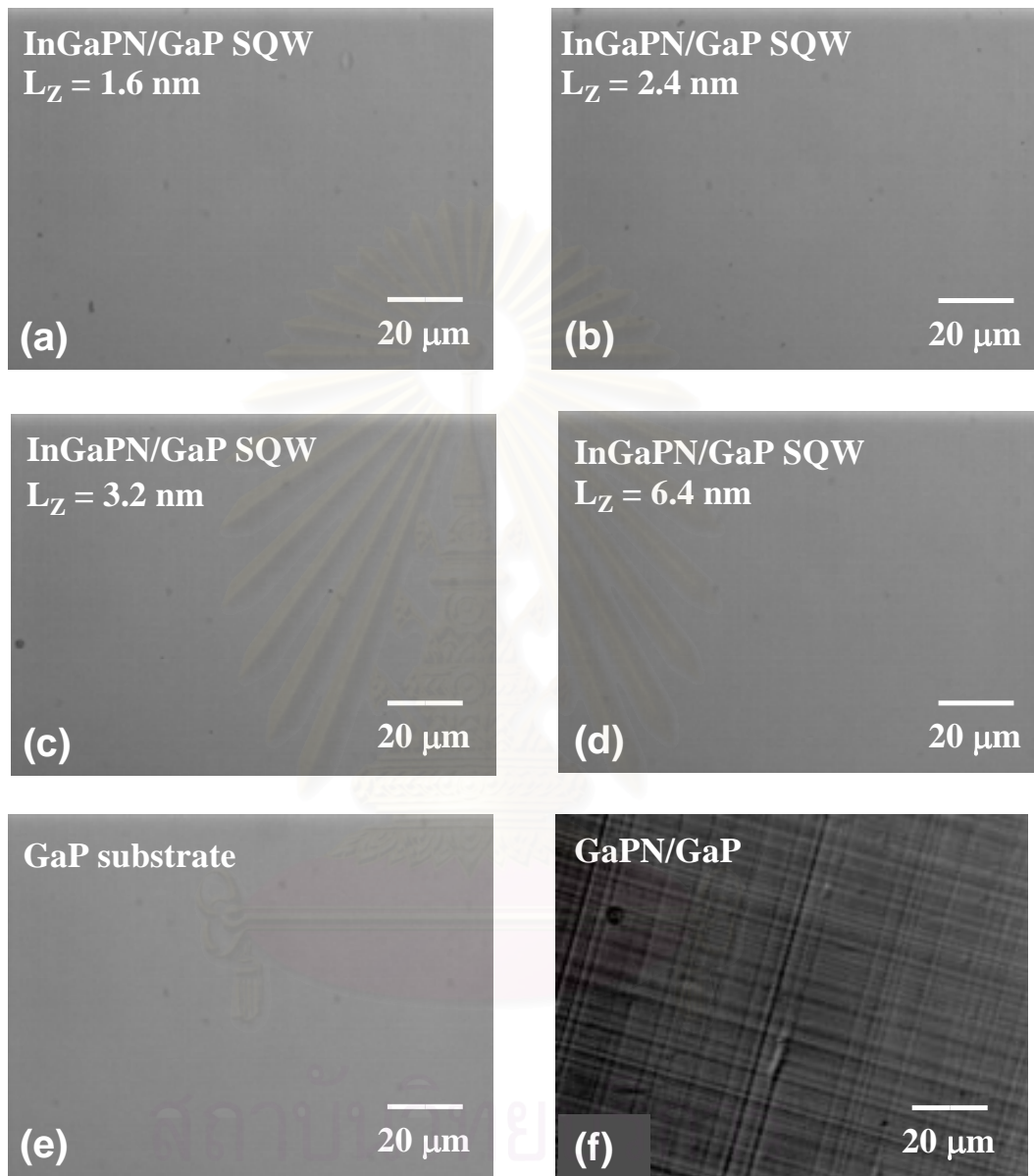
Figure 3.4: Surface images from the optical microscopy: (a) InGaPN/GaP SQW with L_Z = 1.6 nm, (b) InGaPN/GaP SQW with L_Z = 2.4 nm, (c) InGaPN/GaP SQW with L_Z = 3.2 nm, (d) InGaPN/GaP SQW with L_Z = 6.4 nm, (e) GaP substrate, (f) GaPN/GaP bulk layer from Ref. [18].

in Fig. 3.4 (f). It is well known that the cross-hatch pattern is originated from the generation of misfit dislocations at the interfaces, which is due to lattice-mismatch between the layers in the film. This observation indicates that the samples have excellent quality without generation of misfit dislocation at the interface. Such cross-hatches do not appear at all on the surface when the lattice-mismatch is less than 0.3% [18] which is very much small. So, this series of samples are in the lattice-matching condition. The lattice-matched InGaPN/GaP SQWs were confirmed.

3.3   Optical Investigation

3.3.1   Low-temperature Photoluminescence

Figure 3.5 shows the low-temperature (LT, 10 K) PL spectra of $In_{0.050}Ga_{0.950}P_{0.975}N_{0.025}$/GaP lattice-matched SQWs with well-widths of $L_Z = 1.6$, 2.4, 3.2 and 6.4 nm, as well as the $In_{0.050}Ga_{0.950}P_{0.975}N_{0.025}$ bulk layer. All samples show an evidence of the strong light emission in the visible ($\lambda = 560 - 680$ nm) region as shown by the light spectrum above the figure. Compare to the bulk film, the PL peak position of SQWs exhibit a blue-shift of about 38 meV (measure from the top peak) for the narrowest SQW ($L_Z = 1.6$ nm). This blue-shift is much consistent with the quantum confinement by the well. Moreover, it is found that an extra peak appears at higher-energy side of the main peak when the well-width is about $L_Z = 3.2$ nm or narrower. Nevertheless, this feature grows up and shifts toward the higher energies with a decreasing of well-width. Since, for the N concentration close to $y = 0.02$, the average distance between the N atoms is about 1.3 nm [19], which is comparable to the width of the narrowest well of $L_Z = 1.6$ nm. Additionally, thanks to this InGaPN lattice-match to GaP, so they have the lattice constant equal to GaP which is 5.45 Å. The SQW with the narrowest well ($L_Z = 1.6$ nm) is approximated around 2-3 monolayers. So, the N atom might be vanished at some locations. Thus, the N concentration in the $In_{0.050}Ga_{0.950}P_{0.975}N_{0.025}$ well near the interfaces with the GaP barrier is expected as somewhat lower than the inner zone which is $y = 0.025$. As a result, the splitting of this PL sub-peak might be caused by the recombination of

Figure 3.5: Low-temperature (10 K) PL spectra for InGaPN/GaP SQWs ($x = 0.050$, $y = 0.025$) with different well-widths $L_Z = 1.6 - 6.4$ nm as well as the bulk layer. The arrows indicate the extra peak that appears at the higher energy. The light spectrum above the figure shows the emission region of the samples.

excitons due to the lattice fluctuation or well-width fluctuation, as shown in Fig. 3.6 which are induced by random distribution of the N atoms within the well.

As clearly seen from the 10 K PL spectra in Fig. 3.5, the PL spectrum contains several sub-peaks. The number of sub-peaks and the peak positions were preliminary obtained by derivative method. The solid line in Fig. 3.7 is the 10 K PL spectrum of the $In_{0.050}Ga_{0.950}P_{0.975}N_{0.025}$/GaP lattice-matched SQW with L_Z = 1.6 nm which exhibits three distinct spectral features, denoted by arrows. The dotted line is the numerical derivative (with respect to photon energy) of the PL data. The sub-peak positions of the three features were accurately obtained from the zero-crossing (A and B) and an inflection point (C). For in-depth analysis, a quantitative fit to the PL spectra, by assuming a Gaussian distribution of the density of state, has been utilized to accurately evaluate their own energy peak positions. Figure 3.8 (a) and (b) show the fitting results of the bulk film and the example of SQW with well-width of 1.6 nm, respectively. For the bulk film, the fitting result shows the three sub-peaks, which are X, Y and Z. For the SQW shown in Fig.3.8 (b), the four features of sub-peaks denoted as A, B, C and D are visible. The sub-peak Z in the case of bulk film and the sub-peak D in the case of SQW were added in order to fulfill the PL spectrum in the low energy region. The sub-peak Z in the case of bulk film is determined by the
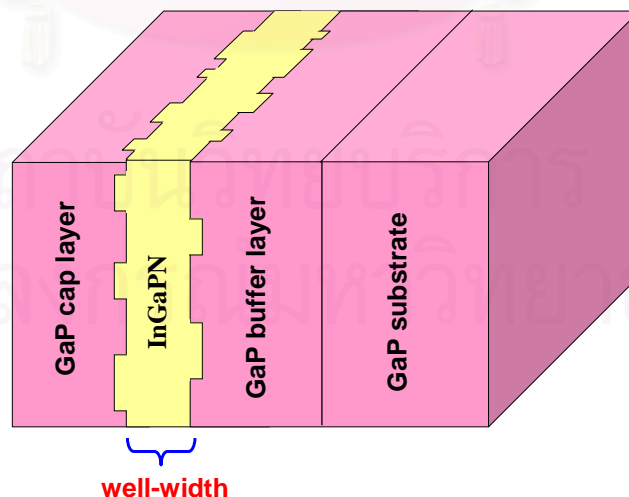
Figure 3.6: Schematic drawing of lattice fluctuation or well-width fluctuation in the InGaPN/GaP SQW.
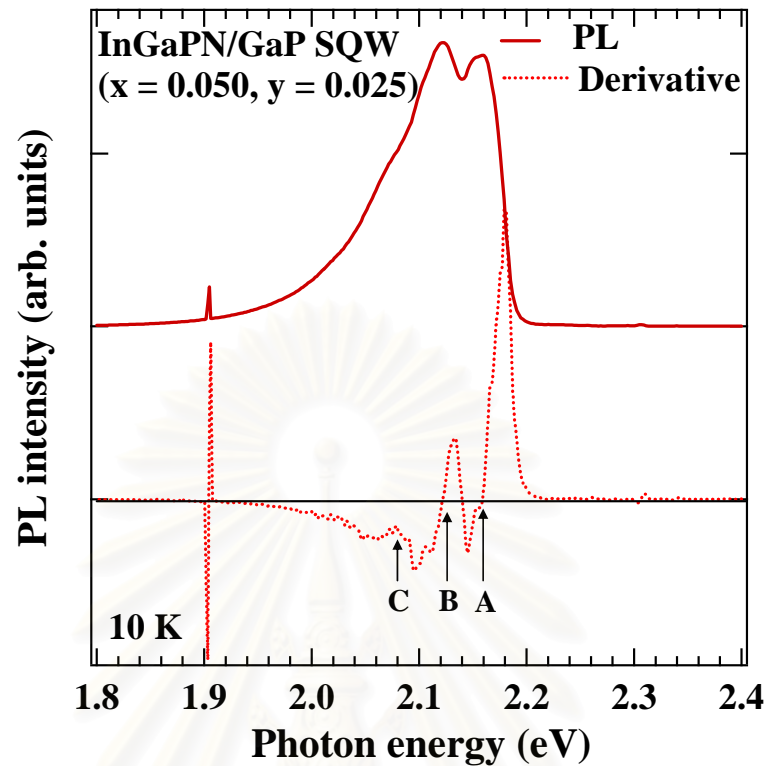
Figure 3.7: 10 K PL spectrum of the $In_{0.050}Ga_{0.950}P_{0.975}N_{0.025}$/GaP lattice matched SQW with well-width of 1.6 nm. The dotted line is the numerical derivative of the PL data (solid line). The energies (A, B and C) denoted by arrows.

band-tail of an electronic structure, which is typically observed in other dilute nitride semiconductors [18, 19]. For an ideal crystal with no impurity perturbation, the conduction band edge should be sharp. However, for the real situation, the crystal is adulterated by impurities [20]. These impurities exert the force on the conduction band and valence band. Since impurities are distributed randomly in the host crystal, this leads the conduction band and valence band are rough bands, as shown in Fig. 3.9. Since the N has high electronegativity (3.0) and N levels close to the conduction band, so the very distinct long band-tail in this InGaPN and other dilute nitride alloys might due to the strong interaction between N and the conduction band. These rough bands might lead to the rising of sub-peak D in the case of quantum well sample.

Evolution of PL sub-peaks of SQWs related to well-width is shown in Fig. 3.10. The progression in the blue-shift of all the PL sub-peaks denoted as A, B, C and D confirms the quantum confinement of the well.
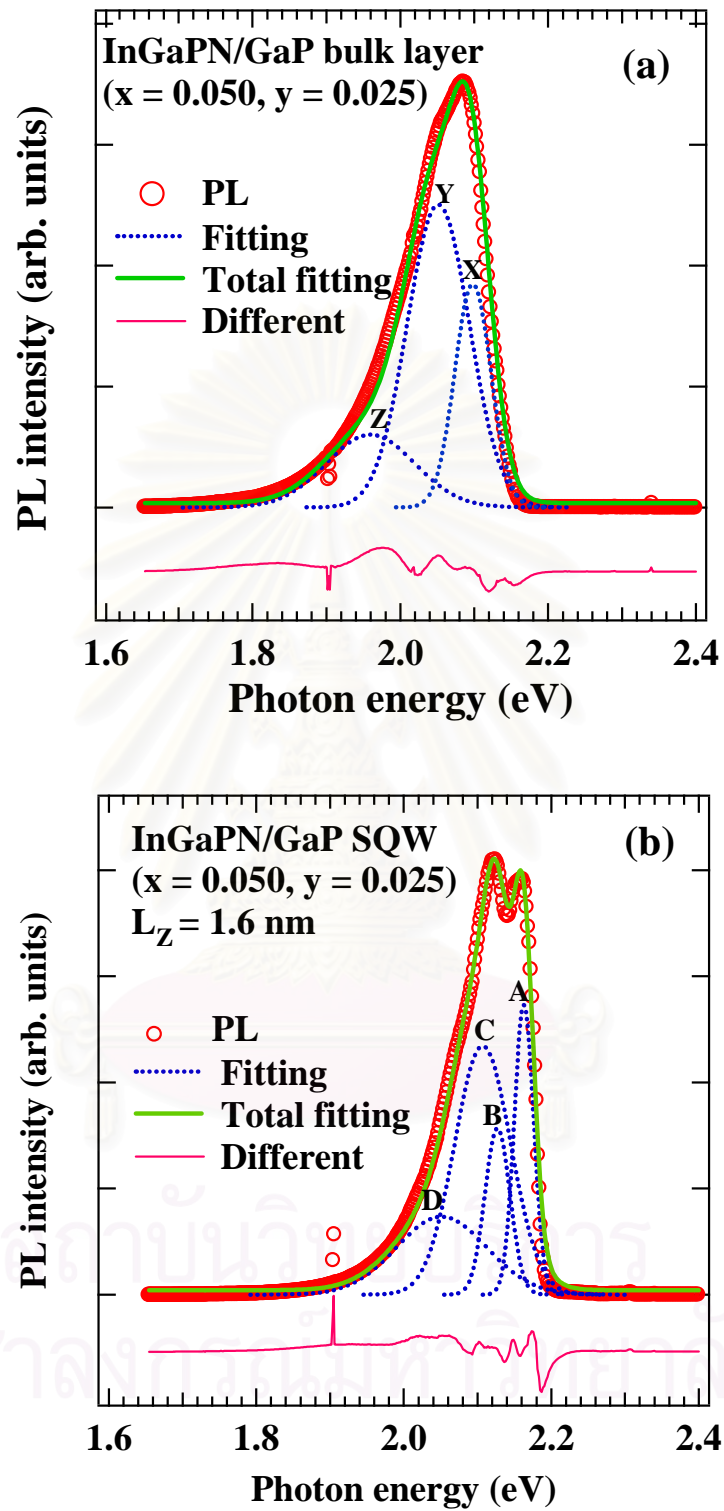
Figure 3.8: (a) 10 K PL spectra for InGaPN/GaP bulk layer (x = 0.050, y = 0.025), as well as the fitting (b) 10 K PL spectra for InGaPN/GaP SQWs (x = 0.050, y = 0.025) with well-widths L_Z = 1.6 nm, as well as the fitting.
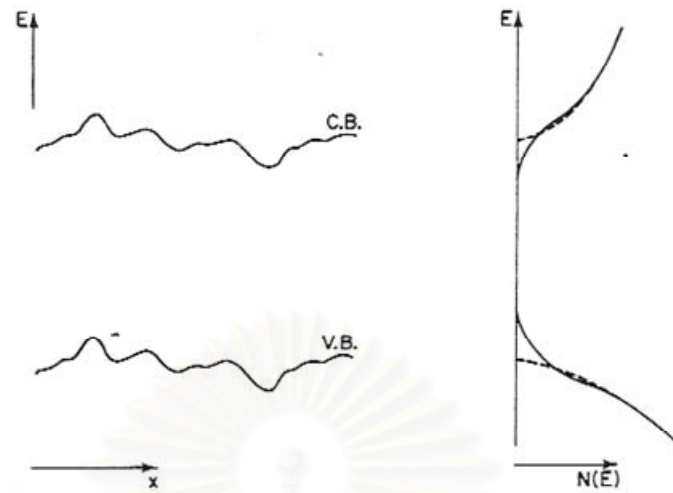
Figure 3.9: (left) the perturbation of the band edge by the inhomogeneous impurities. (right) The formation of tails of states, the dashed lines show the distribution of states in the unperturbed case [20]. N(E) is the density of state.
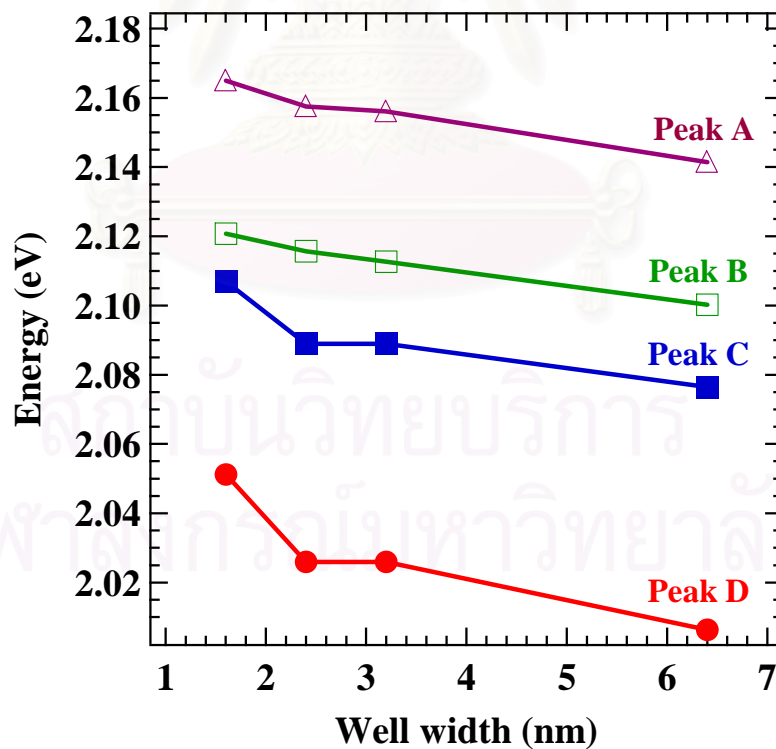
Figure 3.10: Dependence of the PL peak position and the well width for the InGaPN/GaP SQWs ($x = 0.050$, $y = 0.025$) with various well-widths.

3.3.2 Photoluminescence-excitation

Figure 3.11 illustrates the 10 K photoluminescence-excitation (PLE) spectra monitored at 1.89 eV for the $In_{0.050}Ga_{0.950}P_{0.975}N_{0.025}$/GaP SQWs with different well-widths ($L_Z = 1.6 - 6.4$ nm) together with the $In_{0.050}Ga_{0.950}P_{0.975}N_{0.025}$ bulk layer. In the bulk layer, a broad absorption band at about 2.08 - 2.40 eV and a step absorption edge at 2.86 eV are clearly distinguished. It should be noted that these features are similar to those in the $GaP_{1-x-y}As_xN_y$ ($y = 0.02$) [19] and $GaP_{1-y}N_y$ ($y = 0.014$) [21, 22, 23] bulk layers. From the comparison results, there are four notice points in Fig. 3.11, three for no well-width variation and one with well-width variation. The three dotted lines indicated the features that no variation of the energy position with the well-widths. First, the step sharp peak at the energy of 2.87 eV (A) is attributed to the absorption by the direct bandgap of GaP, which is the barrier of SQWs. Second, the sharp peak at 2.31 eV (B) is the A-line or NN_∞ which is the localized state generated by an isolated N atom. Third, the absorption at 2.18 eV (C) is corresponded to the NN_1 state, which is the localized state created by the close nearest neighbor N atom pair.

In the case of incorporating with N, the N atom locates among the Ga atoms. Because N has the electronegativity much higher than P, these N atoms can attract the carriers or exciton to localize around them. In addition, the atomic size of N atom is much smaller than P, leading to the lower potential at this N atom position. Hence, the carriers or exciton are trapped at this position.

In addition, the feature with the well-width variation is the absorption edges indicated by the arrows. Comparing to the bulk film, the PLE spectra have shown the blue-shift of the fundamental absorption edge to 2.17 eV for $L_Z = 1.6$ nm from 2.08 eV for the bulk. The amount of the blue-shift is increased with the decreasing of the well-width. This confirms the quantum confinement by the well. Moreover, from the above results, it could be interpreted that the three features indicated by the dotted line are the absorption of the GaP barriers because they do not change with the well-width variation. In contrast, the absorption edge is the absorption from the InGaPN layer because it exhibits the blue-shift with decreasing the well-width. In SQWs, the

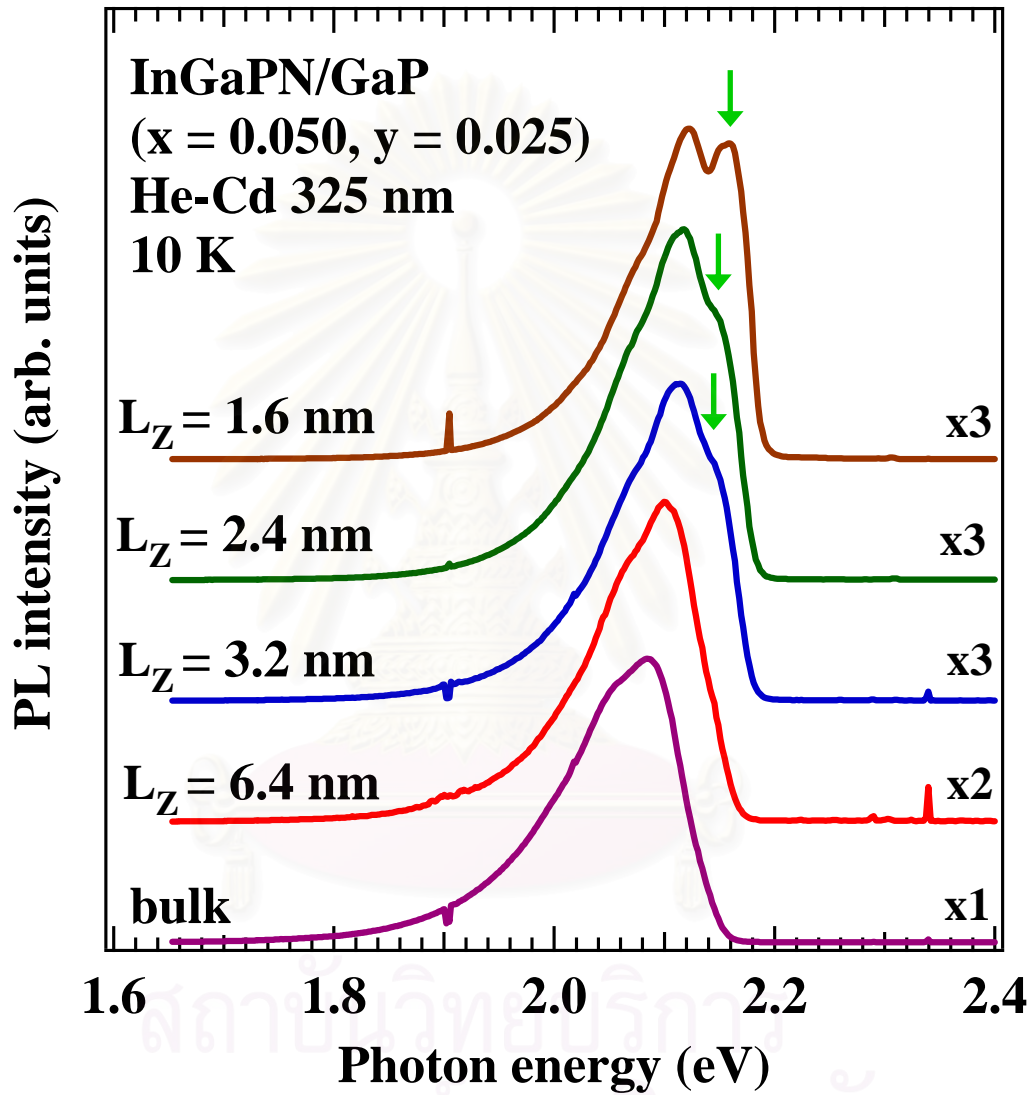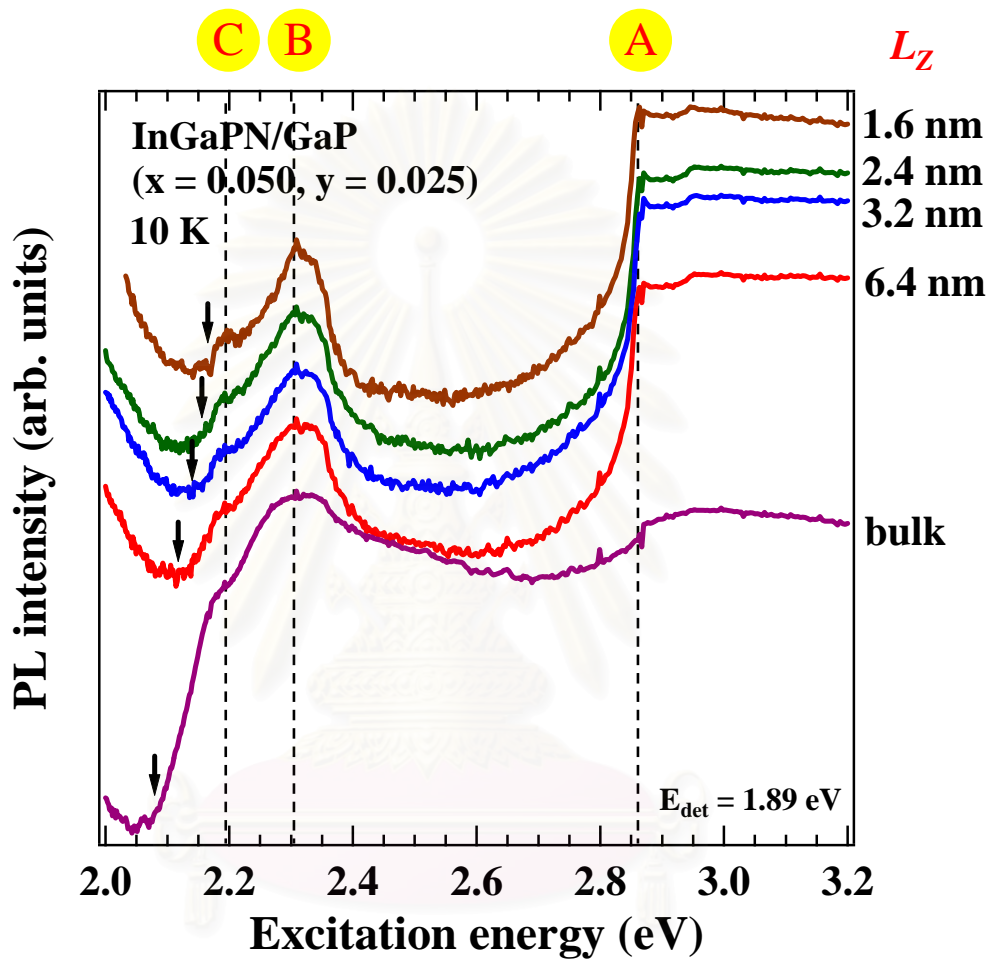**Figure 3.11:** 10 K PLE spectra for InGaPN/GaP SQWs (x = 0.050, y = 0.025) with different well-widths (L_Z = 1.6 – 6.4 nm) as well as the bulk layer. The arrows indicate the absorption edge and the dotted lines indicate the features that no well-width variation.

absorption from the barriers has higher intensity. This indicates that the carriers generate mainly in GaP barriers and then transfer to the InGaPN well layer.

3.4   Temperature Dependent PL

In order to investigate the evolution of the optical transition in the SQWs with the temperature, the temperature dependent PL was done. Figure 3.12 shows the PL spectra for the $In_{0.050}Ga_{0.950}P_{0.975}N_{0.025}$/GaP SQW with $L_Z = 2.4$ nm as dependent on temperature. At the temperature of 5 K, the PL spectrum consists of four PL sub-peaks as describe in previous section. With increasing of temperature, the intensity of sub-peak A gradually decreases with compare to other sub-peaks and be completely quenched at the temperature about 77 K. For the temperature higher than 77 K, the intensity of the sub-peak B decreases and be completely quenched at the temperature around 143 K. On the other hand, only the sub-peaks C and D can be survived for the temperature higher than 143 K and can be observed until 200 K. The SQWs with other well-widths have the similar trend of temperature dependent PL results. According to the theory of the thermodynamic, the increasing of temperature raises the thermal energy of the carriers, as following,

$$E = k_B T \quad , \tag{3.1}$$

where E is the thermal energy of the carriers, k_B is Boltzmann's constant and T is the temperature of the sample. After the carriers obtain this thermal energy, they are activated, and then can escape from the potential well. So, the energy that assists the carriers to "activate" (escape) from the potential well is called "activation energy". From the results, the sub-peaks A and B are quenched at the temperature about 77 K and 143 K. So, the activation energy for the sub-peaks A and B are approximated to be about 6.6 and 12.3 meV, respectively. The lower in activation energy of the sub-peak A than that of the sub-peak B indicate that the emission of sub-peak A is generated from the shallower potential well.

From the temperature dependent PL, we can see that the evolution of PL spectrum with the temperature can be separated into two trends. First, the PL
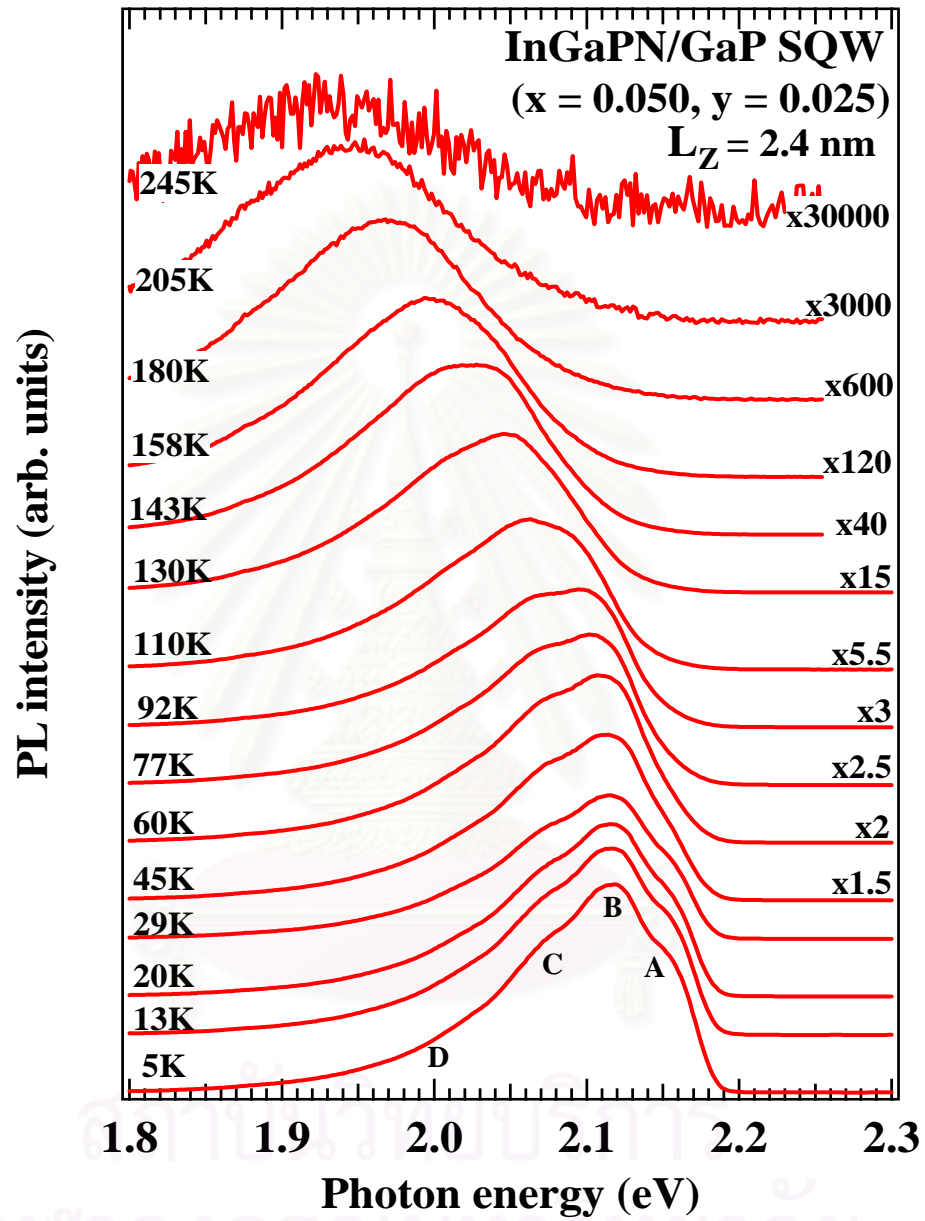
Figure 3.12: Temperature dependent PL of $In_{0.050}Ga_{0.950}P_{0.975}N_{0.025}$/GaP SQW with L_Z = 2.4 nm.

sub-peaks quenched in low temperature region, sub-peak A and B. Secondly, the PL sub-peaks that survive in high temperature region, sub-peak C and D. In addition, the relationship between the positions of PL sub-peaks and well-width, which is shown in Fig. 3.10, indicates that the blue-shift also could be divided into two trends (sub-peaks A and B, and another sub-peaks C and D). Because the sub-peak A is attributed to the lattice fluctuation, so the sub-peak B might be also attributed to the lattice fluctuation. In the quantum well material systems, there are two kinds of fluctuations, the lattice fluctuation and the compositional fluctuation. Thanks to the sub-peak D is the band tail which believed the result of random distribution of N atoms or called compositional fluctuation, so the sub-peak C, which has the same trend of progression, might be also attributed to the compositional fluctuation.

In addition, we can obtain the approximation of activation energy of the sub-peak, which survives for the high temperature, by plotting the natural log of the overall integrated PL intensities as a function of the inverse temperature. So, the natural log of the overall integrated PL intensities of the SQWs is plotted as a function of the temperature shown in Fig. 3.13, together with that of the bulk layer for the comparison. With increasing temperature, the overall integrated emission intensity of the PL spectra gradually decreases. This indicates a large number of non-radiative recombination centers. The activation energy can be obtained from the equation [24],

$$I(T) = \frac{I(0)}{\left(1 + \frac{P_{nro}}{P_r} \exp\left(\frac{-E_a}{k_B T}\right)\right)} \quad , \quad (3.2)$$

where $I(T)$ is the integrated PL intensity at temperature T, $I(0)$ is the integrated PL intensity at temperature 0 K, k_B is Boltzmann's constant, T is the temperature, P_{nro}/P_r is effectively the ratio of non-radiative (P_{nro}) to radiative (P_r) recombination probability and E_a is the activation energy. The best fit above 145 K yields the non-radiative recombination of $P_{nro}/P_r \sim 10^6 - 10^7$. The activation energies of the SQWs together with the bulk layer are shown in Fig. 3.13. The activation energies of the SQWs are higher than that of the bulk layer, indicating the SQWs has the efficiency for confining the carriers better than that of the bulk layer.

Based on the PLE results, it is found that the values of $E_a \sim 200 - 250$ meV are in an agreement well with the energy difference between the PLE absorption edge of
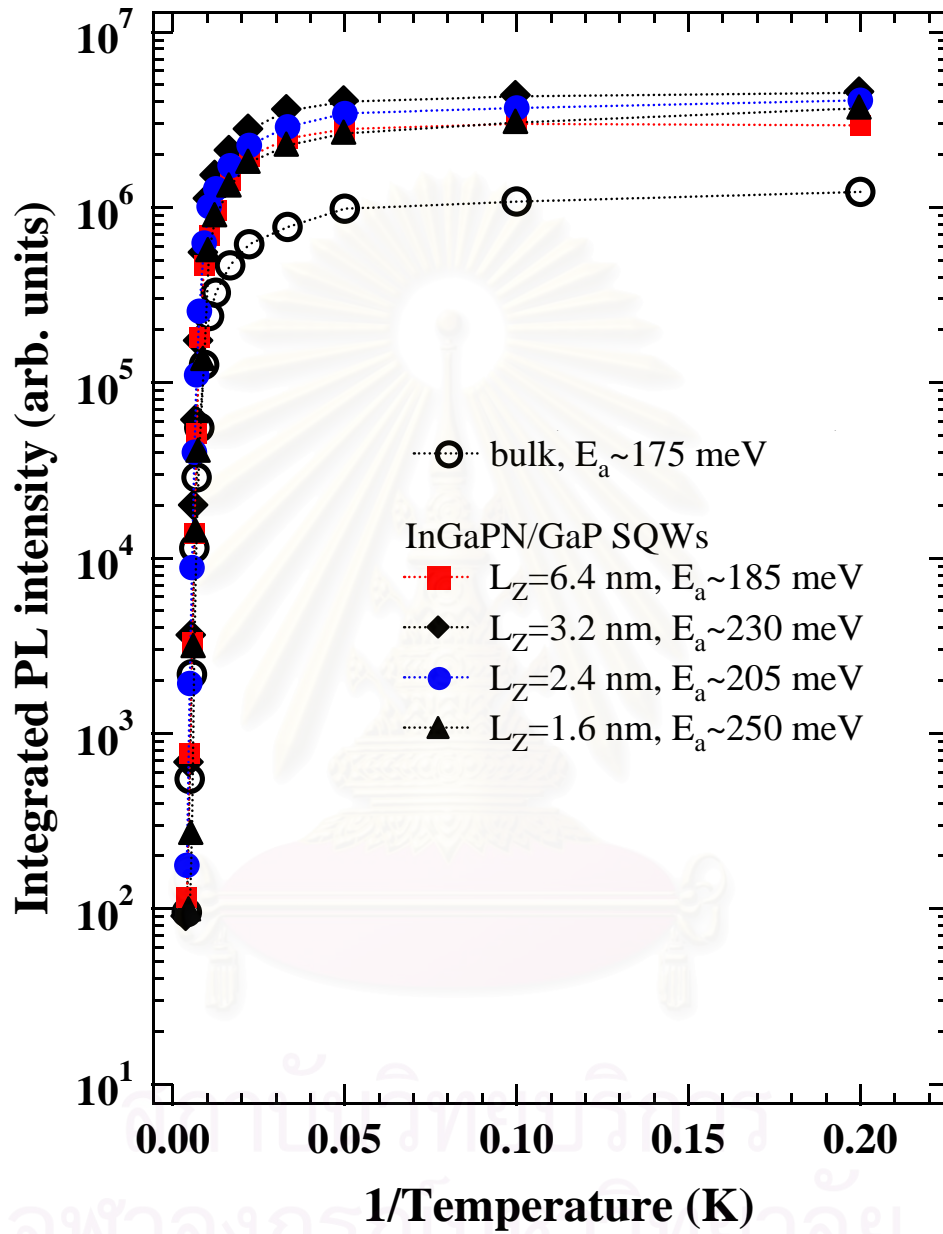
Figure 3.13: Integrated PL intensity of the SQWs plotted as a function of the temperature, together with that of the bulk layer for the comparison. The activation energy of SQWs and the bulk film are also depicted.

the $In_{0.056}Ga_{0.944}P_{0.975}N_{0.025}$ bulk (~ 2.08 eV at 10 K) and the bandgap of GaP (2.35 eV), which amounts to 250 meV. It is also expected by calculation [25, 26] that the most part of the bandgap difference contributes to the conduction-band offset ΔE_c. Therefore, the E_a values for SQWs are considered as coming form the GaP barrier height for the carrier over flow from the quantum well, while for the bulk is from the localization energy of the bound excitons. These results demonstrate an efficient carrier confinement, which is realized in the lattice-matched $In_{0.056}Ga_{0.944}P_{0.975}N_{0.025}$/GaP SQWs with a large conduction band offset ΔE_c ~ 200 - 250 meV, giving the highly efficient PL at higher temperatures.

3.5 Summary

Structural and optical properties of $In_{0.050}Ga_{0.950}P_{0.975}N_{0.025}$/GaP with different well-widths were investigated. The compositions and the well-widths of SQWs were obtained by HRXRD results and their simulation. HRXRD results demonstrate the lattice-matched SQWs. In addition, the surface images from the optical microscopy were used to confirm the lattice-matched SQWs with the strain less than 0.3% and no generation of misfit dislocation. The PL peak position and PLE absorption edge observed from the SQWs exhibit the blue-shift comparing to the bulk film. This blue-shift was increase with decreasing of the well-width, which is attributed to the quantum confinement effect by the well. The temperature dependent PL results show that the SQWs has the activation energy higher than that of the bulk film, indicating the SQWs has the efficiency for confining the carriers better than that of the bulk layer. The larger activation energies in the SQWs are due to the large conduction band offset (200 -250 meV).

CHAPTER IV

EFFECTS OF COMPOSITIONAL VARIATION

In this chapter, structural and optical investigational results of both the $In_xGa_{1-x}P_{1-y}N_y$ bulk layer and the $In_xGa_{1-x}P_{1-y}N_y$/GaP SQWs with different In and N concentrations are described. High-resolution X-ray diffraction (HRXRD) was performed to characterize the structural properties. For the optical characterization, photoluminescence (PL) and photoluminescence-excitation (PLE) techniques were employed.

4.1 Sample Description

All the $In_xGa_{1-x}P_{1-y}N_y$/GaP SQWs and the $In_xGa_{1-x}P_{1-y}N_y$ bulk layers used in this study were grown on GaP (001) substrates using metalorganic vapor phase epitaxy (MOVPE) technique at Prof. Kentaro Onabe's laboratory, the University of Tokyo by Dr. Nobuhiro Nakadan and Dr. Tokuharu Kimura. The precursors for Ga, In, P and N are trimethyl-gallium (TMGa), trimethyl-indium (TMIn), PH_3 and 1,1-dimethyl-hydrazine (DMHy), respectively. The carrier gas is H_2. After the growth of the around 0.3 µm-thick GaP buffer layer at 710°C, a thin $In_xGa_{1-x}P_{1-y}N_y$ well layer and a GaP cap layer were respectively grown at 635°C. The composition of the $In_xGa_{1-x}P_{1-y}N_y$ well layers, which are nominally lattice-matched to GaP, were controlled to be $x = 0.050 - 0.135$ and $y = 0.025 - 0.071$. The well-widths were controlled to be the same in the same series of the samples. The $In_xGa_{1-x}P_{1-y}N_y$ bulk

| GaP cap |
| In$_x$Ga$_{1-x}$P$_{1-y}$N$_y$ |
| GaP buffer |
| GaP substrate |

varied composition

| In$_x$Ga$_{1-x}$P$_{1-y}$N$_y$ |
| GaP buffer |
| GaP substrate |

Single quantum well (SQW)   **Bulk film**
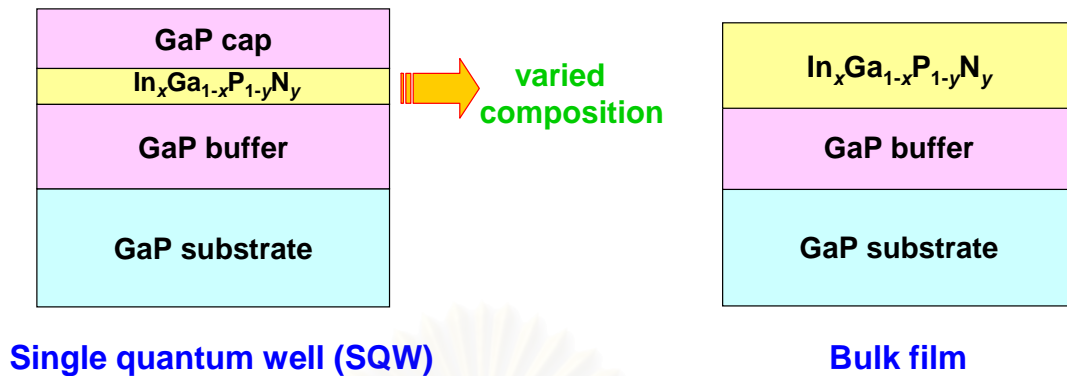
Figure 4.1: Schematic illustration of the InGaPN/GaP SQW and InGaPN bulk layer.

layers without the GaP cap layer were also prepared for a comparative study. The growth parameters such as V/III ratio, [DMHy] molar flow rate, were based on the growth of the In$_x$Ga$_{1-x}$P$_{1-y}$N$_y$ bulk layers [15, 16]. A schematic illustration of the InGaPN/GaP SQW and InGaPN bulk layer are shown in Fig. 4.1.

4.2 Structural Investigation

Figure 4.2 shows the (004) 2θ/ω-scan HRXRD patterns of three In$_x$Ga$_{1-x}$P$_{1-y}$N$_y$ /GaP SQWs, which use different molar flow rates of precursors for the same growth-time. These different molar flow rates lead to the difference in compositions (*x*, *y*) of the In$_x$Ga$_{1-x}$P$_{1-y}$N$_y$ layer. All samples show the similar shape of diffraction patterns. The main sharp peak at the angle of 68.8° correspond to the reflection from the (004) GaP. In addition, the additional diffracted peaks at lower angle of (In)GaP buffer layer, the broad satellite fringes and the frequent Pendellösung fringes are clearly observed. All features are similar to the results discussed in previous chapter (section 3.2.1).

Likewise the previous chapter, the simulation software was used to determine well thickness and the compositions. The simulation results obtained from the software are depicted in Fig. 4.3 together with the experimental diffraction patterns. As shown in the figure, the simulation results are very match to the experimental
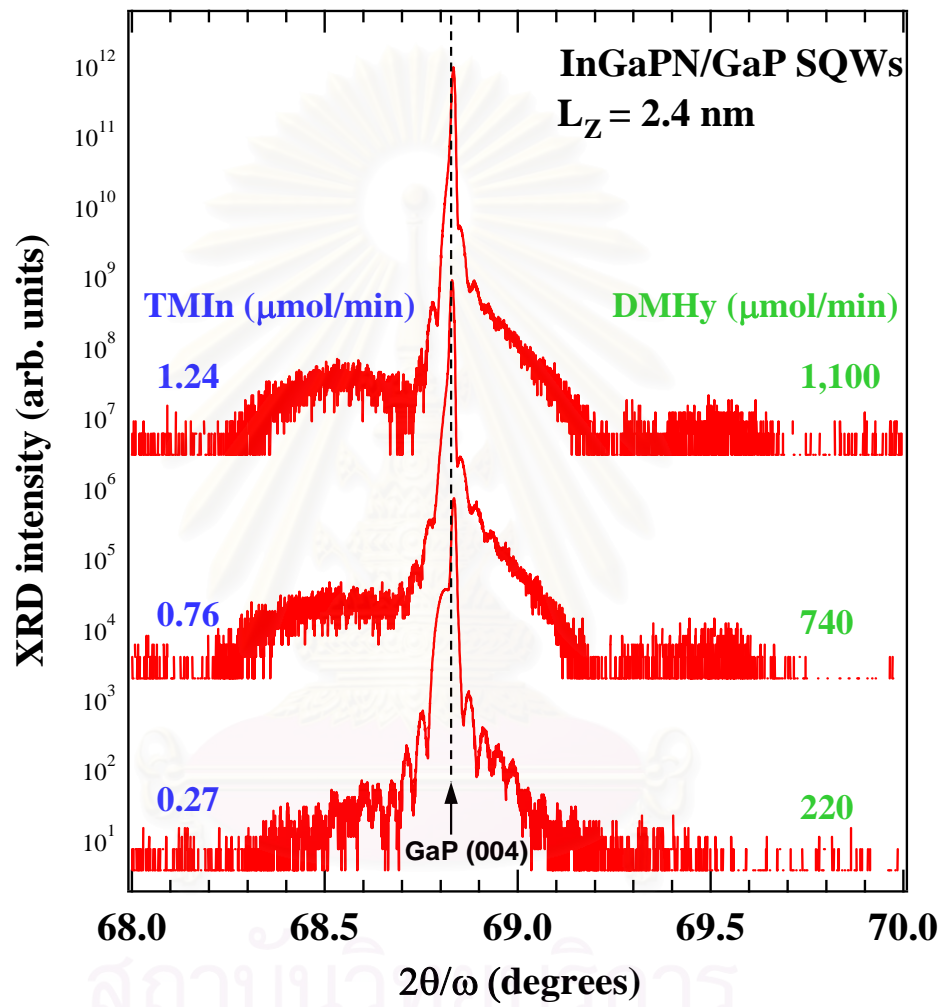
Figure 4.2: HRXRD patterns of InGaPN/GaP SQWs grown using different In and N flow rates.
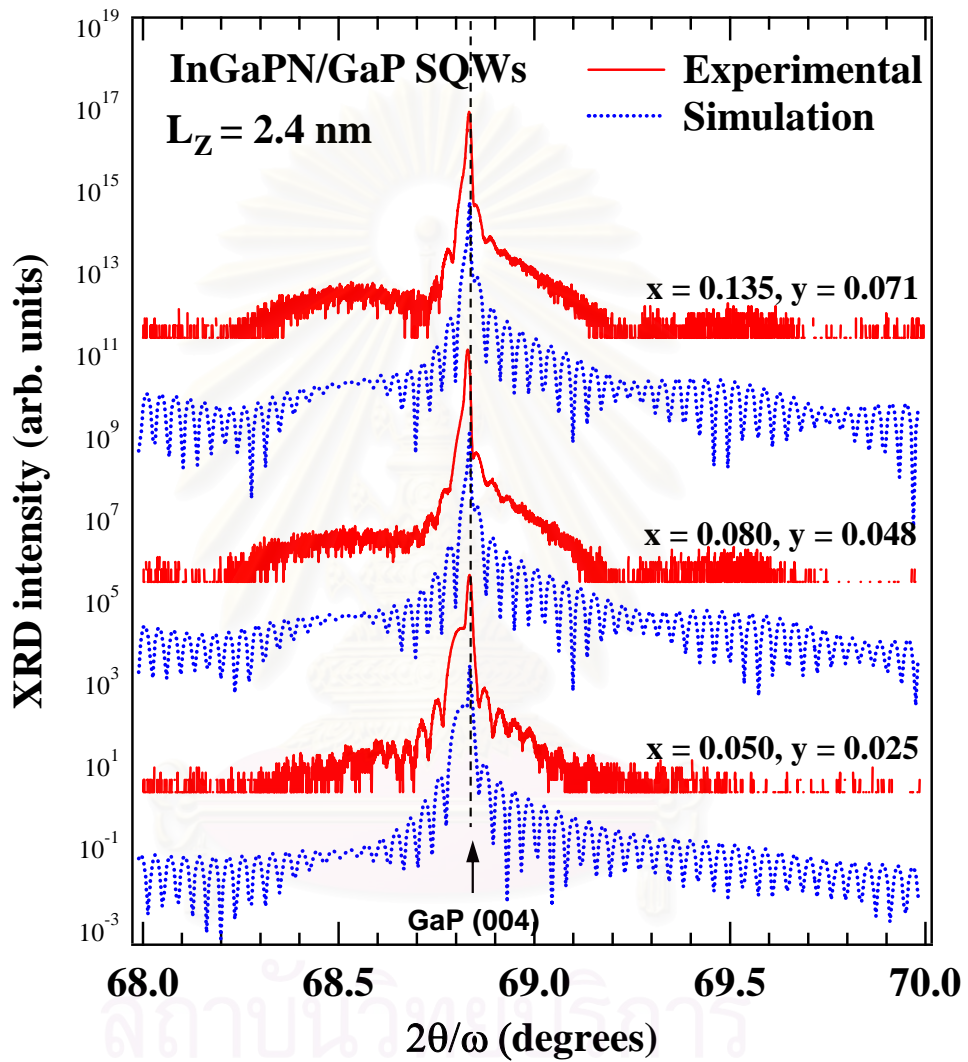
Figure 4.3: HRXRD patterns of InGaPN/GaP SQWs with different In and N concentrations and simulations.

results. According to the simulation, the well thickness or well-width of the $In_xGa_{1-x}P_{1-y}N_y$ well layers of $L_Z = 2.4$ nm are fixed and the same for all the SQWs. But the In and N concentrations in the well layers are different ($x = 0.050$, $y = 0.025$), ($x = 0.080$, $y = 0.048$) and ($x = 0.135$, $y = 0.071$), respectively, as labeled in the figure.

In addition, from the experimental results, the Pendellösung fringes for SQWs with compositions of ($x = 0.080$, $y = 0.048$) and ($x = 0.135$, $y = 0.071$) are not clearly seen than that of the SQW with compositions of ($x = 0.050$, $y = 0.025$). So, the crystal quality degradation caused by high N incorporation. The degradation of the crystal quality might be due to the composition fluctuation of high N containing InGaPN materials. However, they can still be observed, this indicates the fairly flat interfaces. Furthermore, the closely matching between the GaP diffracted peak and the zero order of satellite fringes indicate the lattice-matched InGaPN/GaP SQWs.

4.3   Optical Investigation

4.3.1   Bandgap Energy of $In_xGa_{1-x}P_{1-y}N_y$ Alloys

In order to estimate the bandgap energy of each alloy composition, the PLE results obtained from the bulk layers are considered. Figure 4.4 depicts the PLE spectra of the bulk layers with alloy compositions of ($x = 0.050$, $y = 0.025$), ($x = 0.080$, $y = 0.048$) and ($x = 0.135$, $y = 0.071$), respectively. The absorption edge of the PLE spectra for each alloy composition is determined as the effective bandgap energy of that. The estimated absorption edges are 2.08, 1.96 and 1.86 eV for the compositions of ($x = 0.050$, $y = 0.025$), ($x = 0.080$, $y = 0.048$) and ($x = 0.135$, $y = 0.071$), respectively. With increasing In and N concentrations, the absorption edge exhibits a red-shift. This indicates a reduction of the bandgap energy due to the incorporation of both In and N. For the bulk sample with composition of ($x = 0.135$, $y = 0.071$), the bandgap energy determined by surface photovoltage spectroscopy (SPS) have been reported by Hsu et al. [27]. From their results, the bandgap energies at 0 K and the room temperature are 2.008 ± 0.005 and 1.922 ± 0.025 eV, respectively. This is closely comparable to the effective bandgap energy at 10 K which is 1.86 eV. The difference might come from the difference in characterization methods and the fitting
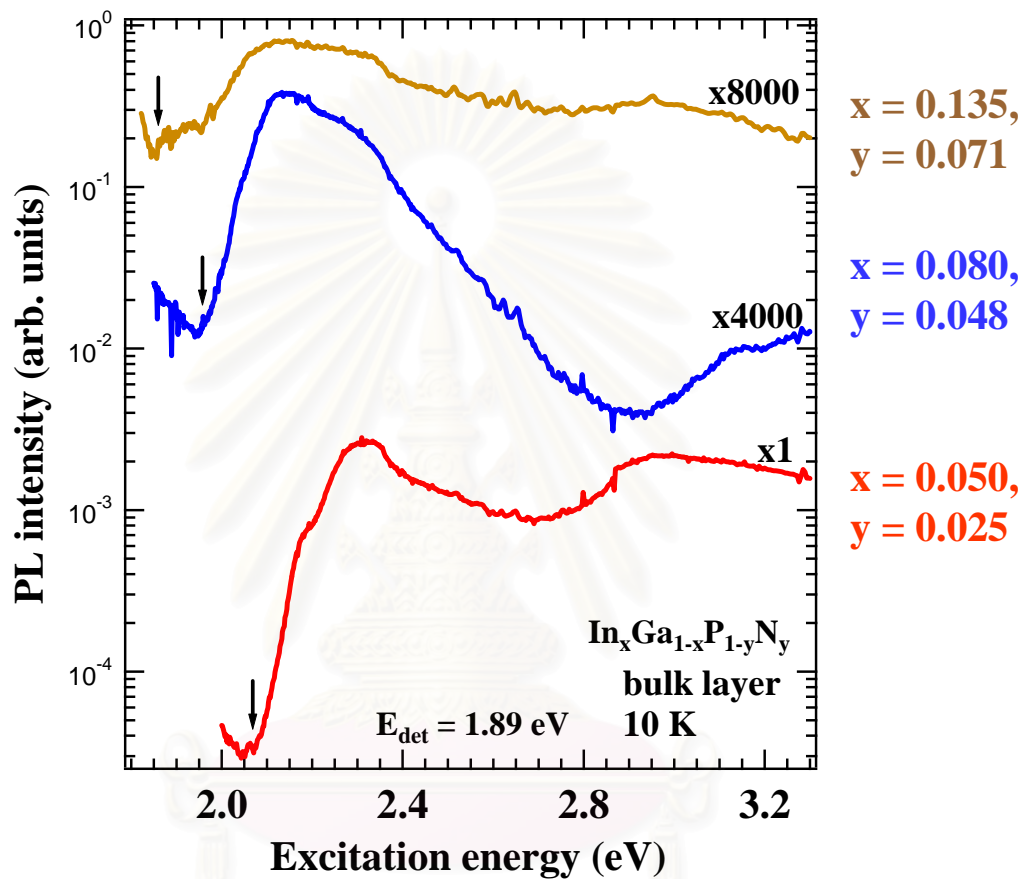
Figure 4.4: 10 K PLE spectra of InGaPN/GaP bulk layers on GaP with different In and N concentrations. The arrows indicate the absorption edge.

procedures. In addition, PL results of the same series are also shown in Fig. 4.5. They also show the red-shift of PL peak positions with increasing both In and N concentrations. This evidence confirms the large lowering of the bandgap energy, which is mainly due to the N incorporation.

From the approximation with no valence band offset for the dilute nitrides [2], the conduction band offsets for the InGaPN/GaP SQWs with the compositions of ($x = 0.050$, $y = 0.025$), ($x = 0.080$, $y = 0.048$) and ($x = 0.135$, $y = 0.071$) can be estimated to be 270, 390 and 490 meV, respectively, as shown in Fig. 4.6. These values indicate the large barrier height for an electron confinement in the InGaPN/GaP quantum structures. In addition, the value of 270 meV for the composition of ($x = 0.050$, $y = 0.025$) is comparable with the activation energy, obtained by the fitting of the temperature dependent PL results described in Chapter 3.

Moreover, to date, fundamental type of bandgap for the InGaPN alloy is still not manifest. Hsu et al. reported that InGaPN is a direct bandgap semiconductor. However, our PLE results show that it seems to be a quasi-direct semiconductor because its PLE absorption edge is not sharp. In the case of direct bandgap semiconductors, in general, their absorptions are very steep (for example, the absorption of direct bandgap of GaP at 2.87 eV as shown in Fig. 3.11). The band formation of InGaPN alloy with low In concentration might be the same for GaPN which is also dilute nitride material. For the incorporation of small amount of N into GaP which is an indirect bandgap semiconductor, the N atoms form many trapping states under the indirect gap of GaP and independent with wave-vector (k) [28]. The most prominent of the N trapping state is the A-line that is originated from an isolated N atom which exhibits as the trapping defect [29]. For N > 1%, these N trapping states merge together and form the new band with independent with wave-vector (k), as shown in Fig. 4.7. Hence, this new band leads GaPN to the quasi-direct semiconductor. The same situation is also expected for InGaPN, which has the concentrations of In and N much smaller than that of Ga and P.
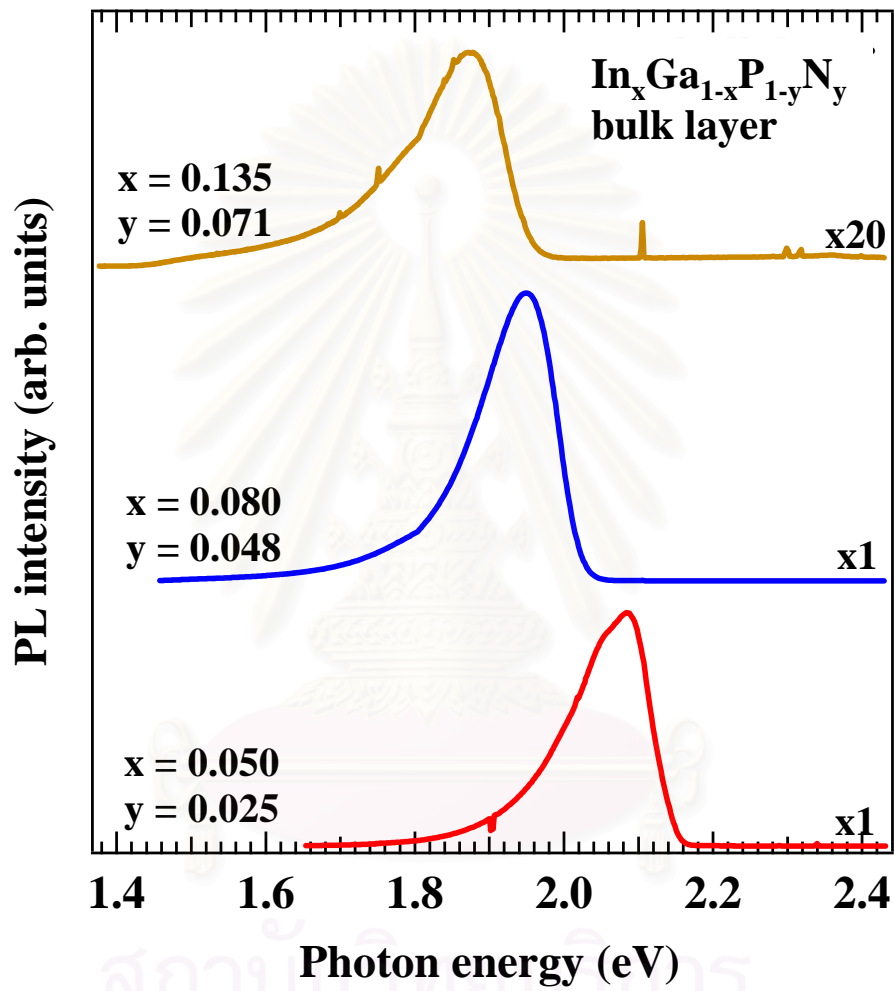
Figure 4.5: 10 K PL spectra for the InGaPN/GaP bulk layers on GaP with different In and N concentrations.

Increasing In and N concentrations

Decreasing the bandgap
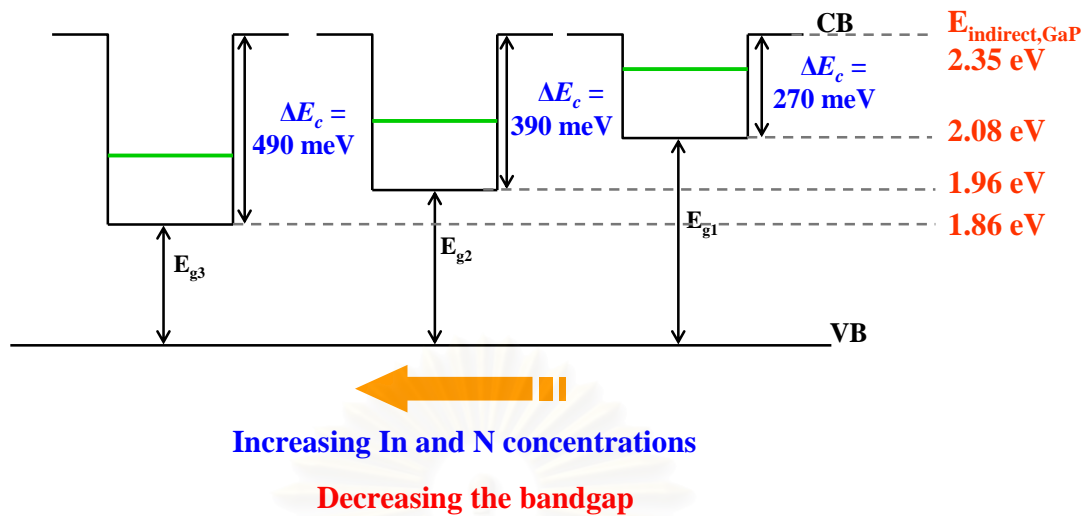
Figure 4.6: Schematic drawing of the approximated conduction band offsets (ΔE_c) of InGaPN/GaP SQWs with different In and N concentrations. The E_{g1}, E_{g2} and E_{g3} are the bandgap energies of the InGaPN bulk layers with the compositions of ($x = 0.050$, $y = 0.025$), ($x = 0.080$, $y = 0.048$) and ($x = 0.135$, $y = 0.071$), respectively.
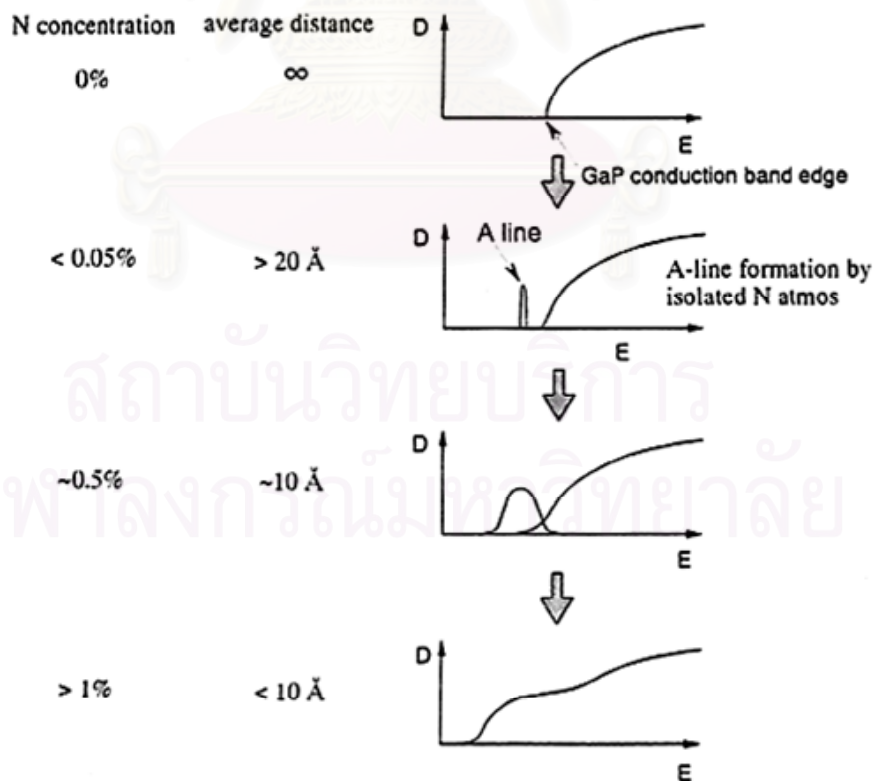
Figure 4.7: Schematic drawing for the formation of the conduction band edge of GaPN alloy [23].

4.3.2 Photoluminescence of InGaPN/GaP SQWs

Low-temperature (10 K) PL spectra of the $In_xGa_{1-x}P_{1-y}N_y$/GaP SQWs with various In and N concentrations of ($x = 0.050$, $y = 0.025$), ($x = 0.080$, $y = 0.048$) and ($x = 0.135$, $y = 0.071$) but the same well-width of $L_Z = 2.4$ nm were shown in Fig. 4.8. With increasing In and N concentrations whereas the well-width was fixed, the PL main peak exhibits red-shift. This indicates a reducing of the optical transition energy which is due to the lowering conduction band edge of $In_xGa_{1-x}P_{1-y}N_y$ well layer. Also, for the highest N-incorporating SQW sample, the intensity of PL main peak rapidly decreases. This is owing to the high-concentration of non-radiative recombination defects in the high N-incorporating SQW. The non-radiative defects are the defects that trap the carriers. So, the carriers cannot recombine or recombine without photon emission (might be phonon emission). In addition, the sharp NN_i lines and their phonon replicas [29] are clearly observed in all SQWs. The dotted lines indicate the NN_i lines which have an intense intensity, i.e., A-line (2.31 eV) and NN_3 (2.26 eV). The A-line and NN_3 are attributed to the recombination from the isolated N atom states and third nearest neighbor N atom site state, respectively [29]. Unlike the PL main peak, these NN_i lines still remain their energy with increasing In and N concentrations. It is interpreted that the PL main peak was emitted from InGaPN well layer. In contrast, the sharp NN_i lines, they were emitted from the GaP barrier. This might due to the N atoms penetration in GaP barriers during the growth, or it is the recombination of excitons near the interface of InGaPN and GaP. Thus, the cause of a large reduction of PL intensity may be owing to the rising of non-radiative defects which related to the incorporation of In and N.

4.3.3 Photoluminescence-excitation of InGaPN/GaP SQWs

Figure 4.9 illustrates the 10 K PLE spectra monitored at 1.89 eV for the $In_xGa_{1-x}P_{1-y}N_y$/GaP SQWs with various In and N concentrations of ($x = 0.050$, $y = 0.025$), ($x = 0.080$, $y = 0.048$) and ($x = 0.135$, $y = 0.071$) but the same well-width of $L_Z = 2.4$ nm. The features of PLE are similar to previous chapter. With increasing In and N concentrations whereas the well-width was fixed, the absorption
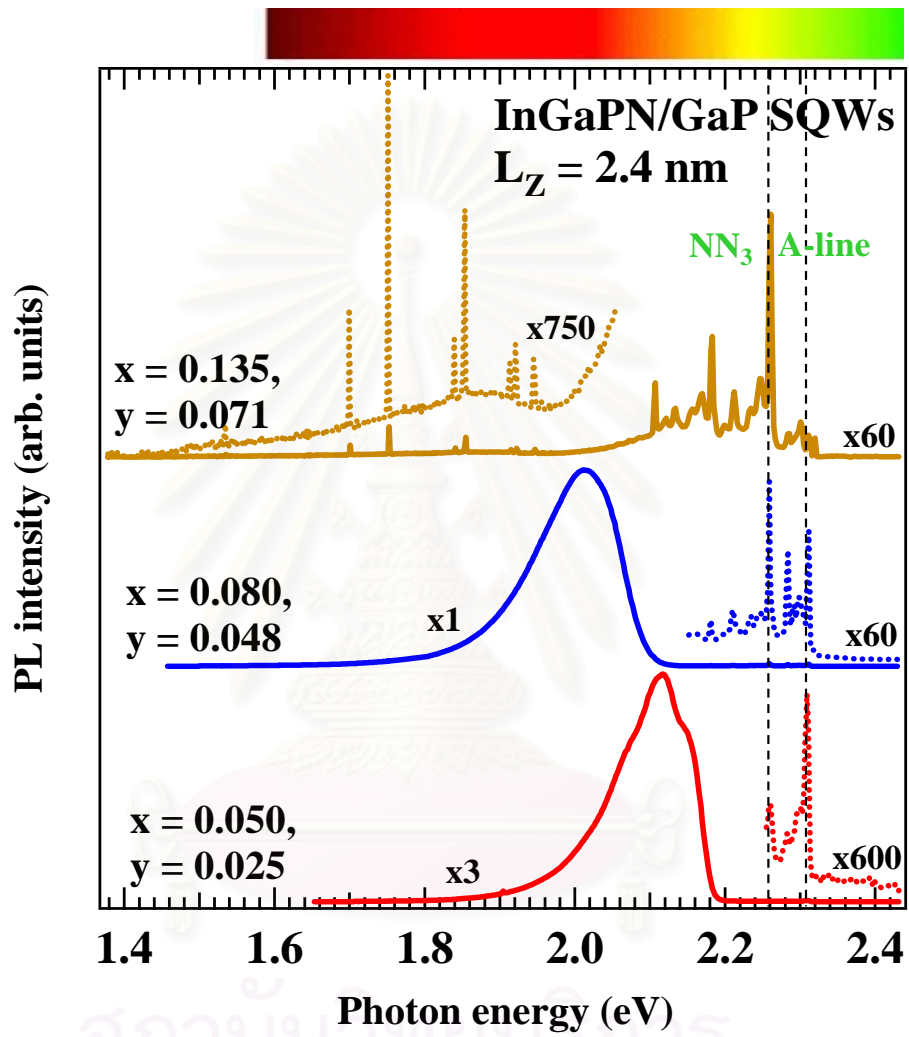
Figure 4.8: 10 K PL spectra for InGaPN/GaP SQWs of well-width 2.4 nm with different In and N concentrations. The dashed lines indicate the A-line and NN_3 line. The light spectrum above the figure shows the emission region of samples.
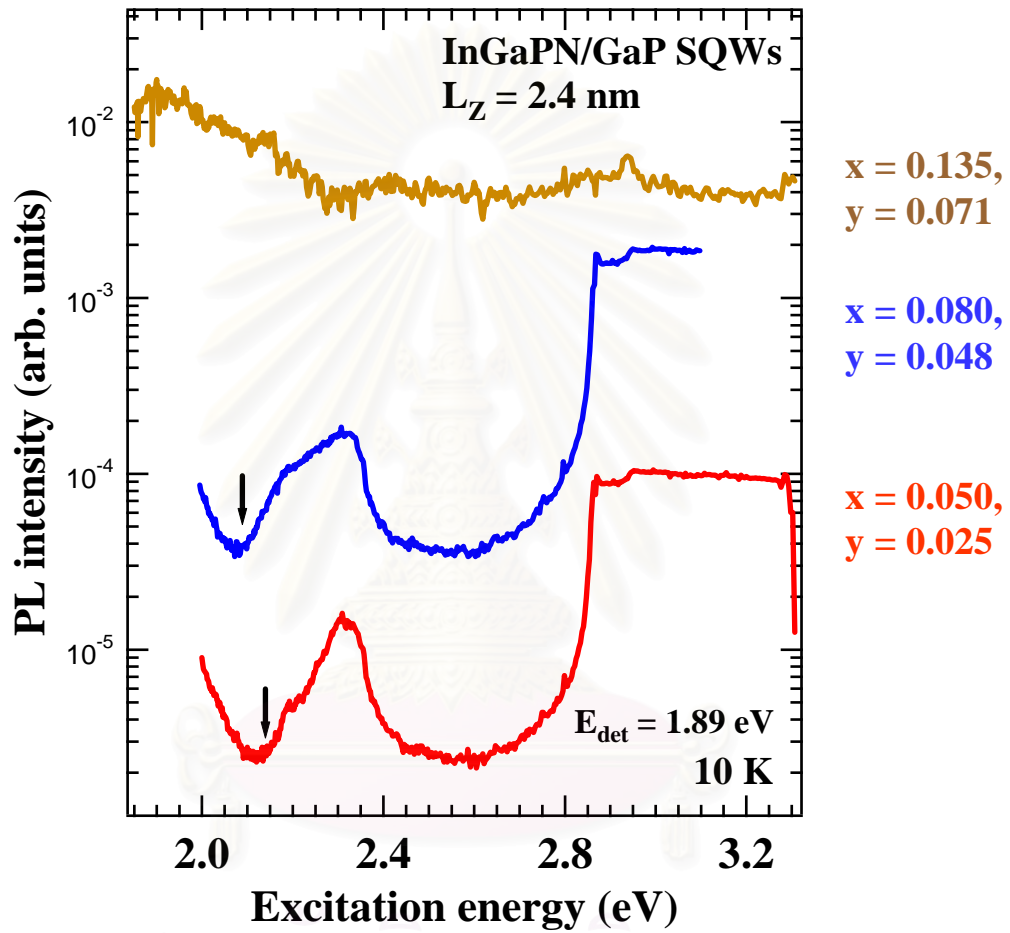
Figure 4.9: 10 K PLE spectra for InGaPN/GaP SQWs with fixed well-width of 2.4 nm and with different In and N concentrations. The arrows indicate the absorption edge.

edges of PLE exhibit the red-shift. This confirms a reduction of the optical transition energy which is due to the lowering conduction band edge of the $In_xGa_{1-x}P_{1-y}N_y$ well layer. The amount of the red-shift is 68 meV from the composition of ($x = 0.050$, $y = 0.025$) to ($x = 0.080$, $y = 0.048$). For the highest N-incorporating SQW, the intensity of the emission is too low for determining the features. So, the well-defined PLE spectrum cannot be observed for such high N-containing sample.

4.4 Summary

Structural and optical properties of $In_xGa_{1-x}P_{1-y}N_y$/GaP with different In and N concentrations, which are ($x = 0.050$, $y = 0.025$), ($x = 0.080$, $y = 0.048$) and ($x = 0.135$, $y = 0.071$), both bulk layers and SQWs were invatigated. For the bulk layers, the absorption edges exhibit a red-shift with increasing In and N concentrations. This indicates the reduction of the bandgap energy due to the incorporation of In and N. It is found that the conduction band offsets for SQWs can be estimated to be 270 - 490 meV. These values indicate the large barrier height for electron confinement in the InGaPN/GaP quantum structures.

For SQWs, the composition and the well-width of SQWs were obtained by the HRXRD results and simulations. The HRXRD results had shown the lattice-matched SQWs and the degradation of the crystal quality which might due to the composition fluctuation of high N-containing in InGaPN materials. Moreover, the PL peak position and PLE absorption edge exhibited the red-shift with increasing In and N concentrations. This is owing to a reduction of the optical transition energy which is due to the lowering conduction band edge of $In_xGa_{1-x}P_{1-y}N_y$ well layer. Our results demonstrate that the large reduction of conduction band edge is mainly due to the incorporation N. With higher incorporation of N, the intensity of PL main peak rapidly decreases, owing to the high-concentration of non-radiative defects which strongly related to the incorporation of N.

CHAPTER V

FINITE-DEPTH SQUARE

POTENTIAL WELL

CALCULATION

In this chapter, the finite-depth square potential well calculation is used to interpret the PL and PLE results that obtained from the InGaPN/GaP SQWs. As an example, the valence band offset of InGaPN/GaP SQW is discussed. The difference of well-widths which causes the lattice fluctuation seen on PL spectra in Chapter 3 is also clarified.

5.1   Comparison between Absorption Edge and Finite-Depth Square Well Calculation

In order to determine the quantum well characteristic of the novel InGaPN/GaP system, the series of $In_{0.050}Ga_{0.950}P_{0.975}N_{0.025}$/GaP SQWs, which have emission in PLE results for all well-widths, are selected for comparing with the potential well calculation as a function of well-width. With benefits of lattice-matched condition, the finite-depth square potential well calculation without the effects of hydrostatic strain can be used to interpret the PL and PLE results obtained from the lattice-matched InGaPN/GaP SQWs. In order to obtain the transition energy, the valence band offset (ΔE_v) of InGaPN/GaP system is required. First, the valence band alignment of the $In_{0.050}Ga_{0.950}P_{0.975}N_{0.025}$ alloy is calculated. In this study, the valence

band lineup of $In_{0.050}Ga_{0.950}P_{0.975}N_{0.025}$ is obtained from the binary materials which are the components of the InGaPN, i.e. GaP, InP, GaN and InN. The interpolation rule for the physical properties (P) of $In_xGa_{1-x}P_{1-y}N_y$ alloy is [30]

$$P_{InGaPN}(x, y) = (1-x)*(1-y)*P_{GAP} + x*(1-y)*P_{InP} + (1-x)*y*P_{GaN} + x*y*P_{InN} \tag{5.1}$$

The data of the valence band alignments for III-V binary compounds is shown in Fig. 5.1. This information is obtained from the theoretical calculation by the Wei and Zunger [31]. However, they have reported that the uncertainty of their calculation is about 0.05 eV (50 meV) and the error can be larger for systems between nitrides and other III-V compounds.

From the interpolation rule, the valence band alignment for the $In_{0.050}Ga_{0.950}P_{0.975}N_{0.025}$ is estimated to be 0.95 eV. So, comparing the GaP which is the barrier, the valence band offset of $In_{0.050}Ga_{0.950}P_{0.975}N_{0.025}$/GaP is small as -0.04 eV. The minus sign indicates that the valence band of $In_{0.050}Ga_{0.950}P_{0.975}N_{0.025}$ is lower than that of GaP which is the barrier. This shows the Type-II quantum well which is hardly possible because the PL results show the strong luminescence. However, the value of valence band offset of 0.04 eV is smaller than the error which
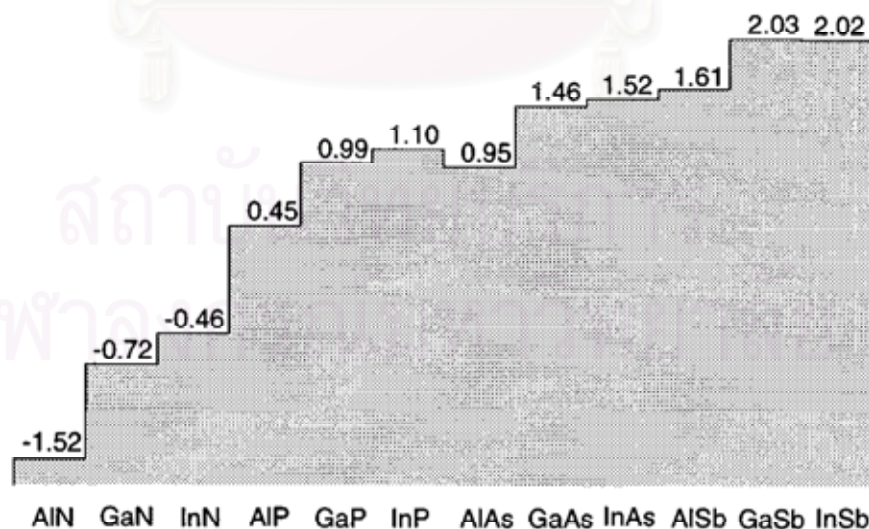
Figure 5.1: Calculated natural valence band alignment of III-V semiconductor compounds [31].

Wei and Zunger gave in their calculation. So, the valence band offset for this system can be approximated to zero. Next, in order to establish the well height, the conduction band offset (ΔE_c) needs to be determined. In this calculation, the PLE absorption edge of $In_{0.050}Ga_{0.950}P_{0.975}N_{0.025}$ bulk layer (~ 2.08 eV) is used as the effective bandgap of the InGaPN well layer. The barrier potential is determined by energy level of the indirect bandgap of GaP (2.35 eV). Consequently, the value of ΔE_c is estimated to be about 270 meV. Although the HRXRD results show that the one side of the barriers is the (In)GaP which is caused by the insertion of small amount of In into the GaP buffer layer, but this small amount of In (~ 0.5%) cannot perturb the indirect bandgap of GaP, as seen in Fig. 1.1. So, the model with the same height of both sides of barriers is still valid.

Because there is only conduction band offset, hence the other required parameter is the electron effective mass (m_e^*) of the $In_{0.050}Ga_{0.950}P_{0.975}N_{0.025}$. The interpolation rule is used again. The electron effective masses of the binary materials [10] and $In_{0.050}Ga_{0.950}P_{0.975}N_{0.025}$ from the interpolation are shown in Table 5.1. The calculation procedures of the finite-depth square potential well have been already shown in Chapter 2. Thus, the optical transition energy (E_T) can be written as

$$E_T = E_{g,InGaPN} + E \tag{5.2}$$

materials	electron effective mass (m_e^*)
GaP	0.13
InP	0.0795
GaN	0.15
InN	0.12
$In_{0.050}Ga_{0.950}P_{0.975}N_{0.025}$	0.128

Table 5.1: The electron effective mass of III-V binary compounds [10] and $In_{0.050}Ga_{0.950}P_{0.975}N_{0.025}$.
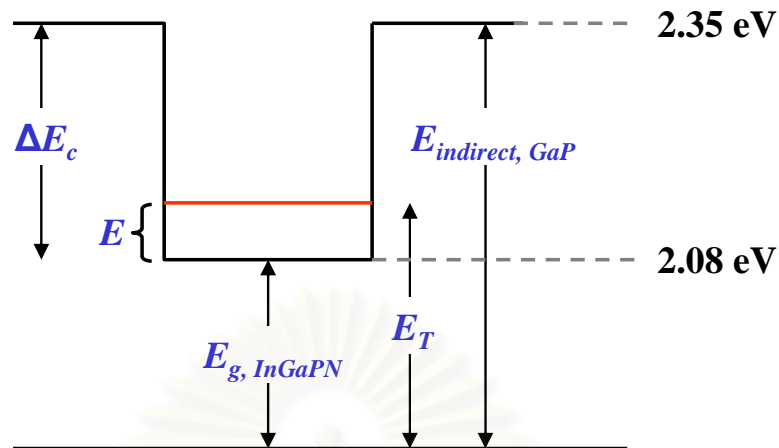
Figure 5.2: Schematic drawing for the calculation of the optical transition energy.

A schematic for the calculation is shown in the Fig. 5.2. The energy positions of the PL main peak and the PLE absorption edges as a function of well-widths are illustrated in Fig. 5.3 together with the calculated transition energies from Eg. (5.2). Both the PL peak position and PLE absorption edge exhibit the same trend with the calculated optical transition energies, confirming the quantum confinement effect of the well. However, both of them show the lower in the energy than the calculated optical transition energies. This difference might be due to the difference in the electron effective mass and the valence band offset. However, in this work, we have calculated the optical transition energies using the electron effective mass obtained from the interpolation rule. It is known that in dilute III-V-N system, the electron effective mass is significantly increased with incorporation of N [33, 34]. So, the electron effective mass in real situation might be heavier than that of the calculation. Moreover, in this InGaPN/GaP structure, the valence band offset might be larger than zero, leading the PLE absorption edge to be lower in energy than the calculation. On the other hand, it is evidence that the PL peak positions are much lower in the energy than the PLE absorption edges and the calculated value of optical transition energies. This evidence implies that the energy at the PLE absorption edge is the energy that excites the electron up to the energy at quantum state but the energy at PL emission might be originated from the emission of exciton. The difference in the transition energy in the case of the PLE and PL might be owing to the exciton binding energy.
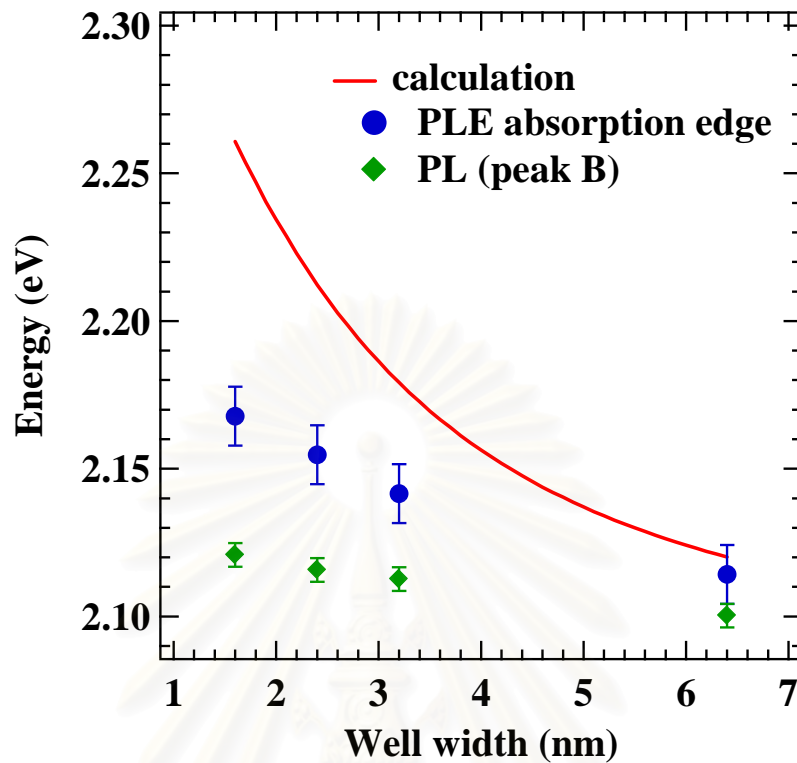
Figure 5.3: The energy positions of the main PL peaks and the PLE absorption edges as a function of well-widths together with the calculated transition energies. The error bars in the case of PLE absorption edges come from the procedure of determination of the absorption edges. The error bars in the case of PL peak positions come from the resolution of PL measurement.

This exciton binding energy will be increased with decreasing well-width since the electron and hole are forced to be closer to each other [35]. This reason might be the cause of increasing the separation between the energy of the PLE absorption edge and that of PL peak position with decreasing well-width.

5.2 Effect of Lattice-fluctuation

In the Chapter 3, the PL results of the well-width dependence (Fig. 3.5) show the splitting of the PL peaks into sub-peak A and sub-peak B which due to the lattice-fluctuation. For the PL spectrum of $In_{0.050}Ga_{0.950}P_{0.975}N_{0.025}$ /GaP SQW with
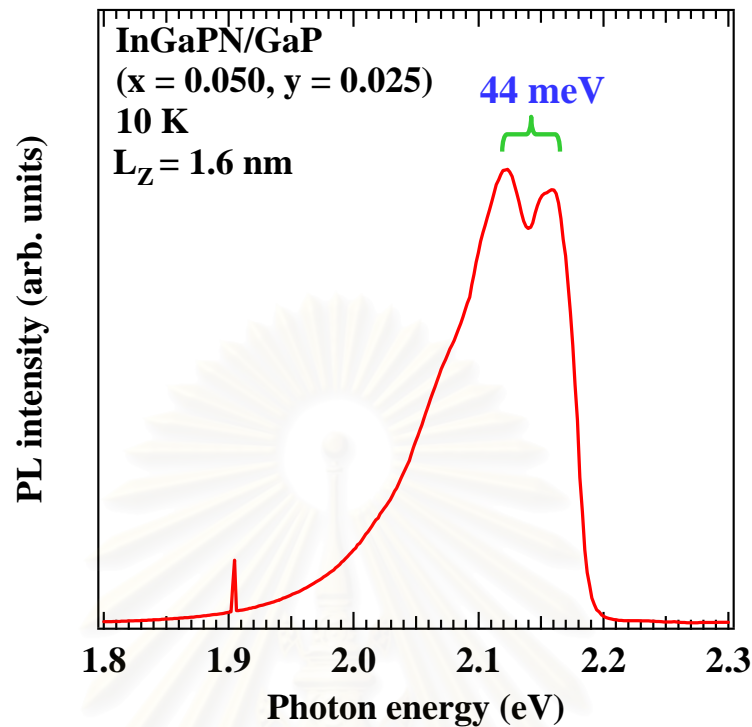
Figure 5.4: PL spectrum of $In_{0.050}Ga_{0.950}P_{0.975}N_{0.025}$/GaP SQW with well-width of 1.6 nm together with the value of difference in energies of the splitting sub-peaks.

well-width of 1.6 nm, the energy difference of sub-peak A and sub-peak B is determined to be 44 meV, as shown for example in Fig. 5.4. If the sub-peak B is the emission from the region, which has the well-width of 1.6 nm, so the sub-peak A which has the emission at higher energy is the emission from the thinner zone. From the finite-depth square potential well calculation, the value of 44 meV is comparable to the difference in the optical transition energy from the SQW which difference in well-width of about one lattice-constant (0.54 nm).

5.3 Summary

The electron effective mass of $In_{0.050}Ga_{0.950}P_{0.975}N_{0.025}$ calculated from the interpolation rule is 0.128. The valence band offset of the $In_{0.050}Ga_{0.950}P_{0.975}N_{0.025}$/GaP structure is discussed. In addition, the results from the interpolation of the valence band alignments of the binary materials show that the valence band edge of

$In_{0.050}Ga_{0.950}P_{0.975}N_{0.025}$ lie at 0.95 eV. This leads the valence band offset of $In_{0.050}Ga_{0.950}P_{0.975}N_{0.025}$/GaP structure to be very small and is approximated to be zero in this calculation.

The comparison between the PLE absorption edge and the optical transition energy from the finite-depth square well calculation are shown. The PLE absorption edges exhibit the same trend with optical transition energies from the calculation, confirming the quantum confinement effect of the well. In addition, by using this calculation, the lattice fluctuation in the novel InGaPN/GaP SQWs is estimated to be about one lattice-constant (0.54 nm).

CHAPTER VI
CONCLUSIONS

In this thesis, the physical properties of the lattice-matched $In_xGa_{1-x}P_{1-y}N_y$/GaP single quantum well (SQWs) grown by MOVPE were analyzed. The structural properties were mainly characterized by high-resolution X-ray diffraction (HRXRD) whereas the optical properties were characterized by photoluminescence (PL) and photoluminescence-excitation (PLE). The $In_xGa_{1-x}P_{1-y}N_y$/GaP SQWs used in this study were separated into two series. First series is the fixed alloy composition $In_xGa_{1-x}P_{1-y}N_y$/GaP SQWs with different well-widths (L_Z = 1.6 -6.4 nm) and the other is the fixed well-width $In_xGa_{1-x}P_{1-y}N_y$/GaP SQWs with different alloy compositions (x, y) in the well layer ((x = 0.050, y = 0.025), (x = 0.080, y = 0.048) and (x = 0.135, y = 0.071)). The analyses were mainly divided into two parts, the effects of well-width variation and the effects of compositional variation. The discussion was focused on the evidences of the quantum confinement effect in the SQWs.

The main results and conclusions obtained in this research work are summarized as follows:

(1) HRXRD results and surface images demonstrate that the lattice-matched $In_xGa_{1-x}P_{1-y}N_y$/GaP SQWs with high crystal quality and fairly flat heterointerface were obtained.

(2) For the fixed composition $In_xGa_{1-x}P_{1-y}N_y$/GaP SQWs with different well-widths, PL peak position and PLE absorption edge shift to higher energy (blue-shift) with decreasing well-width. This confirms the quantum confinement effect of the well. In addition, the well-resolved PL sub-peaks in the SQW with the narrowest well is attributed to the lattice fluctuation (or well-width fluctuation). The

lattice-fluctuation was examined to be about one lattice-constant (1.06 nm) in such SQWs.

(3) For the fixed well-width $In_xGa_{1-x}P_{1-y}N_y$/GaP SQWs with different alloy compositions, PL peak position and PLE absorption edge shift to lower energy (red-shift) with increasing both the In and N concentrations. However, it is believed that the large red-shift is due to the incorporation of N, resulting in a large reduction of the conduction band edge of $In_xGa_{1-x}P_{1-y}N_y$ well layer. This also confirms the quantum confinement effect of the well. However, for the highest In- and N-containing SQWs ($x = 0.135$, $y = 0.071$), the intensity of PL main peak is rapidly decreased. The cause of a large reduction of the PL intensity may be owing to the rising of non-radiative defect density, which is related to the incorporation of In and N.

(4) PL results demonstrate that the $In_xGa_{1-x}P_{1-y}N_y$/GaP SQWs exhibit the luminescence in the visible-wavelength region (yellow to red emission). Particularly, there are strong luminescence in the $In_xGa_{1-x}P_{1-y}N_y$/GaP SQWs with lower compositions of ($x = 0.050$, $y = 0.025$) and ($x = 0.080$, $y = 0.048$).

(5) The conduction band offsets (ΔE_c) of $In_xGa_{1-x}P_{1-y}N_y$/GaP ($x = 0.050 –$ 0.135, $y = 0.025 – 0.071$) SQWs are examined to be 270 – 490 meV. These values indicate the large barrier height for an electron confinement in the InGaPN/GaP quantum structures. However, for the highest In and N incorporating SQWs ($x = 0.135$, $y = 0.071$), although its conduction band offset is as high as 490 meV, the PL and PLE results show the low emission intensity which is caused by the large number of non-radiative defects. This means that these non-radiative defects are possibly related to the In and N. Therefore, the incorporation of In and N for achieving the bandgap in the red region of visible-wavelength is limited due to an insufficient crystal quality of the well layer.

Based on our results, the quantum confinement effect in these lattice-matched $In_xGa_{1-x}P_{1-y}N_y$/GaP SQWs is confirmed. The optical transition energy can be engineered by tuning the well-widths and compositions in the InGaPN quantum well layer. The decreasing of well-width causes the emission in higher transition energy

580	590	600	610	620	630	640	650	660	nm
2.14		2.06		2.00		1.94		1.88	eV
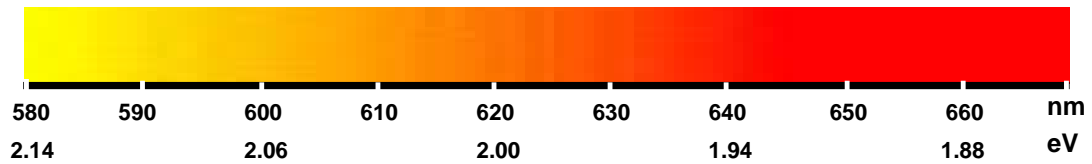
composition \ well-width	$x = 0.050,$ $y = 0.025$	$x = 0.080,$ $y = 0.048$	$x = 0.135,$ $y = 0.071$
bulk	2.084	1.949	1.877
6.4 nm	2.102	1.959	—
3.2 nm	2.112	1.960	—
2.4 nm	2.118	2.011	—
1.6 nm	2.123	2.046	1.945

— no emission or emission in very low intensity

Table 6.1: The transition energies obtained from $In_xGa_{1-x}P_{1-y}N_y$/GaP SQWs as well as the bulk films, and the light spectrum in the yellow to red emission region is also shown.

whereas the increasing of In and N concentrations effects the emission in lower transition energy. However, the increasing of In and N concentrations in the well layer are limited by the degradation of crystal quality. The transition energies of all the $In_xGa_{1-x}P_{1-y}N_y$/GaP SQWs as well as the bulk layers are summarized in Table 6.1. Hence, the lattice-matched InGaPN/GaP SQWs with transparent substrate has the promising for optoelectronic device applications such as light emitting and laser devices in the yellow to red emission region.

REFFERENCES

[1]   J. Y. Duboz, J. A. Gupta, Z. R. Wasilewski, J. Ramsey, R. L, Williams, G. C. Aers, B. J. Riel and G. I. Sproule, Band-gap energy of $In_xGa_{1-x}N_yAs_{1-y}$ as a function of N content. *Phys. Rev. B* **66** (2002): 85313-85318.

[2]   W. Shan, W. Walukiewicz, J. W. Ager III, E. E, Haller, J. F. Geisz, D. J. Friedman, J. M. Olson and S. R. Kurtz, Band Anticrossing in GaInNAs alloys. *Phys. Rev. Lett.* **82** (1999): 1221-1224.

[3]   H. Yaguchi, S. Kikuchi, Y. Hijikata, S. Yochida, D. Aoki and K. Onabe, Photoluminscence study on temperature dependence of band gap energy of GaAsN alloys. *phys. stat. sol. (b)* **288** (2001): 273-277.

[4]   M. Kondow, K. Uomi, A. Niwa, T. Kitatani, S. Watahiki and Y. Yazawa, GaInNAs: A novel material for long-wavelength-range laser diodes with excellent high-temperature performance. *Jpn. J. Appl. Phys*. **35** (1996): 1273-1275.

[5]   I. A. Buyanova, W. M. Chen, E. M. Goldys, H. P. Xin and C. W. Tu, Structural properties of a GaN_xP_{1-x} alloy: raman studies. *Appl. Phys. Lett.* **78** (2001): 3959-3961.

[6]   D. G. Thomas, J. J. Hopfield and C. J. Frosch, Isoelectronic traps due to nitrogen in gallium phosphide. *Phys. Rev. Lett.* **15** (1965): 857-860.

[7]   R. A. Logan, H. G. White and W. Wiegmann, Efficient green electroluminescence in nitrogen-doped GaP p-n junctions. *Appl. Phys. Lett.* **13** (1968): 139-141.

[8]   R. A. Logan, H. G. White and W. Wiegmann, Efficient green electroluminescent junctions in GaP. *Solid State Electron* **14** (1971): 55-70.

[9]   C. W. Tu and P. K. L. Yu, Material properties of III-V semiconductors for lasers and detectors. *MRS bulletin* May (2003): 345-349.

[10]   I. Vurgaftman, J. R. Meyer and L. R. Ram-Mohan, Band parameters for III-V compound semiconductors and their alloys. *Appl. Phys. Rev*. **89** (2001): 5815-5863.

[11] E. Cohen and M. D. Sturge, Excited states of excitons bound to nitrogen pairs in GaP. *Phys. Rev. B* **15** (1977): 1039-1051.

[12] R. A. Faulkner, Toward a theory of isoelectronic impurities in semiconductors. *Phys. Rev.* **175** (1968): 991-1009.

[13] K. Onabe, T. Kimura, N. Nakadan, J. Wu, Y. Ito, S. Yoshida, J. Kikawa and Y. Shiraki. presented at *ICCG-13/ICVGE-11*, Kyoto (2001).

[14] V. A. Odnoblyudov and C. W. Tu, Optical properties of InGaNP quantum wells grown on GaP (100) substrates by gas-source molecular beam epitaxy. *Appl. Phys. Lett.* **89** (2006): 111922.

[15] S. Sanorpim, F. Nakajima, R. Katayama, N. Nakadan, T. Kimura, K. Onabe and Y. Shiraki, MOVPE growth and characterization of high-N content InGaPN alloy lattice-matched to GaP. *phys. stat. sol. (c)* **7** (2003): 2773-2777.

[16] S. Sanorpim, F. Nakajima, R. Katayama, N. Nakadan, T. Kimura and K. Onabe, MOVPE growth and optical investications of InGaPN alloys. *J. Crystal Growth* **275** (2005): 1017-1021.

[17] Mario Birkholz. *Thin film analysis by X-ray scattering*. Germany: WILEY-VCH, 2006.

[18] G. Biwa, H. Yaguchi, K. Onabe and Y. Shiraki, Metalorganic vapor-phase epitaxy of $GaP_{1-x-y}As_yN_x$ quaternary alloys on GaP. *J. Crystal Growth* **189/190** (1998): 485-489.

[19] G. Biwa, H. Yaguchi, K. Onabe and Y. Shiraki, Photoluminescence and photoluminescence-excitation spectroscopy of GaPAsN/GaP lattice-matched multiple quantum well structures. *J. Crystal Growth* **195** (1998): 574-578.

[20] Jacques. I. Pankove. *Optical processes in semiconductors*. New York: Dover Publications, Inc., 1971.

[21] S. Miyoshi, H. Yaguchi, K. Onabe, R. Ito and Y. Shiraki. Metalorganic vapor phase epitaxy of $GaP_{1-x}N_x$ alloys on GaP, *Appl. Phys. Lett.* **63** (1993): 3506-3508.

[22] S. Miyoshi, H. Yaguchi, K. Onabe, Y. Shiraki and R. Ito, Growth mechanism in the metalorganic vapor phase epitaxy of metastable $GaP_{1-x}N_x$ alloys: a growth interruption study. *Jpn. J. Appl. Phys.* **36** (1997): 97.

[23] H. Yagushi, S. Miyoshi, G. Biwa, M. Kibune, K. Onabe, Y. Shiraki and R. Ito, Photoluminescence excitation spectroscopy of $GaP_{1-x}N_x$ alloys: conduction band edge formation by nitrogen incorporation. *J. Crystal Growth* **170** (1997): 353-356.

[24] J. D. Lambkin, L. Considine, S. Walsh, G. M. Oconnor, C. J. McDonagh and T. J. Glynn, Temperature Dependence of the Photoluminescence Intensity of Ordered and Disordered $In_{0.48}Ga_{0.52}P$. *Appl. Phys. Lett.* **65(1)** (1994): 73-75.

[25] S. Miyoshi and K. Onabe, Semi-empirical tight-binding calculation of the electronic structure of $GaP_{1-x}N_x$ (x=0.25, 0.5, 0.75). *Solid State Electron* **41** (1997): 267.

[26] L. Bellaiche, S.-H. Wei and A. Zunger, Composition dependence of interband transition intensities in GaPN, GaAsN and GaPAs alloys. *Phys. Rev. B* **56** (1997): 10233.

[27] H. P. Hsu, P. Y. Wu, Y. S. Huang, S. Sanorpim and K. K. Tiong, Surface photovoltage spectroscopy characterization of InGaPN alloys grown on GaP substrates. *Physica E* (in print).

[28] M. G. Craford and N. Holonyak Jr. *The optical properties of the nitrogen isoelectronic trap in GaAsP*. Netherlands: North-Holland Publishing Company, 1976.

[29] D.G. Thomas and J.J. Hopfield, Isolectronic traps due to nitrogen in gallium phosphide. *Phys. Rev.* **150** (1966): 680-689.

[30] S. Sanorpim, Structural and optical properties of III-III-V-N type alloy films and their quantum wells. (Doctoral dissertation, the University of Tokyo, 2003), p.11.

[31] Su-Huai Wei and Alex Zunger, Calculated natural band offsets of all III-VI and III-V semiconductors: chemical trends and the role of cation *d* orbitals. *Appl. Phys. Lett.* **72** (1998): 2011-2013.

[32] I. Vurgaftman, J. R. Meyer and L. R. Ram-Mohan, Band parameters for III-V compound semiconductors and their alloys. *Appl. Phys. Rev.* **89** (2001): 5815-5863.

[33] H. P. Xin and C. W. Tu, Photoluminescence properties of GaNP/GaP multiple quantum wells grown by gas source molecular beam epitaxy. *Appl. Phys. Lett.* **77** (2000): 2180-2182.

[34]   J. Wu, W. Shan and W. Walukiewicz, Band anticrossing in highly mismatched III-V semiconducting alloys. *Semicond. Sci. Technol.* **17** (2002): 860-869.

[35] Peter Y. Yu Manul Cardora. *Fundamentals of semiconductors*. Germany: Springer, 1996.

APPENDICES

APPENDIX A

Contributions from this thesis to the field

The MOVPE growth samples that have been used in this thesis, were prepared at Prof. Kentaro Onabe's laboratory, the University of Tokyo by Dr. Nobuhiro Nakadan and Dr. Tokuharu Kimura. The photoluminescence and photoluminescence-excitation measurements were also performed at Prof. Kentaro Onabe's laboratory, the University of Tokyo.

I took the raw data from PL and PLE measurements and did the calculation and analysis in Thailand. I participated during the HRXRD measurement at the Scientific and Technological Research Equipment Centre (STREC), Chulalongkorn University. I did the simulation and analysis of the obtained HRXRD results. I performed the optical microscopy at the National Metal and Materials Technology Center (MTEC) and interpreted the obtained results. I summarized all results, concluded the work and wrote two following international scientific papers.

Paper 1: D. Kaewket, S. Tungasmita, S. Sanorpim, F. Nakajima, N. Nakadan, T. Kimura, R. Katayama and K. Onabe, "Photoluminescence and photoluminescence-excitation spectroscopy of InGaPN/GaP lattice-matched single quantum well structures grown by MOVPE", (2007) Journal of Crystal Growth, 298, 531-535.

Paper 2: D. Kaewket, S. Tungasmita, S. Sanorpim, R. Katayama and K. Onabe, "Visible photoluminescence from InGaPN/GaP lattice-matched single quantum well structures grown by MOVPE", (2007) Proceedings of the 2nd IEEE International Conference on Nano/Micro Engineered and Molecular Systems, 695-700.

Moreover, I attended and presented my works in 6 Conferences, as following:

1. "Photoluminescence and photoluminescence-excitation spectroscopy of InGaPN/GaP lattice-matched single quantum well structures grown by MOVPE" *13th International Conference on Metal Organic Vapor Phase Epitaxy* (*ICMOVPE 13*), Miyazaki, Japan, May 22-26, 2006. [Poster presentation]

2. "Visible photoluminescence from InGaPN/GaP lattice-matched single quantum well structures grown by MOVPE" *The 2nd IEEE International Conference on Nano/Micro Engineered and Molecular Systems* (*IEEE-NEMS 2007*), Bangkok, Thailand, January 16-19, 2007. [Oral presentation]

3. "Red emission from InGaPN/GaP lattice-matched single quantum well structures grown by MOVPE" *32nd Congress on Science and Technology of Thailand (STT 32)*, Bangkok, Thailand, October 10-12, 2006. [Oral presentation]

4. "Optical properties of InGaPN/GaP lattice-matched single quantum well structures grown by MOVPE" *6th National Symposium on Graduate Research*, Chulalongkorn University, October 13-14, 2006. [Oral presentation]

5. "Optical characterization of InGaPN/GaP lattice-matched single quantum wells" *Siam Physics congress 2007,* Nakorn Pathom, March 22-24, 2007. [Oral presentation]

6. "Optical investigation of InGaPN/GaP lattice-matched single quantum wells" *14th Academic Conference*, Faculty of Science, Chulalongkorn University, March 16-17, 2006. [Oral presentation]

APPENDIX B

International scientific paper

Photoluminescence and photoluminescence-excitation spectroscopy of InGaPN/GaP lattice-matched single quantum well structures grown by MOVPE

Dares Kaewket[a], Sukkaneste Tungasmita[a], Sakuntam Sanorpim[a],*, Fumihiro Nakajima[b], Nobuhiro Nakadan[b], Tokuharu Kimura[b], Ryuji Katayama[b], Kentaro Onabe[b]

[a]*Department of Physics, Faculty of Science, Chulalongkorn University, Phayathai Rd., Pathumwan, Bangkok 10330, Thailand*
[b]*Department of Advanced Materials Science, The University of Tokyo, 5-1-5 Kashiwanoha, Kashiwa, Chiba 277-8561, Japan*

Available online 20 December 2006

Abstract

$In_{0.056}Ga_{0.944}P_{0.975}N_{0.025}$/GaP lattice-matched single quantum wells (SQWs) have been grown on GaP (0 0 1) substrates by metalorganic vapor phase epitaxy (MOVPE). Low-temperature (10 K) photoluminescence (PL) and PL excitation (PLE) measurements for the varied well widths (L_Z = 1.6, 2.4, 3.2 and 6.4 nm) have been revealed to confirm the quantum confinement by the well. Comparing with the bulk layer, the PL peak position blue shift amounts to 76 meV for the narrowest well of L_Z = 1.6 nm. On the other hand, the PLE spectra have shown the blue shift of the fundamental absorption edge to 2.17 eV for L_Z = 1.6 nm from 2.06 eV for the bulk. The blue shift is about 110 meV. In these samples, the PL and PLE blue shifts are believed to be predominantly determined by the quantum confinement effect to the well. Further results show a high-temperature PL has been far more enhanced than in the bulk due to the large conduction band offset ΔE_c.
© 2006 Elsevier B.V. All rights reserved.

PACS: 78.55.Cr; 78.67.De; 81.15.Kk

Keywords: A1. Photoluminescence (PL); A1. Photoluminescence excitation (PLE); A3. MOVPE; A3. Single quantum wells; B1. III-P-nitrides; B2. InGaPN alloy

1. Introduction

InGaPN is a novel material that can be lattice-matched to GaP [1], with a narrower bandgap than GaP. It is well known that the N incorporation drastically reduces the bandgap energy in the InGaAsN alloy, with the majority of the reduction resulting from lowering of the conduction band [2,3], and hence the similar effect is expected in the InGaPN alloy with N incorporation. Moreover, the InGaPN alloy is an alternative of the GaPAsN alloy that gives a high optical quality quantum well with the lattice-matched GaPAsN/GaP heterostructure [4,5]. These make InGaPN interesting for a well material with a large

barrier height for an electron confinement in the InGaPN/GaP structures. The $In_xGa_{1-x}P_{1-y}N_y$/GaP lattice-matched quantum well (QW) is expected to be an advantageous for laser material in the visible wavelengths.

In spite of the extremely low solid-solution miscibility, we previously reported that nearly 8.7% of N content (y) has been successfully realized in the $In_xGa_{1-x}P_{1-y}N_y$ (x = 0.17) alloy layers by metalorganic vapor phase epitaxy (MOVPE) [6,7]. In this study, based on such growth conditions, $In_{0.056}Ga_{0.944}P_{0.975}N_{0.025}$/GaP lattice-matched single quantum well (SQW) structures have been grown. Photoluminescence (PL) and PL excitation (PLE) measurements for varied well thicknesses have revealed the transitive nature of exciton localization and quantum confinement.

---

*Corresponding author. Tel.: +66 2 218 5110.
E-mail address: Sakuntam.S@chula.ac.th (S. Sanorpim).

2. Experiments

The MOVPE growth of InGaPN/GaP lattice-matched SQW structures was carried out at low pressure (60 Torr) using trimethylgallium (TMGa), trimethylindium (TMIn), PH_3 and 1,1-dimethyhydrazine (DMHy) as the Ga, In, P and N precursors, respectively, H_2 as the carrier. After the growth of a 0.3 μm-thick GaP buffer layer at 710 °C, a thin InGaPN well layer and a GaP cap layer were, respectively, grown at 635 °C. The well widths (L_Z) were controlled to be 1.6, 2.4, 3.2 and 6.4 nm for the different samples. A bulk $In_{0.056}Ga_{0.944}P_{0.975}N_{0.025}$ layer without GaP cap was also prepared for a comparative study. The growth parameters such as V/III ratio, DMHy flow rate, i.e., were based on the growth of the InGaPN bulk layers described elsewhere in Refs. [6,7]. The alloy compositions (x and y) and the well thicknesses were estimated from the bulk growth using high-resolution X-ray diffraction (HRXRD) and secondary ion mass spectroscopy (SIMS). A detailed description of the composition examination can be found in earlier work [6,7]. The optical properties of the SQWs were investigated by PL and PLE measurements. The PL measurement was carried out using CW excitation at power density of $1.0\,W/cm^2$ from the 325 nm line of He–Cd laser. The PLE measurement was performed using monochromatic light dispersed with a 0.27 m monochromator from a 500 W Xenon lamp.

3. Results and discussion

Fig. 1 shows low-temperature (LT, 10 K) PL spectra of $In_{0.056}Ga_{0.944}P_{0.975}N_{0.025}$/GaP lattice-matched SQWs with well widths of $L_Z = 1.6$, 2.4, 3.2 and 6.4 nm, as well as the $In_{0.056}Ga_{0.944}P_{0.975}N_{0.025}$ bulk layer. The He–Cd laser 325-nm line with $1.0\,W/cm^2$ excitation power density was used
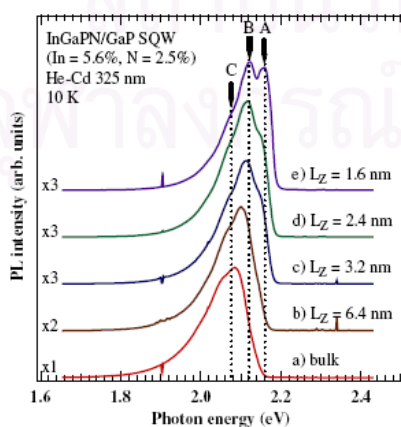
under a weak excitation regime. All the samples show bright and broad luminescence in the red region. The broad PL peak in the bulk layer is typical in $In_xGa_{1-x}P_{1-y}N_y$/GaP [6,7] and $GaP_{1-y}N_y$/GaP [8–10] as well as $GaP_{1-x-y}As_xN_y$/GaP [4,5], and such luminescence occurs at the density of states tails due to the weak localization of excitons. PL peak of $In_{0.056}Ga_{0.944}P_{0.975}N_{0.025}$/GaP lattice-matched SQWs shifts to higher energies with narrower wells. This might be attributed to the quantum confinement by the well.

From the LT-PL spectra of the $In_{0.056}Ga_{0.944}P_{0.975}N_{0.025}$/GaP lattice-matched SQWs displayed in Fig. 1b–e, it is not difficult to see that the PL peaks contain several sub-peaks with different relative intensity. The solid line in Fig. 2 is the 10 K-PL spectrum of the $In_{0.056}Ga_{0.944}P_{0.975}N_{0.025}$/GaP lattice-matched SQW with $L_Z = 1.6$ nm which exhibits three distinct spectral features, denoted by arrows. The dotted line is the numerical derivative (with respect to photon energy) of the PL data. The peak or sub-peak positions of the three features were accurately obtained from the zero-crossing (A and B) and an inflection point (C). It is found from Fig. 1 that an extra peak (feature A) appears at higher-energy side of the main peak (feature B) when the well width L_Z is about 3.2 nm or narrower. Nevertheless, the feature A grows up and shifts toward the higher energies with decreasing L_Z. Comparing with the bulk layer, the peak position of feature A blue shift amounts to 76 meV for the narrowest well of $L_Z = 1.6$ nm, and is much consistent with the quantum confinement by the well. On the other hand, the weaker blue shift for the feature B with decreasing L_Z might be interpreted as the decrease of N concentration in the well. For N concentration (y) nearly 2%, the average distance between the N atoms is about 1.3 nm [4], which is comparable with the width of the narrowest wells

Fig. 1. Low-temperature (10 K) PL spectra for the $In_{0.056}Ga_{0.944}P_{0.975}N_{0.025}$/GaP lattice-matched SQWs as dependent on the well width L_Z, as well as for the bulk $In_{0.056}Ga_{0.944}P_{0.975}N_{0.025}$ layer.
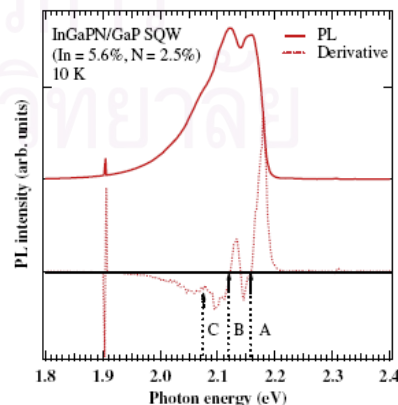

Fig. 2. Low-temperature (10 K) PL spectrum for the $In_{0.056}Ga_{0.944}P_{0.975}N_{0.025}$/GaP lattice-matched SQW having a well width of 1.6 nm. The dotted line is the numerical derivative of the PL data (solid line) yielding the energies (A, B and C) denoted by arrows.

($L_Z = 1.6$ nm). Thus, the N concentration in the well near the interfaces with the GaP barriers is expected as somewhat lower than 2.5%. The additional peak at the lower-energy side (feature C) may be attributed to the significantly localized excitons at N-related states.

Fig. 3 shows the 10 K-PLE spectra monitored at 1.89 eV for the $In_{0.056}Ga_{0.944}P_{0.975}N_{0.025}/GaP$ SQWs as a function of L_Z. In the bulk layer, a broad absorption band at 2.06–2.40 eV and a weak absorption edge at 2.86 eV are clearly distinguished [6]. It should be noted that these features are similar to those in the $GaP_{1-x-y}As_xN_y$ ($x = 0.02$) [5] and $GaP_{1-y}N_y$ ($x = 0.014$) [8–10] bulk layers, and are attributed to the isolated-N (A-line) absorption and to the direct-gap absorption edge, respectively. In the SQWs, the PLE spectra have shown the blue shift of the fundamental absorption edge to 2.17 eV for $L_Z = 1.6$ nm from 2.06 eV for the bulk. The blue shift is about 110 meV for the narrowest well with $L_Z = 1.6$ nm, and is probably due to the quantum confinement in the well. In addition, a sharp rise of absorption at 2.86 eV is not by the well but by the direct-gap absorption of the GaP barriers. This implies that, for the excitation energy higher than the direct-gap energy of GaP, the PL emission would be governed mainly by carriers generated in the GaP barriers and subsequent carriers transfer to the InGaPN well.

In Fig. 4, the LT-PL and PLE spectra shown above are collectively shown at the near-band-edge region. It is found that the PL sub-peaks B and C are associated with the band-tail states which are much lower in energy than the PLE absorption edge. On the other hand, the PL sub-peak A for the narrower wells ($L_Z \leqslant 3.2$ nm) is identical in its energy to the PLE absorption edge. This evidence demonstrates that the PL peaks B and C are due to the localized excitons whose spatial extent is shorter than the well width. Therefore, the weaker blue shift of these PL sub-peaks can be understood as the decrease of N
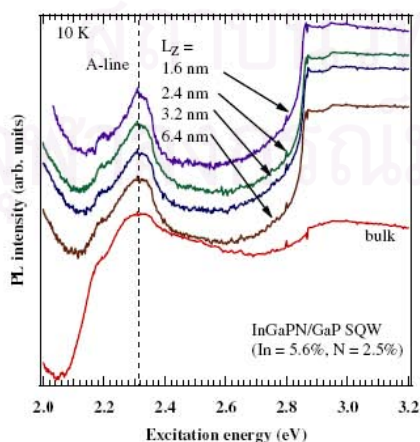
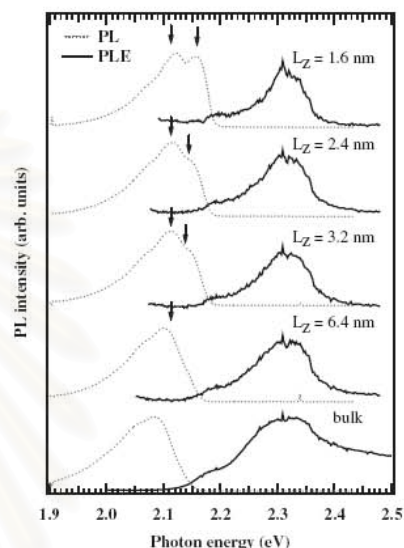

Fig. 4. Low-temperature (10 K) PL and PLE spectra at the near-band-edge region for the $In_{0.056}Ga_{0.944}P_{0.975}N_{0.025}/GaP$ lattice-matched SQWs as dependent on the well width L_Z, as well as for the bulk $In_{0.056}Ga_{0.944}P_{0.975}N_{0.025}$ layer. The arrows indicate the main (feature B) and the extra (feature A) peaks of the PL spectra.

concentration in the well. Since, these PL sub-peaks have shown less sensitive to the well width. From the energy difference between the absorption edge of PLE and the PL peak energy, we can expect the extra PL sub-peak A is due to less localized excitons, as will be described later.

Fig. 5 shows the PL spectra for the $In_{0.056}Ga_{0.944}P_{0.975}N_{0.025}/GaP$ SQW with $L_Z = 2.4$ nm as dependent on temperature. The temperature-dependent PL shows some characteristics generally observed for the InGaPN/GaP SQWs as follows: (i) The PL sub-peaks B and C is in agreement with a temperature dependence of the strongly localized luminescence. (ii) The emission intensity of the PL sub-peak A is quenched completely at about 80 K. This confirms that the feature A is attributable to a less-bounded exciton recombination.

The natural log of the overall integrated PL intensities of the SQWs is plotted as a function of temperature, shown in Fig. 6, together with that of the bulk layer for comparison. With an increase in temperature, the overall integrated emission intensity of the PL spectra gradually decreases, indicating the presence of a large density of non-radiative recombination centres. This behaviour corresponds to the thermal activated non-radiative recombination mechanism. The PL emission (efficiency) can simply be described by a model involving non-radiative process [11], $\eta(T) = [1 + (P_{nro}/P_r)\exp(-E_a/k_BT)]^{-1}$, where k_B is the Boltzmann constant, T is the sample temperature. P_{nro}/P_r is effectively the ratio of non-radiative (P_{nro}) to radiative (P_r)
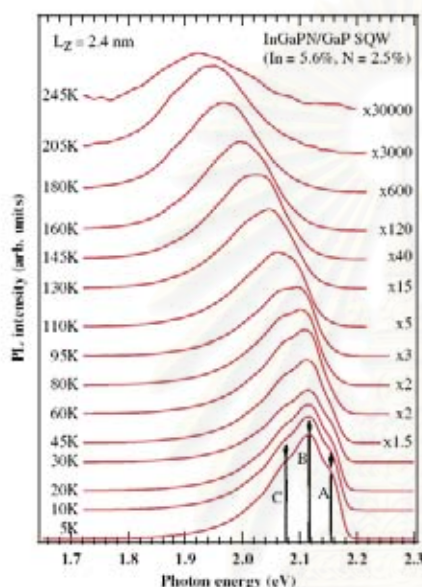

Fig. 3. Low-temperature (10 K) PLE spectra for the $In_{0.056}Ga_{0.944}P_{0.975}N_{0.025}/GaP$ lattice-matched SQWs as dependent on the well width L_Z, as well as for the bulk $In_{0.056}Ga_{0.944}P_{0.975}N_{0.025}$ layer.

Fig. 5. PL spectra for $In_{0.056}Ga_{0.944}P_{0.975}N_{0.025}$/GaP lattice-matched SQW ($L_Z = 2.4$ nm) as dependent on temperature.
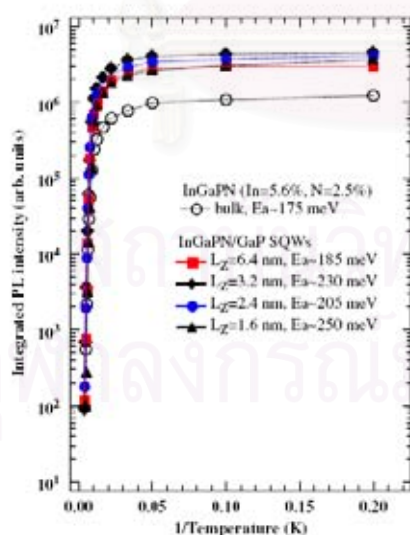

Fig. 6. Integrated PL intensity of for $In_{0.056}Ga_{0.944}P_{0.975}N_{0.025}$/GaP lattice-matched SQWs as dependent on temperature. A theoretical fitting gives the activation energies $E_a \sim 175$ meV for the bulk layer and $E_a \sim 200-250$ meV for the SQWs.

recombination probability for the loss mechanism. The best fit above 145 K yields the non-radiative recombination of $P_{nro}/P_r \sim 10^6 - 10^7$ and the activation energy (E_a) values

increased with decreasing L_Z, as shown in Fig. 6. Based on the PLE results, it is found that the values of $E_a \sim 200-250$ meV are in an agreement well with the energy difference between the PLE absorption edge of the $In_{0.056}Ga_{0.944}P_{0.975}N_{0.025}$ bulk (~ 2.09 eV at 10 K) and the bandgap of GaP (2.34 eV), which amounts to 250 meV. It is also expected by calculation [12,13] that the most part of the bandgap difference contributes to the conduction-band offset ΔE_c. Therefore, the E_a values for SQWs are considered as coming form the GaP barrier height for the carrier over flow from the quantum well, while for the bulk is from the localization energy of the bound excitons. These results demonstrate an efficient carrier confinement, which is realized in the lattice-matched $In_{0.056}Ga_{0.944}P_{0.975}N_{0.025}$/GaPSQWs with a large conduction band offset $\Delta E_c \sim 200-250$ meV, giving the highly efficient PL at higher temperatures.

4. Conclusions

$In_{0.056}Ga_{0.944}P_{0.975}N_{0.025}$/GaP lattice-matched SQW structures were successfully grown by MOVPE. LT-PL and PLE results for the SQWs with varied well widths have been revealed to confirm the quantum confinement by the well. Comparing with the bulk layer, the PL peak position and the fundamental absorption edge of PLE blue shift amounts to 76 and 110 meV, respectively, for the narrowest well of $L_Z = 1.6$ nm. In these samples, the blue shifts are believed to be predominantly determined by the quantum confinement effect to the well. The dependence on temperature of the PL spectra from the bulk and the SQWs indicates the presence of the localized excitons and the carrier over flow from the quantum well, respectively. The larger activation energies (E_a) in the SQWs are due to the large conduction band offset $\Delta E_c (200-250$ meV).

References

[1] K. Onabe, T. Kimura, N. Nakadan, J. Wu, Y. Ito, S. Yoshida, J. Kikawa, Y. Shiraki, Presented at ICCG-13/ICVGE-11, Kyoto, 2001.
[2] M. Kondow, T. Kitatani, S. Nakatsuka, M.C. Larson, K. Nakahara, Y. Yazawa, M. Okai, IEEE J. Select. Topics Quantum Electron. 3 (1997) 719.

[3] M. Kondow, K. Uomi, A. Niwa, T. Kitatani, S. Watahiki, Y. Yazawa, Jpn. J. Appl. Phys. 35 (1996) 1273.

[4] G. Biwa, H. Yaguchi, K. Onabe, Y. Shiraki, J. Crystal Growth 195 (1998) 574.

[5] G. Biwa, H. Yaguchi, K. Onabe, Y. Shiraki, Mater. Res. Soc. Symp. 482 (1998) 173.

[6] S. Sanorpim, F. Nakajima, R. Katayama, N. Nakadan, T. Kimura, K. Onabe, Y. Shiraki, Phys. Stat. Solidi (c) (7) (2003) 2773.

[7] S. Sanorpim, F. Nakajima, R. Katayama, N. Nakadan, T. Kimura, K. Onabe, J. Crystal Growth 275 (2005) e1017.

[8] S. Miyoshi, H. Yaguchi, K. Onabe, R. Ito, Y. Shiraki, Appl. Phys. Lett. 63 (1993) 3506.

[9] S. Miyoshi, H. Yaguchi, K. Onabe, Y. Shiraki, R. Ito, Jpn. J. Appl. Phys. 36 (1997) 97.

[10] H. Yagushi, S. Miyoshi, G. Biwa, M. Kibune, K. Onabe, Y. Shiraki, R. Ito, J. Crystal Growth 170 (1997) 353.

[11] J.D. Lambkin, L. Considine, S. Walsh, G.M. Oconnor, C.J. McDonagh, T.J. Glynn, Appl. Phys. Lett. 65 (1) (1994).

[12] S. Miyoshi, K. Onabe, Solid State Electron. 41 (1997) 267.

[13] L. Bellaiche, S.-H. Wei, A. Zunger, Phys. Rev. B 56 (1997) 10233.

APPENDIX C

International proceeding

Visible Photoluminescence from InGaPN/GaP Lattice-Matched Single Quantum Well Structures Grown by MOVPE

D. Kaewket[1], S. Tungasmita[1,*], S. Sanorpim[1,#], R. Katayama[2] and K. Onabe[2]

[1]Department of Physics, Faculty of Science, Chulalongkorn University, Thailand
[2]Department of Advanced Materials Science, The University of Tokyo, Japan

Abstract— Optical properties of $In_xGa_{1-x}P_{1-y}N_y$/GaP lattice-matched single quantum wells (SQWs) with different well widths ($L_z = 1.6 - 6.4$ nm) at different In ($x = 0.050 - 0.135$) and N ($y = 0.025 - 0.071$) concentrations have been investigated by low-temperature photoluminescence (PL) and PL-excitation (PLE). The PL spectra showed the strong visible emission from the samples which attracted to a variety of optoelectronic device applications such as light emitting and laser diodes. Comparing to the bulk film, the PL peak position and the fundamental absorption edge of PLE spectra exhibit blue-shift, which correspond to the principally determined by the quantum confinement effect to the well. Comparison between the absorption edge of PLE spectra and the finite square well calculation demonstrate that the effective bandgap energy of InGaPN/GaP system is might be originated from the N-related localized states. With increasing N concentration, the PL peak position exhibits red-shift, which is due to the lowering conduction band edge of InGaPN. On the other hand, the integrated PL intensity is significantly decreased for the SQW with higher In and N concentrations. This probably caused by the larger number of non-radiative process which associated to N-induced trap states.

Keywords- InGaPN; metalorganic vapor phase epitaxy (MOVPE); photoluminescence (PL); photoluminescence-excitation (PLE); single quantum wells (SQWs)

I. INTRODUCTION

InGaPN is a novel material that can be lattice-matched to GaP, with a narrower bandgap than GaP [1]. The material is of interest for a variety of high-brightness light-emitting and laser applications such as automotive lighting, optical media reader/writer, billboard, media display panel and traffic lights, etc. It is well known that the incorporation of N drastically reduces the bandgap energy with the majority of the reduction resulting from the lowering of conduction band, as in the case of InGaAsN [2]. Although InGaPN is an indirect bandgap semiconductor, since the GaP which is the majority material is the indirect bandgap semiconductor. The InGaPN/GaP structure can be invented for optoelectronic devices, like GaPN/GaP and GaPAsN/GaP structures. In the late 1960s, Thomas and Hopfield discovered the N isoelectronic trap in GaP:N for low N concentration ($\sim 10^{18}$ cm^{-3}) [3], which led this structure to fabrication of high-efficient green light emitting diodes (LED's) [4, 5]. This phenomenon causes by the producing of localized N-related trap states in the bandgap

which lower than the indirect bandgap energy level of GaP. As a result, the carriers are attracted by these strong localized states and then recombination. These make the GaPN and GaPAsN materials to be the quasi-direct semiconductor with lowering the effective bandgap. The same effect is expected for InGaPN material. These introduce the InGaPN/GaP structure as an alternative heterostructure with a large barrier height for an electron confinement in the InGaPN/GaP quantum structures, and exhibit higher characteristic temperature for laser application. V. A. Odnoblyudov *et al.* reported that the conduction band offset (ΔE_C) of this structure is about 225 meV which much larger than the commercial AlInGaP/GaAs structure (75 meV) [6].

Due to the limit of the extreme immiscibility which is the characteristic of the III-(III)-V-N type alloys, it is well known that the high quality InGaPN layer with high N content is difficult to grow. Thus, it is also a challenge that how far the N atoms can be incorporated in the InGaPN alloy. G. Biwa *et al.* reported on the metalorganic vapor phase epitaxy (MOVPE) growth of high quality GaP$_{1-y}$N$_y$ films with N content up to y = 0.023 at relatively high growth temperature [7]. Based on such growth conditions, the In$_x$Ga$_{1-x}$P$_{1-y}$N$_y$ layers ($0 \le x \le 0.176$ and $0 \le y \le 0.087$) were successfully grown on the GaP (001) substrates [8, 9]. The successful growth of the lattice-matched In$_x$Ga$_{1-x}$P$_{1-y}$N$_y$ layer with the N content as high as y = 0.071 was demonstrated. However, only little information about optical properties of the InGaPN/GaP heterostructure has been reported nowadays [6]. In this work, luminescence properties of In$_x$Ga$_{1-x}$P$_{1-y}$N$_y$/GaP lattice-matched single quantum wells (SQWs) which various well-widths and In (x = 0.050, 0.080, 0.135) and N (y = 0.025, 0.048, 0.071) concentrations have been investigated by low-temperature photoluminescence (PL). Structural characterization has been done by high-resolution X-ray diffraction (HRXRD). We have also investigated the confinement effect in In$_x$Ga$_{1-x}$P$_{1-y}$N$_y$/GaP lattice-matched SQWs by PL-excitation (PLE) measurements and used the finite-depth single-square well mode in evaluation.

II. EXPERIMENTS

All the In$_x$Ga$_{1-x}$P$_{1-y}$N$_y$/GaP lattice-matched SQWs and the In$_x$Ga$_{1-x}$P$_{1-y}$N$_y$ bulk layers used in this study were grown on GaP (001) substrates by MOVPE, using trimethylgallium (TMGa), trimethylindium (TMIn), PH$_3$ and 1,1-dimethylhydrazine (DMHy) as the Ga, In, P and N precursors, respectively, H$_2$ as the carrier gas. After the growth of the
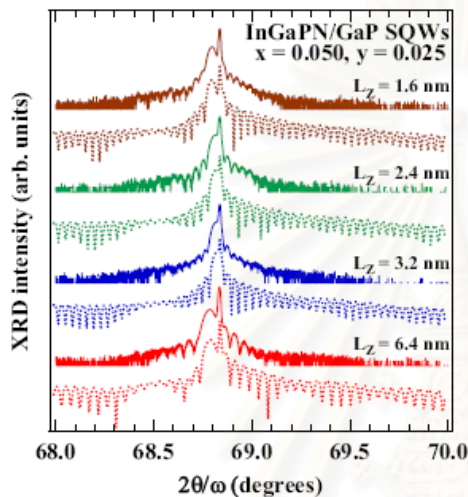
Figure 1. HRXRD patterns of the InGaPN/GaP SQWs with similar In and N concentration (x = 0.050, y = 0.025) and different well widths (solid lines), as well as the simulation (dotted lines).
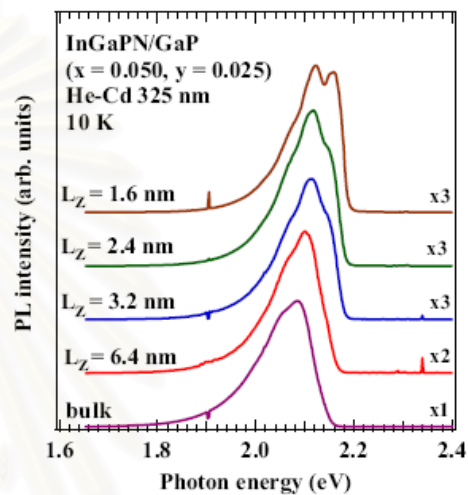

Figure 2. Low-temperature (10 K) PL spectra for InGaPN/GaP SQWs (x = 0.050, y = 0.025) with different well-widths L_Z = 1.6 – 6.4 nm as well as the bulk layer.

around 0.3 μm-thick GaP buffer layer at 710°C, a thin InGaPN well layer and a GaP cap layer were respectively grown at 635°C. The well-width and composition of the $In_xGa_{1-x}P_{1-y}N_y$ well layers, which are nominally lattice-matched to GaP, were controlled to be L_Z = 1.6 - 6.4 nm and x = 0.050 – 0.135 and y = 0.025 – 0.071, respectively. The $In_xGa_{1-x}P_{1-y}N_y$ bulk layers without the GaP cap layer were also prepared for a comparative study. The growth parameters such as V/III ratio, DMHy flow rate, were based on the growth of the InGaPN bulk layers described in elsewhere [8, 9]. The well-width and the composition of single quantum wells (SQWs) were determined by high–resolution X-ray diffraction (HRXRD) measurement via the dynamical-theory simulation software. The optical experiments at low temperature (10 K) were carried out using PL and PLE spectroscopes. PL measurement was performed using the 325 nm-line of He-Cd laser (1.0 W/cm^2) as the excitation source. PLE measurement was done using monochromatic light dispersed with a 0.27 m monochromator from a 500 W Xenon lamp.

III.   RESULTS AND DISCUSSION

A.   Effects on well-width variation

All the samples were examined by HRXRD in order to determine the well-width and composition and check the structural quality. The (004) 2θ/ω-scan HRXRD patterns of the $In_{0.050}Ga_{0.950}P_{0.975}N_{0.025}$/GaP SQWs with various well-widths (L_Z = 1.6 - 6.4 nm) are shown as in Fig. 1. The main sharp diffracted peak at the angle of 68.8° is corresponded to the

reflection from the (004) GaP and the additional diffracted peak at the lower angle is corresponding to the (004) InGaP. The existence of InGaP is due to the diffusion of a small amount of In (x ~ 0.5%), which is existed in the growth system, into the GaP buffer layer during the growth. The distinct Pendellösung fringes indicate the finite thickness of the (In)GaP buffer layer (~300 nm). This indicates that structural quality of $In_{0.050}Ga_{0.950}P_{0.975}N_{0.025}$/GaP lattice-matched SQWs were successfully grown. The dynamical-theory simulation results are also displayed as the dotted curves in Fig. 1. The good agreement between the simulated and experimental data indicates that the $In_{0.050}Ga_{0.95}P_{0.975}N_{0.025}$/GaP lattice-matched SQWs with excellent crystal quality and fairly flat interfaces have been grown on the GaP substrate.

As shown in Fig. 2, the 10 K-PL spectra for the corresponding $In_{0.050}Ga_{0.950}P_{0.975}N_{0.025}$/GaP SQWs with various well widths (L_Z = 1.6 - 6.4 nm) together with the $In_{0.050}Ga_{0.950}P_{0.975}N_{0.025}$ bulk film. The emission from the $In_{0.050}Ga_{0.950}P_{0.975}N_{0.025}$/GaP SQWs with narrower well-widths is shifted to higher energies. The PL also shows an evidence of the strong light emission in the visible (λ = 560 – 680 nm) region. Compare to the bulk film, the PL peak position and the fundamental absorption edge of PLE spectra (see Fig. 4a) exhibit a blue-shift, which is much consistent with the quantum confinement by the well. Moreover, it is found that an extra peak appears at higher-energy side of the main peak when the well-width is about L_Z = 3.2 nm or narrower. Nevertheless, this feature grows up and shifts toward the higher energies with a decreasing of well-width. Since, for the
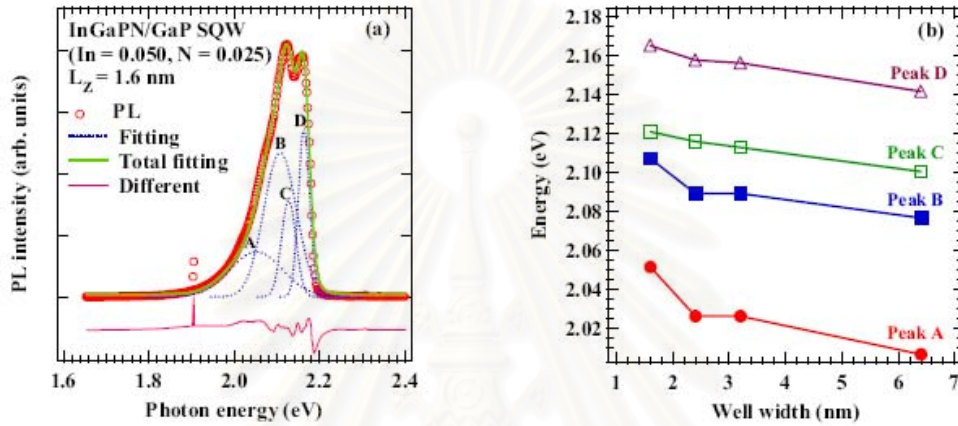
Figure 3. a) Low-temperature (10 K) PL spectra for InGaPN/GaP SQWs (x = 0.050, y = 0.025) with well-widths L_Z = 1.6 nm, as well as the fitting.
b) Dependence of the peak position and the well width for the InGaPN/GaP SQWs (x = 0.050, y = 0.025) with various well-widths.

N concentration close to y = 0.02, the average distance between the N atoms is about 1.3 nm [10], which is comparable to the width of the narrowest well (L_Z = 1.6 nm). Thus, the N concentration in the $In_{0.050}Ga_{0.950}P_{0.975}N_{0.025}$ well near the interfaces with the GaP barrier is expected as somewhat lower than y = 0.025. As a result, the splitting of this PL sub-peak might be caused by the recombination of localized excitons due to the well-width fluctuations, which are induced by random distribution of the N atoms within the well.

As seen from the 10 K-PL spectra as in Fig. 2, the PL spectrum contains several sub-peaks. A quantitative fit to the PL spectra, by assuming a Gaussian distribution of the density of state, has been utilized to accurately evaluate their own energy peak positions. An example of the fitting procedures is shown in Fig. 3a for the SQW with well-width of 1.6 nm. The evolution of all these PL sub-peaks related to well-width shown in Fig. 3b. The progression of the PL sub-peaks denoted as A, B, C and D are attributed to the quantum confinement by the well. The small difference of the blue-shift of each PL sub-peak might be owing to the different in the effective mass of the localized exciton which depends on the

trapping defects. We do not have sufficient evidence here to clarify the origin of these emissions. However, the A, B, C and D sub-peaks indicate that there are four different emission bands. These PL emissions are most likely as a result from localized defect states form near the conduction band in the InGaPN material [8, 9, 11].

Next, we focus on the quantum well characteristic of the novel InGaPN/GaP structure, which we have proposed [1]. Adding In into GaP, resulting an increasing of the lattice constant in InGaP alloy. On the other hand, adding N to GaP results in a decreasing of lattice constant in GaPN alloy. InGaPN can therefore be lattice-matched to GaP by adjusting In and N concentrations. As a result, the finite-depth single-square well model without the effects of hydrostatic strain can be used to interpret the PL and PLE results obtained from the lattice-matched InGaPN/GaP SQWs. Linear interpolation is applied to obtain the material parameters of $In_{0.050}Ga_{0.950}P_{0.975}N_{0.025}$ alloy, i.e., the electron effective mass (m_e) and Luttinger parameters [12]. All the input parameters are summarized in Table I. To calculate the conduction-band offset (ΔE_C), the PLE absorption edge of $In_{0.050}Ga_{0.950}P_{0.975}N_{0.025}$ bulk layer (2.08 eV) is used as the effective bandgap of the InGaPN well layer. The barrier potential is determined by energy level of the indirect bandgap of GaP (2.35 eV). In addition, it is known that adding small amount of N decreases the bandgap, which mainly affects the conduction band (CB) states leading to a large ΔE_C and only a small valence-band offsets (ΔE_V) [6]. Thus, the value of ΔE_V can be approximated to be zero, in our case. Consequently, the value of ΔE_C is estimated to be about 270 meV.

For $In_{0.050}Ga_{0.950}P_{0.975}N_{0.025}$ well layer, the heavy-hole effective mass (m_{hh}) is giving by

$$m_{hh} = m_0 \; / \; (\gamma_1 - 2\gamma_2) \qquad (1)$$

TABLE I. PARAMETERS USED IN THE CALCULATION [13]

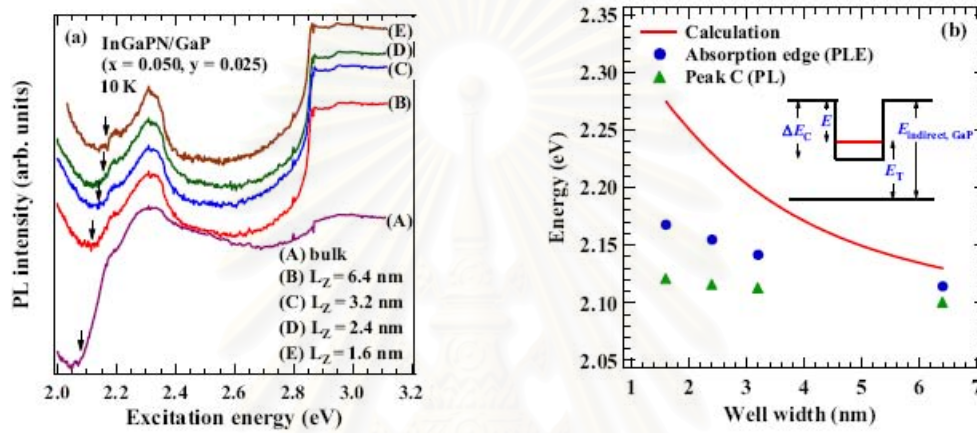| Binary materials	Luttinger parameters		Electron effective mass (m_e)
	γ_1	γ_2	
GaP	4.05	0.49	0.13
InP	5.08	1.60	0.15
GaN	2.67	0.75	0.08
InN	3.72	1.26	0.12

Figure 4. a) Low-temperature (10 K) PLE spectra for InGaPN/GaP SQWs (x = 0.050, y = 0.025) with different well-widths L_Z = 1.6 – 6.4 nm as well as the bulk layer. The arrows indicate the absorption edge.

b) Dependence of the energy and the well width for the theoretical calculation and the absorption edge, as well as the peak C of PL. The inset shows the band alignment of the InGaPN/GaP SQW structure.

The value of m_{hh} calculated in (1) is equal to $0.34m_0$. The exciton effective mass (m), which is obtained from the reduced mass, was estimated to be $0.09m_0$. For the GaP barrier, the electron effective mass and the heavy-hole effective mass are m_e = $0.13m_0$ and m_{hh} = $0.33m_0$, respectively. Thus, the exiton effective mass of the GaP barrier was determined to be $0.09m_0$, which is comparable to that of the well layer.

Taking into account the exiton effective masses, we now turn to solve the finite-depth single-square well problem, without the effects of hydrostatic strain. Confined exiton energies were calculated by numerically finding the root of the following equations:

$$\alpha \tan \alpha = \beta \qquad (2)$$

and

$$\alpha^2 + \beta^2 = \frac{2m|V|}{\hbar^2} \left(\frac{L_z}{2} \right)^2 \qquad (3)$$

where $\alpha = \dfrac{L_z}{2} \sqrt{\dfrac{2m}{\hbar^2}(-|E| + |V|)}$, $\beta = \dfrac{L_z}{2} \sqrt{\dfrac{2m|E|}{\hbar^2}}$,

L_Z and m stand for the well-width and the exciton effective mass in the confinement direction. E is the energy of the state in the well (see inset in Fig. 4b) and V is the barrier potential (or band discontinuity, ΔE_C). Thus, the optical transition energy (E_T) can be written as

$$E_T = E_{indirect, GaP} - E \qquad (4)$$

where $E_{indirect, GaP}$ is the indirect gap of GaP (2.35 eV). Fig. 4(b) shows the PL and PLE absorption edge as a function of well-width together with the dependence calculated optical transition energies from (4). The PLE absorption edge has the same trend with the calculated optical transition energies, confirming the quantum confinement effect by the well. However, the PLE absorption edges exhibit the lower in the energy than the calculated optical transition energies. This difference might be due to the difference in exciton effective mass. It is known that in dilute III-V-N system, the electron effective mass is significantly increased with incorporation of N [14, 15]. However, in this work, we have calculated the optical transition energies using the same value of the exiton effective mass for the well and barrier layers. Particularly note that, it is also include the behavior mass effect to explain the well-width dependence of the transition optical energies. On the other hand, it is evidence that the PL peak positions are much lower in the energy than the PLE absorption edges and the calculated value of optical transition energies. This evidence implies that such PL emission might be originated from the localized states which are attributable to the N-related band edge fluctuation in the well.

B. Effects on compositional variation

The experimental and simulated (004) HR-XRD patterns for $In_xGa_{1-x}P_{1-y}N_y$/GaP lattice-matched SQWs with various In and N concentrations are illustrated in Fig. 5. The solid curves are experimental results, while the dotted curves are the results from the best fitting using dynamical-theory simulation software. The fitted well-width of these SQWs was 1.6 nm. As can be seen in Fig. 5, the lattice-matched $In_xGa_{1-x}P_{1-y}N_y$/GaP SQWs were obtained with the fitted In and N concentrations of (a) (x = 0.050, y = 0.025), (b) (x = 0.080, y = 0.048) and (c) (x = 0.135, y = 0.071). The Pendellösung fringes from the
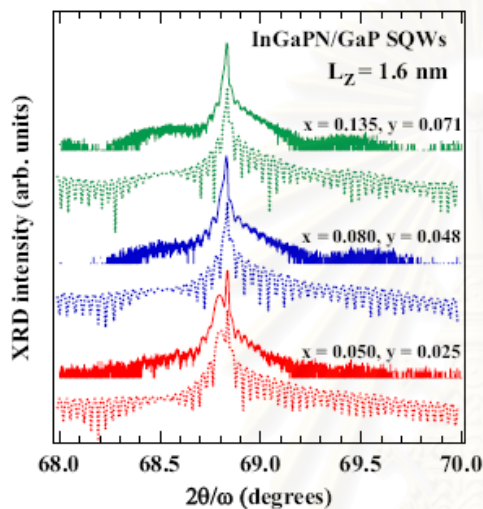
Figure 5. HRXRD patterns of the InGaPN/GaP SQWs with similar well width and different In and N concentrations. The lower curves are the simulation.

Figure 6. Low-temperature PL spectra for InGaPN/GaP SQWs with fixed L_Z = 1.6 nm and various In and N concentrations.

(In)GaP buffer layer in the SQW with the lowest In and N concentrations (x = 0.050, y = 0.025) are clear and have better fitting results than those of SQWs with higher In and N concentrations showing that flatter hetero-interfaces are achieved in InGaPN/GaP SQWs due to its smaller lattice mismatch. The inferior interface fringe features is due to crystal quality degradation caused by high N incorporation. The degradation of the crystal quality might be due to the composition fluctuation of high N containing InGaPN materials as relatively high growth temperature was used.

The 10 K-PL spectra for the corresponding $In_xGa_{1-x}P_{1-y}N_y$/GaP SQWs with various In and N concentrations of (a) (x = 0.050, y = 0.025), (b) (x = 0.080, y = 0.048) and (c) (x = 0.135, y = 0.071) were shown in Fig. 6. With increasing In and N concentrations whereas the well-width was fixed, the PL main peak exhibits red-shift, indicating a reducing of the optical transition energy which is due to the lowering conduction band edge. It was found that the red–shift is amounts to 0.17 eV for the highest N-incorporating SQW sample. Also, for the highest N-incorporating SQW sample, the intensity of PL main peak rapidly decreases, owing apparently to the high-concentration of non-radiative recombination centers in such a high N-incorporating SQW. In addition, the sharp NNi lines and their phonon replicas [16] are clearly observed in all SQWs. The dotted guide lines indicate the NNi lines which have an intense intensity, i.e., A-line (2.31 eV) and NN3 (2.26 eV). The A-line and NN3 are attributed to the recombination from the isolated N atom states and third nearest neighbor N atom site state, respectively [16]. Unlike the PL main peak, these NNi lines still remain their energy with increasin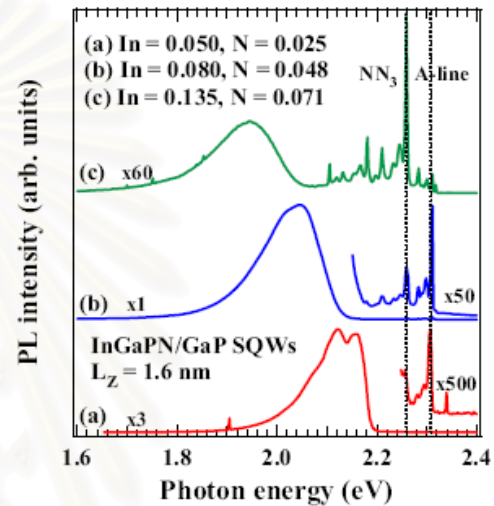g In and N concentrations. It is interpreted that the PL main peak was emitted from InGaPN well layer but the sharp NNi lines were emitted from the GaP barrier due to the N atoms penetration during the growth. Thus, the cause of a large reduction of PL intensity may be owing to the rising of non-radiative defects, which are related to the incorporation of N.

IV. CONCLUSION

We investigated the optical properties of $In_xGa_{1-x}P_{1-y}N_y$/GaP lattice-matched SQW structures with various well widths (L_Z = 1.6 - 6.4 nm) and different In (x = 0.050 - 0.135) and N (y = 0.025 - 0.071) concentrations grown by MOVPE. Low-temperature PL and PLE results for the lattice-matched SQWs with varied well-widths and In and N concentrations have been revealed to confirm the quantum confinement by the well. Comparing with the bulk layer, the PL peak position and the fundamental absorption edge of PLE exhibit blue-shift for SQWs with narrower well-widths and lower In and N concentrations. These blue-shifts were interpreted using the finite-depth single-square well mode which believed to be predominantly determined by the quantum confinement effect to the well. The highest In and and N concentrations in this study is x = 0.135 and y = 0.071, respectively, and its low-temperature PL emission in the visible wavelength was clearly observed. This result shows the potential for the fabrication of a variety of high-brightness light-emitting and lasers on GaP substrates.

REFERENCES

[1] K. Onabe, T. Kimura, N. Nakadan, J. Wu, Y. Ito, S. Yoshida, J. Kikawa and Y. Shiraki, presented at ICCG-13/ICVGE-11, Kyoto, 2001.

[2] M. Kondow, K. Uomi, A. Niwa, T. Kitatani, S. Watahiki and Y. Yazawa, "GaInNAs: A novel material for long-wavelength-range laser diodes with excellent high-temperature performance," Jpn. J. Appl. Phys., vol. 35, pp. 1273, 1996.

[3] D. G. Thomas, J. J. Hopfield and C. J. Frosch, "Isoelectronic traps due to nitrogen in gallium phosphide," Phys. Rev. Lett., vol. 15, pp. 857-860, 1965.

[4] R. A. Logan, H. G. White and W. Wiegmann, "Efficient green electroluminescence in nitrogen-doped GaP p-n junctions ," Appl. Phys. Lett., vol. 13, pp. 139-141, 1968.

[5] R. A. Logan, H. G. White and W. Wiegmann, "Efficient green electroluminescent junctions in GaP," Solid state electron, vol. 14, pp. 55-70, 1971.

[6] V. A. Odnoblyudov and C. W. Tu, "Optical properties of InGaNP quantum wells grown on GaP (100) substrates by gas-source molecular beam epitaxy," Appl. Phys. Lett., vol. 89, pp. 111922, 2006.

[7] G. Biwa, H. Yaguchi, K. Onabe and Shiraki, "Metalorganic vapor-phase epitaxy of GaPAsN quaternary alloys on GaP," J. Cryst. Growth, vol. 189/190, pp. 485-489, 1998.

[8] S. Sanorpim, F. Nakajima, R. Katayama, N. Nakadan, T. Kimura, K. Onabe and Y. Shiraki, "MOVPE growth and characterization of high-N content InGaPN alloy lattice-matched to GaP," Physica status solidi (c), vol. 7, pp. 2773-2777, 2003.

[9] S. Sanorpim, F. Nakajima, R. Katayama, N. Nakadan, T. Kimura and K. Onabe, "MOVPE growth and optical investications of InGaPN alloys," J. Cryst. Growth, vol. 275, pp. 1017, 2005.

[10] G. Biwa, H. Yaguchi, K. Onabe and Y. Shiraki, "Photoluminescence and photoluminescence-excitation spectroscopy of GaPAsN/GaP lattice-matched multiple quantum well structures," J. Cryst. Growth, vol. 195, pp. 574-578, 1998.

[11] D. Kaewket, S. Tungasmita, S. Sanorpim, F. Nakajima, N. Nakadan, T. Kimura, R. Katayama and K. Onabe, "Photoluminescence and photoluminescence-excitation spectroscopy of InGaPN/GaP lattice-matched single quantum well structures grown by MOVPE," J. Cryst. Growth, in press.

[12] P. Lawaetz, "Valence-band parameters in cubic semiconductors," Phys. Rev. B, vol. 4, pp. 3460-3467, 1971.

[13] I. Vurgaftman, J. R. Meyer and L. R. Ram-Mohan, "Band parameters for III-V compound semiconductors and their alloys," Appl. Phys. Rev., vol. 89, pp. 5815-5863, 2001.

[14] H. P. Xin and C. W. Tu, "Photoluminescence properties of GaNP/GaP multiple quantum wells grown by gas source molecular beam epitaxy," Appl. Phys. Lett., vol. 77, pp. 2180-2182, 2000.

[15] J. Wu, W. Shan and W. Walukiewicz, "Band anticrossing in highly mismatched III-V semiconducting alloys," Semicond. Sci. Technol., vol. 17, pp. 860-869, 2002.

[16] D.G. Thomas and J.J. Hopfield, "Isolectronic traps due to nitrogen in gallium phosphide," Phys. Rev., vol. 150, pp. 680-689, 1966.

VITAE

Miss Dares Kaewket was born on October 13, 1981 in Phitsanulok, Thailand. She received her Bachelor degree of Science in Physics from Chulalongkorn University in 2003, and continued her Master's degree study in 2004.